Development of multifunctional nanoparticles for drug delivery and bioimaging

Von der Naturwissenschaftlichen Fakultät der

Gottfried Wilhelm Leibniz Universität Hannover

zur Erlangung des Grades

Doktor der Naturwissenschaften

(Dr. rer. nat.)

genehmigte Dissertation

von

Muharrem Seleci, Master`s Degree (Türkei)

geboren am 27.09.1986 in Giresun, Türkei

2017

Referent: Prof. Dr. Thomas Scheper

Korreferent: Prof. Dr. Cornelia Blume

Tag der Promotion: 01.12.2017

Dedication

In generosity and helping others be like a river.

In compassion and grace be like the sun.

In concealing others' faults be like the night.

In anger and fury be like the dead.

In modesty and humility be like the earth.

In tolerance be like a sea.

Either exist as you are or be as you look.

Mevlânâ Rûmî

This dissertation is dedicated to my dear wife Didem and my parents Fatma and İsmail, my sister Gözde and everybody who contributed me to achieve this success. This would not have been possible without you.

Muharrem
Hannover, 2017

Acknowledgement

First of all, I would like to thank my supervisor, Prof. Dr. Thomas Scheper, for welcoming me into his group and for his valuable support during the past few years. I also would like to express my deepest gratitude to Dr. Frank Stahl for his help, guidance and enthusiastic encouragement throughout my thesis. He believed in me every time and never doubted my abilities.

Prof. Dr. Suna Timur and Assoc. Prof. Dr. Dilek Odaci Demirkol contributed substantially efforts to come here. Since my bachelor, they have supported me all the time, always make me feel special and I appreciate them.

I wish to thank Dr. Johanna Walter for sharing her time and for her valuable scientific critiques. I would like to also express my thanks to Martin Paehler and Martina Weiss who made everything easily accessible in the institute, Ivo Havlik and Michael Dors for IT support, and Ulrike Dreschel and Cornelia Alic who were very kind helping me prepare and complete my documents.

I am extremely grateful to Dr. Ashwath Jayagopal, section head at Roche Pharma Research and Early Development, for his support, encouragement, and extension of the contract. He gave me an opportunity to get a new perspective and to learn how science and research are conducted in a big company. All the RIDDL (Retinal Imaging and Drug Delivery Group) members were very helpful and considerate. I must say, I am very fortunate to work with them.

Dr. Rebecca & Patrick Jonczyk deserve a special thanks and appreciation. There is nothing worse than feeling all alone somewhere foreign, however you have made your presence felt in Hannover and I am sure that our friendship will always remain. I wish to thank Dr. Mehriban Ulusoy as she was so eager to share her experience with us and mediated to meet with Hermann and Sigrid. I am so glad that we turned over a new leaf in our friendship which is continuing over the years.

I would like to express my thanks to all the members of Institute Technical Chemistry but especially to Harshvardhan Modh for having a good time. I also thank Nuran & Özgür, Zeynep & Hakan, and Bahar & Erkan for spending pleasant time together.

I consider myself lucky to meet with you, Hermann "Amca" and Sigrid. I appreciate our meetings with informative discussions in Campus Suite. It provided me different aspects of my life and was an opportunity to get to learn more about Germany.

Last but not least, I would like to express my deepest thanks to my mother, father, sister and grandfather; the family of my wife, my cousins, and friends for being patient and their endless support. I owe very special thanks to my dear wife Didem for her love, her friendship, and especially making it possible for me to get a PhD degree in Germany. I would never have predicted this outcome when we met in organic chemistry lab nine years ago. Without her support, I could not have done what I was able to do. I love you all.

Abstract

The rapid development of nanotechnology has offered novel therapeutic and diagnostic strategies to overcome limitations of conventional therapy. Creation of the materials at nanometer scale and manipulation of their properties have enabled to employ them in a number of biological applications such as in controlled drug delivery and bioimaging.

Within this thesis, the physical parameters for construction of multifunctional nanoparticles were summarized and the application potential of polymeric nanoparticles and liposomes as a drug carrier and imaging vehicle were evaluated. Initially, amphiphilic hyperbranched copolymer as a drug nanocarrier was designed with dual peptides which can specifically bind to integrin αvβ3 with RGD, while Cys-TAT facilitates penetration through the cell membrane. After drug (doxorubicin (DOX)) encapsulation with detailed characterization, the applicability of the polymeric micelles was tested in glioblastoma and breast cancer cell lines that are αvβ3 integrin positive and negative, respectively. Thus, the effects of targeting ligand on the surface of nanoparticle were analyzed in terms of cellular uptake as well as toxicity. Targeted drug-loaded micelles showed stronger inhibition on the integrin αvβ3 receptor overexpressed cells compared to the drug-loaded micelles without peptides on the surface.

Finally, liposome-nanoparticle hybrids were designed for co-delivery of imaging and therapeutic agents. Both hydrophobic nanoparticle (quantum dot (QD)) and hydrophilic drug (topotecan (TPT)) were encapsulated into liposomes and their further characterization was performed in detail. Drug release profile was observed under neutral and acidic conditions. *In vitro* analysis of the formulations was performed on cervical cancer cells. As a result, even though no targeting ligand was used on liposome surface, liposomal formulations were uptaken to the cells more efficiently compared to the free drug. Thus, the bioavailability of the imaging agent and therapeutic efficiency of the drug were enhanced by using theranostic liposome-QD hybrids.

Overall, novel multifunctional polymeric and liposomal tools for drug delivery and bioimaging were designed and developed with different targeting strategies. These approaches might offer new possibilities for development of novel platforms in nanomedicine.

Key words: *multifunctional nanoparticles, hybrid nanomaterials, bioimaging, targeted drug delivery, nanomedicine*

Kurzfassung

Die rasante Entwicklung in der Nanotechnologie hat neue therapeutische und diagnostische Strategien ermöglicht, um die Grenzen der konventionellen Therapie zu überwinden. Die Herstellung von Materialien im Nanometer-Bereich mit definierten Eigenschaften ermöglicht eine Anwendung beispielsweise in der kontrollierten Arzneimittelabgabe und der Bildgebung.

Im Rahmen dieser Arbeit wurden Parameter für den Bau multifunktionaler Nanopartikel zusammengefasst. Das Anwendungspotential von Liposomen und polymeren Nanopartikeln als Arzneimittelträger und Vehikel in der Bildgebung wurde untersucht. Zunächst wurde ein amphiphiles hyperverzweigtes Copolymer als Arzneimittelträger mit zwei zielgerichteten Peptiden (RGD, Cys-TAT) entwickelt. Nach Verkapselung eines Medikamentes (Doxorubicin (DOX)) und der detaillierten Charakterisierung wurden *in-vitro* Zellen, die Integrin αvβ3 positiv oder negativ waren, mit den polymeren Micellen behandelt. So wurde der Einfluss der Oberflächen-Peptide auf die zelluläre Aufnahme sowie Toxizität der Nanopartikel analysiert. Zielgerichtete, wirkstoffbeladene Mizellen zeigten eine stärkere Hemmung der Zellwachstum an den Integrin αvβ3-Rezeptor überexprimiert Zellen im Vergleich zu wirkstoffbeladenen Mizellen ohne Peptide auf der Oberfläche.

Außerdem wurden Liposom-Nanopartikel-Hybride für die Co-Abgabe von bildgebenden und therapeutischen Mitteln entwickelt. Sowohl hydrophobe, fluoreszierende Nanopartikel (Quantum dots (QD)) als auch hydrophile Arzneimittel (Topotecan (TPT)) wurden in Liposomen verkapselt und charakterisiert. Die Arzneimittelfreisetzung wurde unter neutralen und sauren Bedingungen verfolgt. -Die Untersuchung der zellulären Aufnahme der Liposom-QD-Hybride . *in-vitro* ergab, dass Zellen die Liposom-QD-Hybride effizienter aufnahmen als das freie Arzneimittel, obwohl sich kein zielgerichteter Ligand auf der Liposomoberfläche befand.

Insgesamt wurden multifunktionale Polymere und Liposome für die gezielte Bioverfügbarkeit eines Bildgebungsmittels und eine spezifische Verabreichung von Arzneimitteln mit hoher therapeutischer Wirsamkeiterfolgreich entwickelt. Hierdurch bieten sich neue Möglichkeiten für die Entwicklung theranostischer Plattformen in der Nanomedizin.

Stichwörter: *multifunktionale Nanopartikel, hybride Nanomaterialien, Bioimaging, gezielte Arzneimittelabgabe, Nanomedizin*

Table of Contents

List of Tables

List of Figures

Supplementary Information

List of Abbreviations

ABCs	Amphiphilic block copolymers
AFM	Atomic force microscopy
ANOVA	One-way analysis of variance
ATRP	Atom transfer radical polymerization
AuNP	Gold nanoparticles
BEMA	2-Bromoethyl methacrylate
BS3	Bis(sulfosuccinimidyl)suberate
CEA	Carcinoembryonic antigen
CDI	N,N'-carbonyldiimidazole
CPPs	Cell penetrating peptides
cryo-TEM	Cryo-transmission electron microscopy
DAPI	4′,6-diamidino-2-phenylindole dihydrochloride
DLC	Drug loading content
DLE	Drug loading efficiency
DLS	Dynamic light scattering
DMEM	Dulbecco's modified eagle medium
DMPC	Dimyristoylphosphatidylcholine
DOX	Doxorubicin
DSPC	Distearoylphosphatidylcholine
DTT	Dithiothreitol
EDC	1-ethyl-3-(3-dimethylaminopropyl)carbodiimide hydrochloride
EE	Encapsulation efficiency
EGFR	Epidermal growth factor receptor
EPC	Egg phosphatidylcholine
EPR	Enhanced permeability and retention
FCS	Fetal calf serum
FF-TEM	Freeze-fracture transmission electron microscopy
FITC	Fluorescein isothiocyanate
FT-IR	Fourier transform infrared
GPC	Gel-permeation chromatography
GUVs	Giant unilamellar vesicles
HANPs	Hyaluronic acid nanoparticles

HBS	HEPES buffered saline
HEMA	2-Hydroxyethyl methacrylate
HPLC	High performance liquid chromatography
IgG	Immunoglobulin G
IR	Infrared
LUVs	Large unilamellar vesicles
mAbs	Monoclonal antibodies
MEM	Minimum Essential Medium Eagle
MeOH	Methanol
MLVs	Multilamellar vesicles
MMA	Methyl methacrylate
MMP	Matrix metalloproteinase
MTT	3-[4,5-dimethylthiazol-2-yl]-2,5-diphenyltetrazolium bromide
MVVs	Multi-vesicular vesicles
NHS	*N*-hydroxysuccinimide
NTA	Nanoparticle tracking analysis
O/W	Oil-in-water
PAMAM	Poly(amidoamine)
PBS	Phosphate buffered saline
PCL	Poly(ε-caprolactone)
PDI	Polydispersity index
PEG	Polyethylene glycol
PI	Propidium iodide
pI	Isoelectric point
PL	Payload
PLGA	Poly(lactic-coglycolide)
PMMA	Poly(methyl methacrylate)
PMMA-*b*-PHEMA	Poly(methyl methacrylate)-*block*-poly(hydroxyethyl methacrylate)
PMPI	N-(*p*-Maleimidophenyl) isocyanate
PNPs	Polymeric nanoparticles
P/S	Penicillin/streptomycin
QD	Quantum dot
RES	Reduce reticuloendothelial system

RI	Refractive index
SCVP	Self-condensing vinyl polymerization
SEC	Size-exclusion chromatography
SMCC	Succinimidyl-4-(*N*-maleimidylmethyl)cyclohexane-1-carboxylate
SPDP	*N*-succinimidyl-3-(2-pyridyldithio)propionate
SUVs	Small unilamellar vesicles
SWCNT	Single-walled carbon nanotubes
TCEP	Tris-(2-carboxyethyl)phosphine
Tc	Phase transition temperature
TFA	Trifluoroacetic acid
TPT	Topotecan
ULVs	Unilamellar vesicles
UV	Ultraviolet
2D	Two-dimensional
3D	Threedimensional
β-CD	Beta-cyclodextrin
ζ-potential	Zeta potential

1.Introduction

Nanoscience and nanotechnology have become one of the most discussed and popular science in the last two decades. Investigation the changes of the physical and chemical properties of the materials in nanoscale can be refered as nanoscience. Nanotechnology is the production of new materials and devices using their nanoscale properties. The application of nanotechnology in medicine referred as nanomedicine. It is offering several exciting possibilities such as controlled drug/gene delivery, bioimaging for diagnostics, and targeted photothermal/chemothermal therapy. In this context, nanoparticles play a key role in nanomedicine with unique chemical, physical and optical properties that can be distinct from their bulk counterparts. Their composition and the properties can be exquisitely tailored to overcome some of the limitations found in conventional therapeutic and diagnostic agents due to poor bioavailability and instability. Thereby, nanoparticles can protect the loaded agents from biological degradation with improving their stability and bioavailability, assist co-localized release and improve therapeutic performance of the agents. A number of nanoparticle-based delivery systems have been already approved for cancer therapy in clinics and many others are under pre- and post-clinical trials [1].

Nanoparticles also offer multifunctionality by combining both therapeutic and diagnostic properties in one formulation and this combination is known as theranostics. These theranostic agents enable therapy, diagnosis, real time monitoring of the disease progression and treatment efficiency [2]. Theranostic agents are expected to accumulate in diseased sites. Thus, agent concentration is enhanced in target tissue while unwanted toxicity in the healthy tissue can be limited. This has been accomplished either *via* passive accumulation of the agent through the disorganized leaky vasculature or *via* active targeting by conjugating of the targeting ligands (e.g. antibodies, peptides, small molecules, or aptamers) on the nanoparticle surface [3]. Targeting ligands can be covalently or non-covalently attached to the nanoparticle surface. In covalent binding, the conjugation is performed through reactive functional groups on the nanoparticle surface. The main noncovalent attachment method is direct adsorption to the surface.

The use of multifunctional nanoparticles as a carrier for therapeutic and/or imaging agents can improve the pharmaceutical and pharmacological properties of commonly used compounds in diagnosis and treatment. Several materials including lipids, polymers, metals, and semiconductors have been used to formulate nanoparticles.

However, understanding of the events at the nano-bio interface, reproducible controlled synthesis and the fate of the nanoparticles in the cellular level could be some examples of limitations to overcome. In this regard, development of novel nanocarrier systems is essential to overcome these limitations and as well as physicological barriers.

Liposomes and polymeric nanoparticles are the most often used nanoparticles for this purpose. Since these compounds are biodegradable and don't accumulate in the body [4]. Besides, both hydrophilic and hydrophobic agents can be loaded at the same time. Liposomes are artificially prepared, self-assembled spherical vesicles composed of natural phospholipids. Their uni/multi-lamellar structure exhibit a flexible scaffold with high loading capacity, bioavailability and lack of immunogenicity. Polymeric nanoparticles made from natural or synthetic polymers would be prefered due to their stability and ease of surface modification [5]. Solid polymeric nanoparticles, polymeric micelles, dendrimers, polymersomes and polymer-lipid hybrids are mostly used polymer based drug delivery systems. The coating of hydrophilic polyethylene glycol (PEG) polymer to nanoparticle surface (PEGylation) has been used to reduce reticuloendothelial system (RES) uptake by shielding effect and increases circulating time [6]. Semiconductor quantum dots (QDs) with unique photophysical properties have become important fluorescent probes for *in vitro* and *in vivo* bioimaging research.

2. Aim and Scope

The development of novel multifunctional vehicles and investigation of their applicability in drug delivery and bioimaging are the objectives of this study. In the theoretical part, some of the commonly used nanostructures such as liposomes, polymeric nanoparticles, and quantum dots to improve therapeutic efficiency of the agents were summarized. Several parameters that should be considered in the design of "smart" nanoparticles were discussed in detail. Afterwards, the designed polymeric and liposomal delivery systems were addressed within the present thesis, respectively.

In the first study, the using potential of polymeric micelles in drug delivery was tested. The aim of using nanoparticles in drug delivery is to decrease normal tissue toxicity by improving specificity, and increase the stability and bioavailability of the agent by encapsulating into the nanoparticles. For this purpose, micelle surface was functionalized and enabled for conjugation of targeting moieties which enable accumulation in the target tissue. On the one hand, two peptides, Cys-TAT and RGD, were conjugated to each other and used to obtain effective targeting ligand with high penetration property. On the other hand, a fluorescent topoisomerase II inhibitor, doxorubicin (DOX), was encapsulated into the hydrophobic core of the micelles, and meanwhile enhanced the drug solubility. The cellular uptakes and cytotoxicities of the well characterized micelles with/without targeting ligands were investigated and the results were compared with free drug. Thus, the effects of active targeting on nanoparticle-cell interaction could be also evaluated.

In the second part, a theranostic nanoparticle-liposome hybrid, which integrates therapeutic function and diagnostic imaging into a single vehicle, was designed for co-delivery of the agents. Liposomes were synthesized by thin film hydration method. Hydrophobic quantum dot (QD) was incorporated into the lipid bilayer of the liposomes. Thereby, its biocompatibility was enhanced with keeping fluorescence property. A water soluble analog of camptothecin, topotecan (TPT) was encapsulated into the aqueous core of the liposomes *via* pH gradient method by keeping its pharmacologically active form. The cellular uptake and cytotoxicity studies of the detailed characterized liposomal formulations were carried out *in vitro* and the results were discussed. Thus, both hydrophilic anticancer drug TPT and hydrophobic QD were loaded into one vehicle.

3. Theoretical Background

This chapter is divided into two sub-chapters. First, chapter 3.1 provides general information about nanoparticles and surface engineering strategies for drug delivery and bioimaging. The second part presents a review article (chapter 3.2) summarizing the physical parameters of nanoparticles relevant for the construction of "smart" multifunctional nanoparticles as well as passive and active targeting.

3.1 Nanoparticles for drug delivery and bioimaging

With the rapid development in nanotechnology, using of nanomaterials has increased tremendously and has released a wide range of products. Among them, nanoparticle-based systems are utilized to deliver drugs, heat, light, or other substances to the specific cells and as well as to monitor alterations in the tissues. A number of nanoparticle-based formulations of chemotherapies have been approved by the authorities or are currently undergoing clinical trials for the effective treatment of the various cancers (see also the tables in Ref. [7]). Even though at a relatively its infancy stage, the field of multifunctional nanoparticles has shown great promise in the emerging medical fields such as multimodal imaging, theranostics, and image-guided therapies [8]. In this chapter, liposomes and polymeric nanoparticles with the ability to load multiple agents of different properties were elaborated below as carrier platform. Besides, quantum dots with unique optical properties were addressed as an imaging agent.

3.1.1 Liposomes

Liposomes are spherical vesicles having an aqueous core enclosed by one or more lipid bilayers or lamellae. They were discovered in the early 1960's by Dr. Alec D. Bangham [9-10]. Liposomes are mostly composed of phospholipids. Phospholipids are amphipathic molecules exhibiting a phospholipid has a hydrophilic headgroup, a glycerol backbone and two fatty acid chains (hydrophobic tails) (Figure 3.1a). In aqueous environments, the phospholipids tend to self-assemble into vesicles. They align themselves closely in planer bilayer membrane-like structures with the hydrophilic part (the polar head) in contact with the water phase, and the hydrophobic part (the apolar tail or hydrophobic chains) placed in the interior (Figure 3.1b) [11]. Hydrophilic interactions and hydrophobic effect lead to the formation of liposomes. Liposomes can be classified according to their size and number of bilayers (Figure 3.1c). Based on their number of bilayers, liposomes can be classified into three categories: (1) multi-vesicular vesicles

(MVVs 1.6-10.5 μm), (2) multilamellar vesicles (MLVs 0.1-15 μm) and (3) unilamellar vesicles (ULVs 25 nm-1.0 μm). Unilamellar vesicles can also be classified on the basis of their size into three categories: (1) small unilamellar vesicles (SUVs 25-50 nm) (2) large unilamellar vesicles (LUVs 100 nm-1.0 μm) and (3) giant unilamellar vesicles (GUVs larger than 1 μm) [12-13].
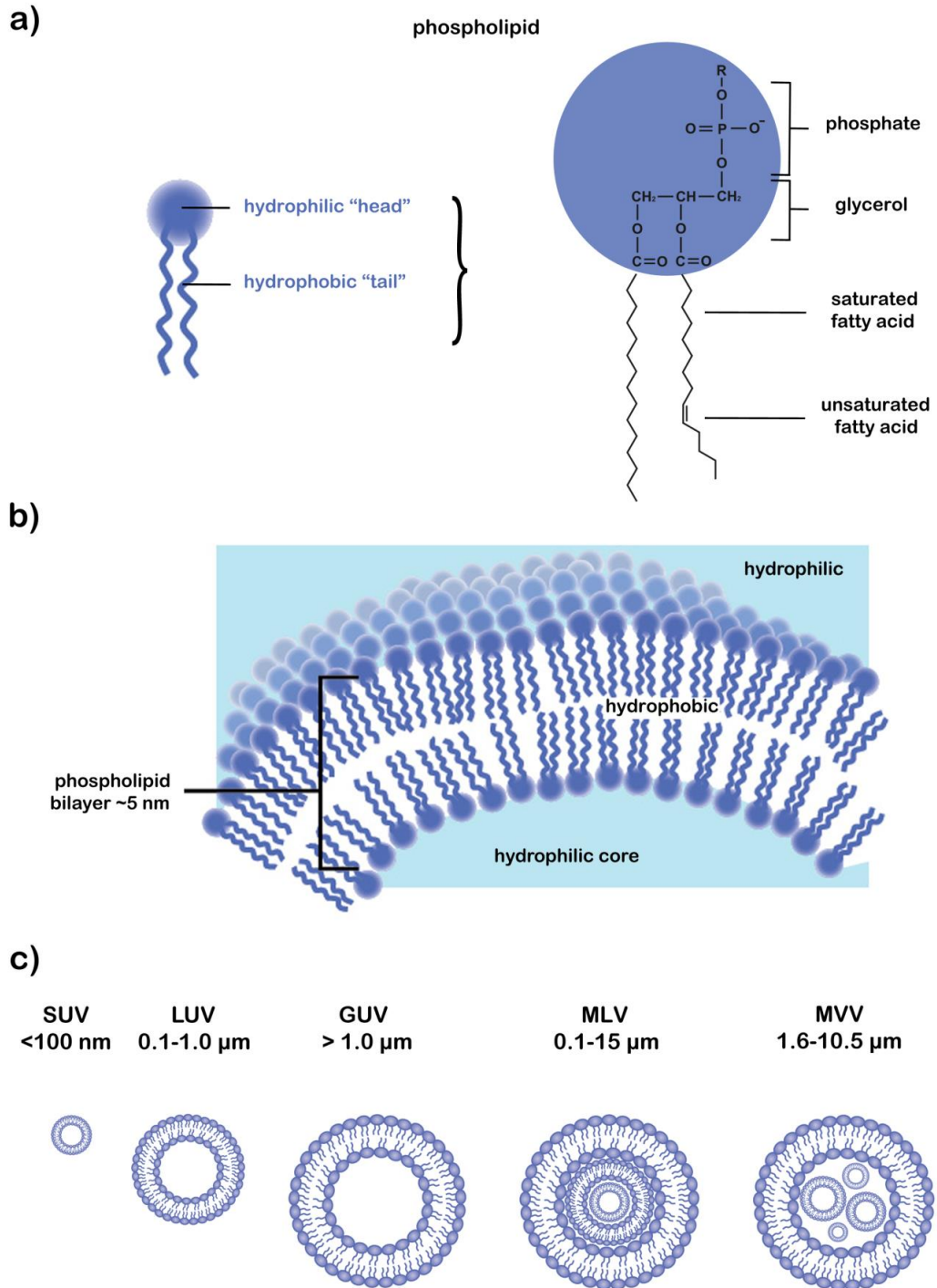
Figure 3.1 (a) The structure of a phospholipid, showing hydrophilic head and hydrophobic tail. (b) Phospholipid bilayer composed of hydrophilic polar head and hydrophobic non-polar tails.

(c) The common vesicle size and lamellarity classification system. Figure 3.1b modified from reference [14].

The relative fluidity and the mobility of each lipid molecule within the bilayer play key roles for the properties of the liposomes. The lipid bilayer has the tendency to allow some molecules to pass through it. This tendency is called as selective permeability. Small non-polar molecules move across the lipid- bilayer quickly, whereas large molecules and charged molecules cross the membrane slowly [15-16]. The degree of fatty acid saturation also affects the permeability of the lipid bilayers to the molecules. Temperature is another parameter that can affect the mobility of the lipids within the bilayer. The fluidity of the liposomal bilayer depends on the lipid phase transition temperature (Tc) and its ambient temperature. When the ambient temperature is increased and reaches Tc, the membrane passes from a solid gel phase, where the hydrocarbon chains are fully extended and closely packed, to a fluid liquid-crystal phase, where molecules have more freedom of movement [17]. The Tc varies depending on the length and nature (saturated or unsaturated) of the fatty acid chains. Thus, selection and combinations of lipids can control the fluidity of bilayers [18].

When the ambient temperature is below the Tc, phospholipids are in the gel phase and the bilayer presents low fluidity and permeability. At a temperature above the Tc, the phospholipids are in a fluid phase and the bilayer has high fluidity, but relatively low permeability. The lipid bilayer increases the permeability by several orders of magnitude when the temperature is equal to Tc. This phenomenon is attributed to the presence of highly permeable interfacial regions between coexisting gel (<Tc) and fluid (>Tc) bilayer domains [19].

Cholesterol is mostly integrated in the liposome preparation. Cholesterol molecule orients itself among the phospholipid molecules, with its hydroxyl group facing the water phase, the tricyclic ring sandwiched between the first few carbons of the fatty acyl chains, into the hydrocarbon core of the lipid bilayer [20]. The addition of cholesterol at a low concentration into the bilayer leads to an increase in the transmembrane permeability. The lipid bilayer becomes more fluid when compared with the pure phospholipids below the Tc (gel phase). Incorporation of higher amounts (>30 mol%) of cholesterol can eliminate phase transition and decrease the membrane permeability and fluidity at a temperature above the Tc (fluid phase) [21].
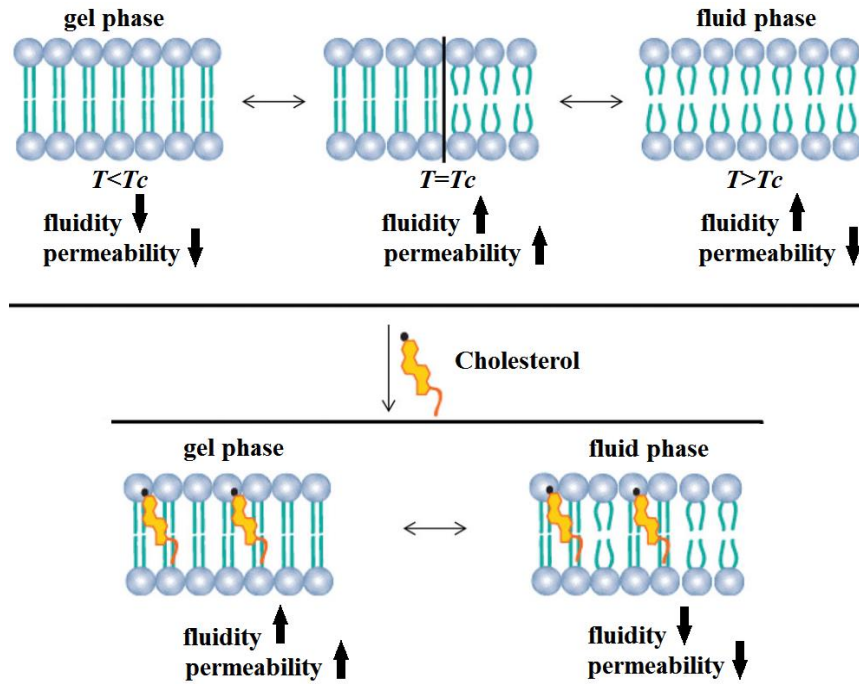
Figure 3.2 Effect of temperature and cholesterol on permeability of phospholipid bilayer. Cholesterol eliminates the transition phase of the lipid bilayer and increases the lipid bilayer permeability in the gel phase, while decreases permeability in the fluid phase. Modified from reference [13].

Cholesterol can also stabilize the membrane in the presence of biological fluids. Liposome without cholesterol interacts with plasma proteins such as albumin, transferrin, and macroglobulin. These proteins tend to extract tightly packed phospholipids from liposome, hence depleting the monolayer of the vesicles leadings to physical instability [22].

3.1.1.1 Preparation methods and size reduction techniques

Thin film hydration method

The thin-film hydration method is the most common and simple technique for preparation of MLV and it is the original method of Bangham [23]. It includes the use of organic solvents, mainly chloroform, ether or methanol, to dissolve or solubilize the lipids. A thin and homogeneous lipid film is formed when the organic solvent is evaporated by a rotary evaporation. Nitrogen gas is applied in order to completely remove the residual solvent. An aqueous buffer is added to the thin film lipids, allowing their hydration, at a temperature above the Tc of the lipid.

Solvent (ether or ethanol) injection technique

The solvent injection methods involve the dissolution of the lipid into an organic phase (ethanol or ether), followed by the injection of the lipid solution into aqueous media, forming liposomes [24]. When ethanol is injected, it dissolves in water and dilution of ethanol below a critical concentration forces the dissolved phospholipids to self-assemble in the aqueous phase and form SUVs. In contrast, on injecting an ether solution of phospholipids into warmed water (above the boiling point of the ether), SUV formation occurs after the evaporation of ether [25].

Reverse-phase evaporation

In this method, the lipids are firstly dissolved in organic solvents, then the solvent is removed under pressure by a rotary evaporation. The thin film is re-suspended in diethyl ether or isopropyl ether, followed by the addition of water. The preparation is then sonicated during a brief time period, forming a homogeneous emulsion. The organic solvents are removed by rotary evaporation, resulting in the formation of a viscous gel-like intermediate phase. This method is used for the preparation of LUV dispersion [26].

Sonication and extrusion

Sonication is a commonly used method for the reduction of liposomal size. MLVs can be sonicated either with a bath type sonicator or with a probe sonicator. The sonication method enables homogenous dispersion of small vesicles. The tip of a sonicator is directly immersed into the liposome dispersion and delivers high energy to the lipid suspension. The coupling of energy at the tip results in overheating; therefore, the vessel must be engrossed into an ice bath. Sonication tips tend to release titanium particles into the lipid suspension, which must be removed by centrifugation prior to use. The bath sonicators are the second types of instrumentation for preparation of SUV. Controlling the temperature of the lipid dispersion is easier with this method, in contrast to sonication by using the tip.

Extrusion is an easy and reproducible process, resulting in no detectable degradation of the phospholipids. Here, a suspension of heterogeneous size liposomes is passed through a polymer filter. Finally, liposomes of defined size and homogeneity can be produced by sequential extrusion of the usual multilamellar vesicles [27].

3.1.1.2 Characterization of liposomes

Characterization of the liposomes is of great importance in understanding their suitability for a range of applications. Rapid, reliable and quantitative characterization is an important consideration as part of the development and quality control processes.

Morphology and size

Microscopic techniques can provide information about the structures of liposomes. Cryo-transmission electron microscopy (cryo-TEM) and freeze-fracture TEM (FF-TEM), which keep a sample at cryogenic temperatures without staining, are the two most frequently used techniques for liposome analysis. Atomic force microscopy (AFM) is also a powerful tool to examine the morphology, dimensions and surface properties of liposomes with different compositions [28-29]. Furthermore, fluorescence microscopy and confocal fluorescence microscopy has been widely used in the analysis of fluorescently labeled liposomes [30].

The average size of liposomes is an important parameter, especially when the liposomes are designed for therapeutic use. Several techniques are available for assessing liposome size, which include microscopy techniques, size-exclusion chromatography (SEC), field-flow fractionation, and static or dynamic light scattering (DLS). DLS measures the time-dependent fluctuations in the intensity of scattered light, which occur because particles (liposomes) in a suspension undergo random Brownian motion due to collisions between suspended particles and solvent molecules. An analysis of the intensity fluctuations allows the determination of the distribution of the diffusion coefficients of the liposomes, which are converted into a size distribution using established theories. DLS is a simple and rapid method, but it provides an average property of liposome bulk. Nanoparticle tracking analysis (NTA) is another newly developed technology which tracks and measures nanoparticles moving under Brownian motion. Under microscopy, the moving paths of nanoparticles are recorded. According to the theory of Brownian motion, particle size exhibits a negative correlation with the diffusion rate, thus the size and size distribution can be obtained [31].

Surface charge

Generally, zeta potential measurement is used to determine the surface charge of liposomes by applying voltage across a pair of electrodes at either end of a measurement cell containing the particle dispersion. Charged particles are attracted to the oppositely

charged electrode. The particles move in an electrical field of known strength through the interference pattern of two laser beams and produce scattered light which depends on the speed of the particles [32].

3.1.1.3 Liposomes in drug delivery

Liposomes are appropriate drug-delivery vehicles due to their non-immunogenic, biocompatible and biodegradable nature. The liposomal structure allows to entrap both hydrophilic and hydrophobic drugs. The encapsulation of the active form of a drug into the lipid bilayer protects it against enzymatic degradation and immunological and chemical inactivation. Thus, liposomes increase the circulation lifetimes of a drug and prevent a drug from being metabolized prior to reaching target tissues. Furthermore, increased circulation lifetimes result in higher levels of passive accumulation at disease sites as compared to free drug. Moreover, coating of the liposome surface with polymers, such as PEG, which extends blood circulation time while reducing reticulo endothelial system uptake (stealth liposomes). Following the modification of terminal PEG molecule, stealth liposomes can be actively targeted with targeting moieties [33]. These advantages eventually enhance the targeting efficiency with a better therapeutic index. Liposomes are the first nano drug delivery systems with real time clinical applications. The milestone in liposome technology was the introduction of PEGylated liposome product, Doxil to the U.S. market in 1995 for the treatment of patients with ovarian cancer and AIDS-related Kaposi's sarcoma. Nowadays, various liposomal products are available in the market in diverse areas including the delivery of anti-cancer, anti-inflammatory, anti-fungal and anti-bacterial preparations [34].

Drug loading techniques

The methods by which drugs can be loaded into liposomes depend on the properties of the drugs and the lipids. There are two ways to encapsulate drugs into liposomes: passively, when the bioactive agent is encapsulated during the liposome formation; or actively, when the bioactive agent is encapsulated after liposome formation [35].
Payload (PL) and encapsulation efficiency (EE) are the terms used to determine the amount of drug entrapped into the liposomes. PL is the drug–lipid (mol mol^{-1}) ratio and EE is the PL in the final liposome formulation compared with the initial PL used for liposome preparation. When the amount of lipid is not quantified, the EE is used to

indicate the percentage of drug encapsulated in relation to the amount of drug offered for encapsulation during liposome preparation (EE%).

Hydrophilic drugs

During liposome preparation, hydrophilic drugs are dissolved in the external aqueous phase and become entrapped within the inner core of the liposome after solvent evaporation [36]. Thin-film hydration (passive loading) is the most commonly used method for the encapsulation of hydrophilic drugs. To improve the EE of hydrophilic drugs, some other methods, such as reverse-phase evaporation, dehydration–rehydration of empty liposomes and freeze–thaw cycling can also be used. The pH gradient technique (active loading) is another strategy to increase the EE of hydrophilic drugs into liposomes. This method includes two steps, the generation of the pH gradient with low intraliposomal pH and the subsequent loading of the drug. Haran *et al.* introduced an ammonium sulfate method for the generation of a pH gradient and the encapsulation of amphipathic weak bases [37]. In this technique, the pH of the interior part of the liposome is such that the unionized drug, which enters the liposome by passive loading, is ionized inside the liposome, and ionized drug molecules lose their ability to diffuse through the lipid membrane. Therefore, high concentration of the ionized drug is obtained inside the liposome [38].

Liposomes are generally prepared in a 300 mM solution of the ammonium sulfate salt with a pH of 5.5. By means of extraliposomal ammonium sulfate exchange to the pH 7.4 buffer, a pH gradient is generated. The higher concentration of ammonium in the aqueous phase causes the diffusion of the neutral ammonia molecules. For every ammonia molecule that leaves the liposome, one proton is left behind. Thus, a pH gradient is formed (Figure 3.3).
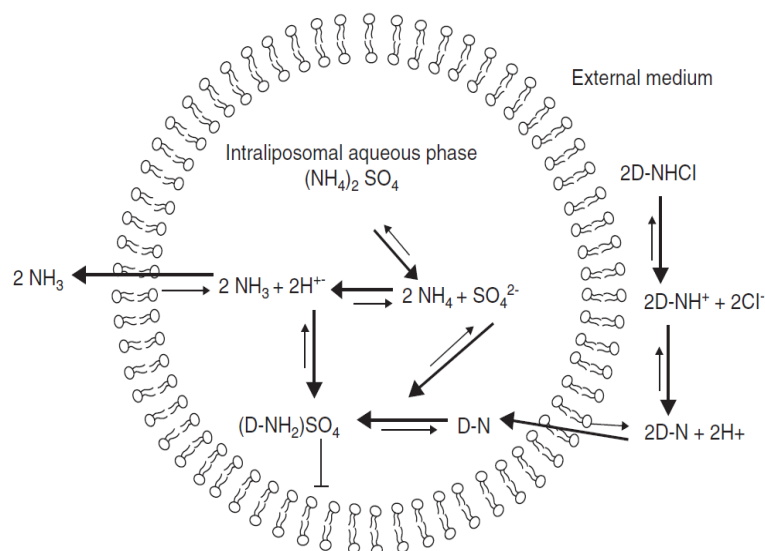
Figure 3.3 Schematic representation of the process occurring during drug loading in the case of the ammonium sulfate method. Reprinted from reference [39].

Lipophilic drugs

During the preparation of liposomes, hydrophobic drugs are solubilized in the organic solvent along with the phospholipids and the solvent is evaporated to form a thin-lipid film. After that, this mixture is rehydrated in the buffer and the free drug is separated from the liposome-associated drug. Once trapped, they remain in the liposome bilayer as they have a very low affinity towards the inner or outer aqueous regions of the liposomes. The interaction of lipophilic drug within the lipid bilayer depends on the amount and structure of the drug, which results in changes in the vesicle properties such as permeability, size, and stability of the bilayer [40]. Amphotericin B and paclitaxel are the most commonly investigated hydrophobic drugs in liposome formulations.

3.1.2 Polymeric nanoparticles

Polymeric nanoparticles (PNPs) are composed of synthetic polymers (poly-*e*-caprolactone, polyacrylamide, polyacrylate), natural polymers (chitosan, gelatin) and pseudosynthetic polymers (synthetic polypeptides) and have already been used for drug delivery [41]. Polymer chemistry allows the development of various polymeric nanoparticles that can be modified without the loss of their desired physical, chemical, and biological properties. Drugs can either be immobilized on the PNPs surface after a polymerization reaction or can be encapsulated in PNP structure during a polymerization step [42]. Polymers are able to ensure a sustained release of encapsulated drugs and to protect drugs from the body's degradation mechanisms. They can provide targeting

capabilities to drugs due to their tendency for passive accumulation in tumors. Furthermore, they enable to overcome the poor aqueous solubility of hydrophobic drugs [43].

3.1.2.1 Amphiphilic Block Copolymers

Amphiphilic block copolymers (ABCs) contain at least two blocks of different chemical nature. These blocks form phase separation due to chain association in solvents that selectively dissolve one of the blocks. This process results in the formation of core/shell structures, i.e., polymeric micelles [44]. Here, the hydrophobic blocks associate to form the core region and the hydrophilic blocks serve as an interface between the bulk aqueous phase. If the soluble block is predominant, the insoluble block aggregates to form spherical micelles. As the length of the soluble block decreases relatively to that of the insoluble block, cylindrical micelles or vesicles are formed [45]. Due to the presence of various types of block copolymer architectures (linear block copolymers, dendritic polymers, graft copolymers, starlike polymers, cyclic polymers), diverse morphologies of micelles are formed under specific conditions. The unique structure enables the use of polymeric micelles as a carrier for water-insoluble agents for pharmaceutical applications. Moreover, they stabilize the drug and enhance the pharmacokinetic properties of incorporated compounds. Hydrophobic drugs are loaded by using physical, chemical or electrostatic methods. The loading method is chosen according to the specific features of the core-forming block, as elaborated below.

Drug loading

There are five types of drug loading techniques for block copolymers, depending on their physicochemical properties (Figure 3.4). First one is direct dissolution of the amphiphilic copolymer and drug in water. This is an easy technique of preparing drug-loaded polymeric micelles. The copolymer and the drug self-assemble in water to form drug-loaded micelles. This technique can be combined with an increase in temperature to enhance drug loading [46]. The second category of drug-loading procedures is suitable for water-insoluble amphiphilic copolymers. Water-insoluble polymers and drugs need an organic solvent to solubilize. After dissolving, the organic solvent is removed by evaporation and a thin film of copolymer and drug is obtained. Drug-loaded polymeric micelles are obtained by dehydration of film with water. The third method is the dialysis technique. The drug and the polymer in an organic solvent are placed in the dialysis bag

and immersed into water. The replacement of organic solvent with water induces micelle formation. This technique is needed, when the core forming blocks are long and more hydrophobic. Another method is physical entrapment of a hydrophobic drug through an oil-in-water (O/W) emulsion process. Here organic solvents which are not able to mix with water are used. Last procedure is freeze drying. In this method, the polymer and the drug are dissolved in a water/tert-butanol mixture. After that, the mixture is subjected to freeze drying or lyophilization. Drug-loaded micelles are formed spontaneously upon reconstitution of the freeze-dried polymer–drug film in an injectable vehicle.
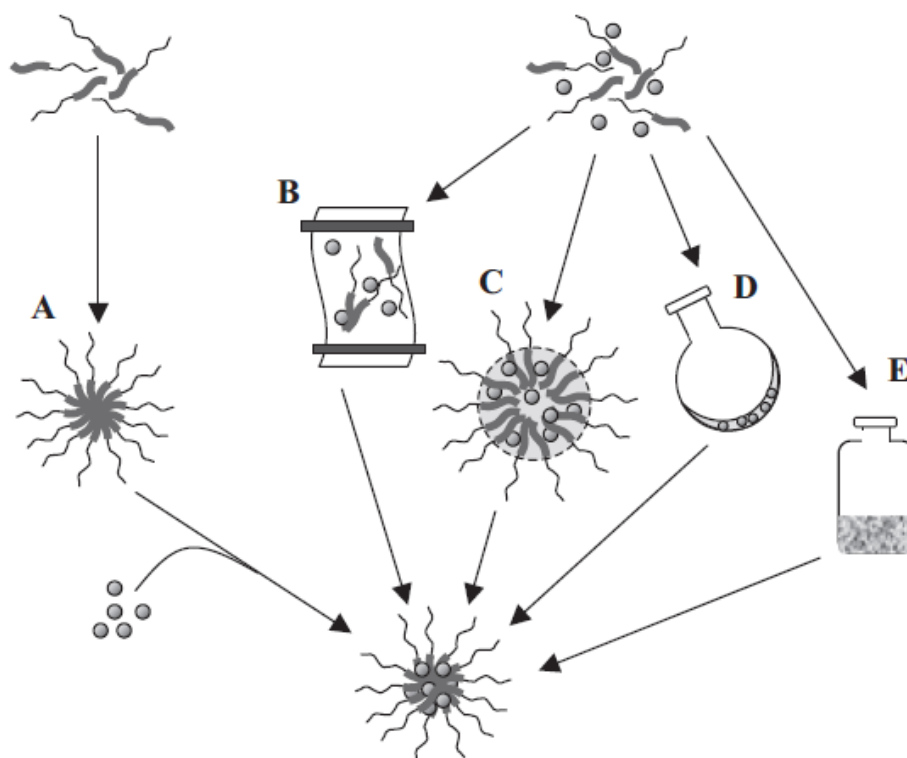
Figure 3.4 Drug-loading procedures for polymeric micelles: (A) direct solution, (B) dialysis, (C) O/W emulsion, (D) solvent evaporation, and (E) freeze-drying. Reprinted from reference [47].

3.1.3 Quantum dots

Quantum dots (QDs) are colloidal semiconductor nanocrystals with a size ranging from 2-10 nm. QDs exhibit many outstanding optical properties compared to conventional fluorophores, such as high quantum yields, broad absorption spectra, narrow and size-tunable emission, and strong resistance to photobleaching [48]. These properties make them very attractive for bioimaging applications. Traditional dyes require specific excitation wave lengths, whereas QDs can be excited over a wide range of wave lengths. Moreover, conventional dyes have a wide spectrum of emissions and this causes the overlay of large-area spectrums of different dyes. On the contrary, QDs have narrow

emission spectra that can be controlled through the variation of core size, composition and surface coatings. QDs can easily be designed to emit light at various wavelengths from ultraviolet (UV) to infrared (IR). Narrow emission and broad absorbance spectra make QDs suitable for multi-color imaging studies [49]. Photostability is a critical issue for most fluorescence applications, and QDs have a unique advantage in this field. While organic fluorophores quench when exposed to light for only a few minutes, QDs exhibit photostability with high brightness despite repeated excitation cycles [50]. In addition, due to the large surface area of QDs, they are easily modified with surface-conjugated biomolecules and proteins.

QDs have been successfully used for *in vitro* and *in vivo* imaging [51]. *In vitro* imaging is divided into three parts namely, cellular imaging, biomolecular tracking in cells and tissue staining. Cellular imaging is performed using fixed or live cells. After fixing cells, QDs can easily entry to the cells *via* chemically created pores. When live cells are labeled, the process must be performed sensitively to maintain cellular viability. As QDs enter inside the cytoplasm of cells, dispersion of the QDs depends on their surface coating and pH stability. Wu *et al.* linked QDs to immunoglobulin G (IgG) and streptavidin to label breast cancer marker human epidermal growth factor receptor 2 (HER2), actin and microtubule fibers, and nuclear antigens at different subcellular locations (Figure 3.5a). Their results showed that all labeling signals were specific for the targets and bright and photostable [50]. Biomolecule detection in cells is another issue, which has practical clinical importance. Especially, the presence and amount of tumor markers indicate the formation of tumor tissues and differentiation of tumor cells. Yezhelyev *et al.* used QDs for detection of five tumor biomarkers (nuclear hormone receptors (ER and PR), epidermal growth factor receptor (EGFR), the mechanistic target of rapamycin (mTOR), and HER2 in human breast cancer cells and on clinical tissue sections. QDs in different colors were conjugated with five antibodies. A mixture of five different kinds of QD-antibody conjugates was incubated with three different tissues. After staining, all three tissues showed different expression levels for the five targets (Figure 3.5b). They compared their results with traditional methods including immunohistochemistry, western blotting, and fluorescence in situ hybridization. A close correlation between the results was obtained. These outcomes proved that the QD-based technology is promising for the determination of tumor biomarkers *in vitro* [52]. Furthermore, Park *et al.* synthesized QDs-antibody conjugates specific for colon cancer markers of carcinoembryonic antigen (CEA), matrix metalloproteinase (MMP) 9, MMP

14 and IgG as a negative control for the specific detection of cancer in colonoscopy [53]. QDs-antibody probes were applied to human colon adenoma tissues. The staining results between carcinoma targeted-QDs probes and the IgG-QDs control probe were compared (Figure 3.5c). MMP9-QDs probe showed the lower signal intensity than that from the control IgG. However, MMP14-QDs and CEA-QDs probes showed significantly higher signals than that from the control IgG.
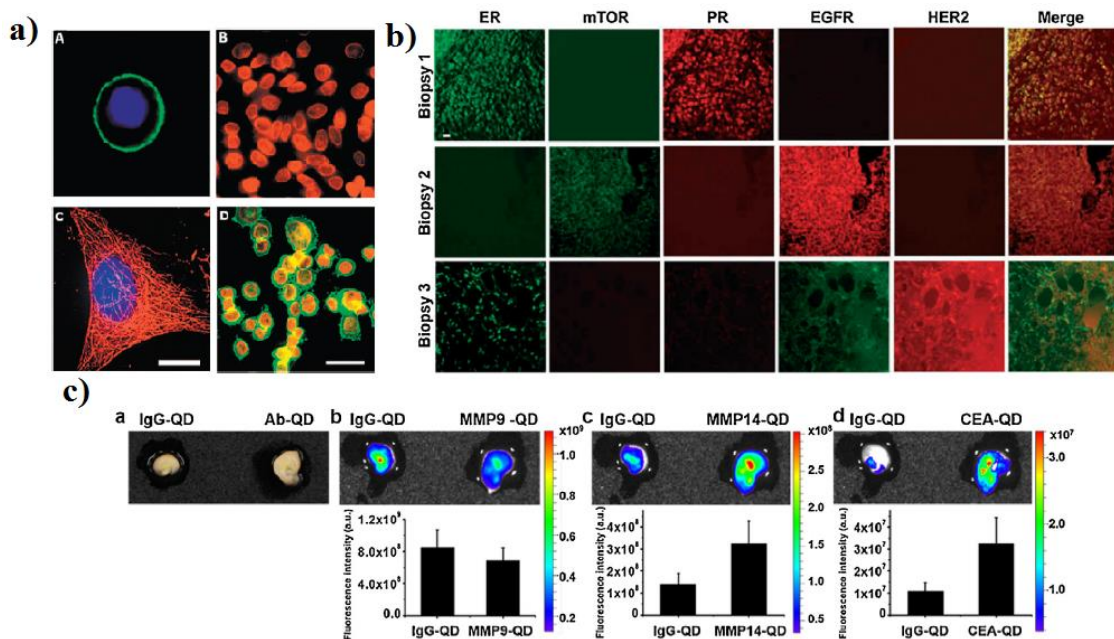
Figure 3.5 (a) Labeling of cell surface and intracellular targets with QD probes. In single-color examples membrane-associated HER2 receptors are detected with primary antibodies and QD-labeled secondary IgG (A, green), while intracellular nuclear antigens (B, red) and microtubules (C, red) are visualized with primary IgG/secondary IgG-biotin/QD-Streptavidin cascade. Both labeling routes can be applied simultaneously for a two-color staining (D). The nuclei are counterstained with Hoechst 33 342 (blue) in A and C. (b) Multiplexed molecular profiling of three tissue sections using QDs-Antibody conjugates against ER, mTOR, PR, EGFR and HER2 for direct staining. (c) (Top) (left panel) White light images and (right three panels) merged pseudocolor fluorescence images of a human colon adenoma stained with QDs-Antibody probes (right) of control QDs-IgG (left); and (bottom) average QDs fluorescence signal intensities from three human colon adenoma specimens. Modified from references [51-53].
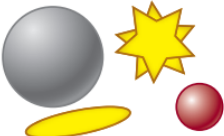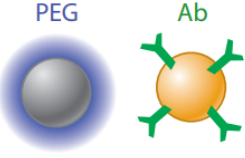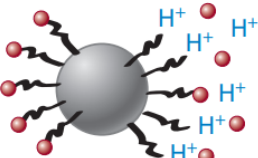
3.1.4 Surface engineering strategies

The prepared nanomaterials often need surface modifications such as ligand exchange and bioconjugation for various biosensor, bioanalytical, bioimaging, drug delivery, diagnostic and therapeutic applications. Surface modifications can help us to control the physicochemical, toxicological and pharmacological properties of nanomaterials. Furthermore, attachment of various reactive functional groups on the surface of nanomaterials allows to conjugate a wide range of contrast agents, antibodies, peptides,

ligands, drugs and genes, and construct multifunctional and hybrid nanomaterials for the bioimaging and treatment of the diseases [54].

Nanoparticles have evolved according to their responses in biological investigations. Three generations of nanoparticles have been developed for biomedical applications. The first generation nanomaterials have primary surface chemistries to possess biocompatibility. The surface chemistries are optimized to enhance stability and targeting properties with a high delivery performance for second generation nanomaterials. The third generation is "smart" nanoparticles that are environment-responsive and enable the targeted co-delivery of the bioactive agents (Figure 3.6).

Figure 3.6 The illustration highlights the interactions between the evolution of nanomaterial design and fundamental nano-bio studies. Abbreviations: Ab, antibody; EPR, enhanced permeation and retention; MPS, mononuclear phagocyte system; PEG, polyethylene glycol. Reprinted from reference [55].

Bioconjugation methods

Bioconjugation includes the attachment of one molecule to another, generally through a covalent bond, to create a complex [56]. Bioconjugation enables to produce different bioconjugates having unique features for a wide variety of industries such as medical, pharmaceutical, diagnostics, and material sciences. In general, four main functional groups, that are primary amines (-NH$_2$), carboxyls (-COOH), sulfhydryls (-SH) and carbonyls (-CHO), are frequently used in bioconjugation process for biological molecules [57].

Direct conjugation is one of the bioconjugation processes to create "intelligent" nanoparticular systems for biomedical applications. Nanoparticles with amine and aldehyde functional groups can directly be conjugated to fluorescent dyes or drugs. Amine functionalized nanoparticles react with fluorescence dyes, such as fluorescein isothiocyanate (FITC) (Figure 3.7A). For instance, Huang *et al.* conjugated primary amine group of chitosan nanoparticles to isothiocyanate group of FITC to investigate the cellular uptake mechanism of chitosan nanoparticles [58]. Morover, nanoparticles can directly be conjugated with drugs using the hydrazone bond between aldehyde and hydrazide group (Figure 3.7B). Prabaharan *et al.* synthesized folic acid conjugated amphiphilic hyperbranched block copolymer for tumor-targeted drug delivery. The doxorubicin hydrochloride (DOX) was conjugated to the hydrazide groups of the polymer by pH sensitive hydrazone linkage. The results showed that DOX released rapidly at acidic pH values such as those encountered in tumor tissue due to the hydrolysis of hydrazone bond [59].
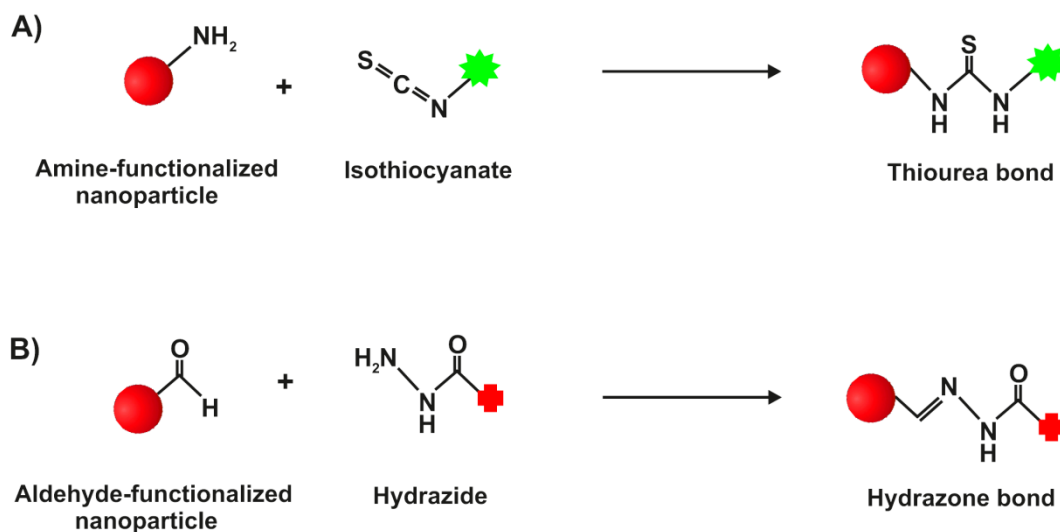
Figure 3.7 Schematic representation of direct conjugation reactions for amine-functionalized (A) and aldehyde-functionalized nanoparticles (B).

Cross-linkers

Using crosslinkers is the second process of creating bioconjugates. Crosslinkers provide appropriate reactive groups to link molecules together. Zero-length crosslinkers are the smallest available reagent systems for bioconjugation. These linkers mediate the conjugation of two molecules by forming a bond containing no additional atoms.

Carbodiimides are the most popular type of zero-length crosslinkers. They are used to facilitate the formation of amide linkages between carboxylates and amines. EDC, (1-

ethyl-3-(3-dimethylaminopropyl)carbodiimide hydrochloride), is one of the commonly used water soluble carbodiimides in protein conjugation. Its application in particle and surface conjugation procedures can be performed along with NHS (*N*-hydroxysuccinimide) or water soluble sulfo-NHS esters to improve reaction efficiency or stable intermediates (Figure 3.8A). CDI, (*N*,*N'*-carbonyldiimidazole), includes two acylimidazole leaving groups. In non-aqueous conditions, CDI reacts with the carboxylates of the molecule to form a reactive intermediate that is subsequently reacted with amines to form amide bonds.
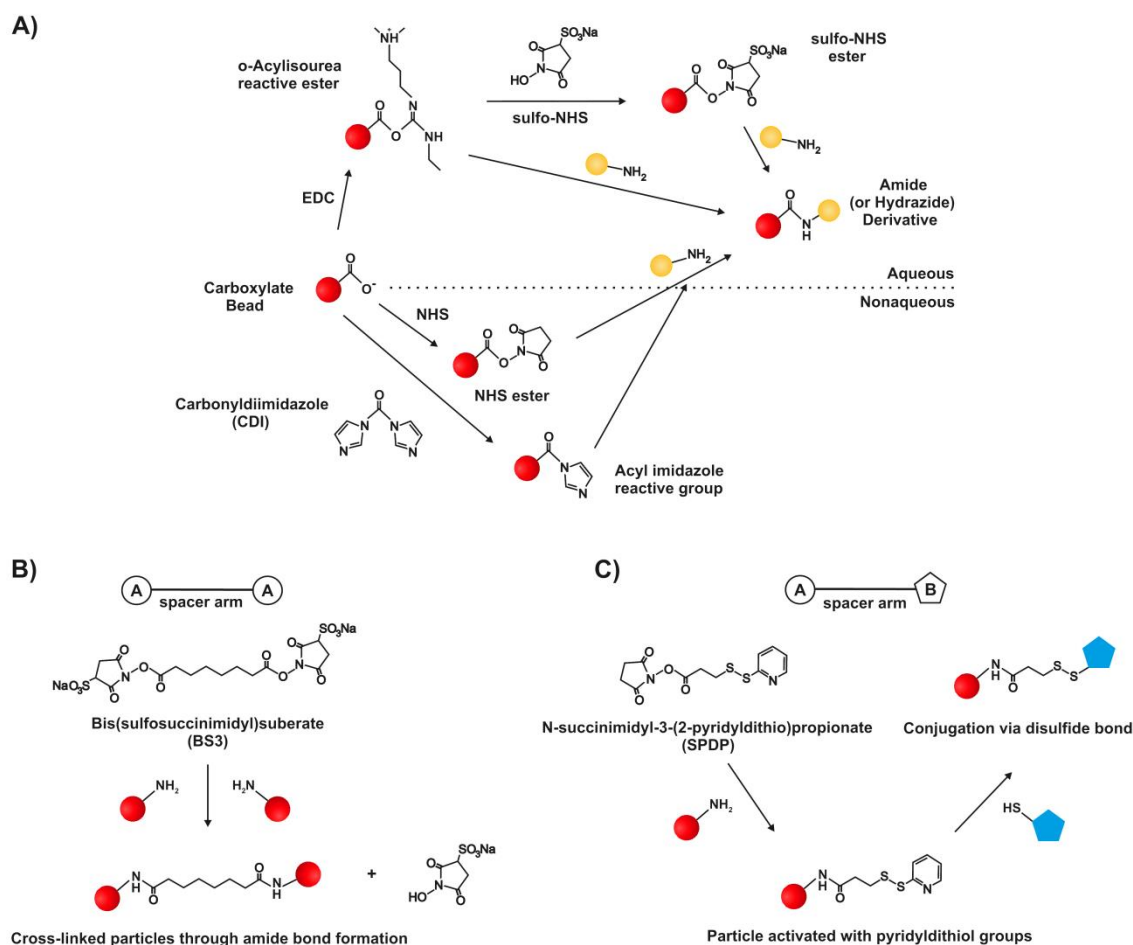
Figure 3.8 Reaction scheme of cross-linking strategies for bioconjugation towards therapeutics and imaging applications. (A) Carboxylate particles can be conjugated with amine-containing molecules through various reaction strategies. (B) Conjugation *via* amine-reactive homobifunctional crosslinker BS3. (C) Conjugation *via* amine-to-sulfhydryl heterobifunctional crosslinker SPDP**.**

The bifunctional crosslinkers can be divided into two groups dependent on similarity of the reactive groups: Homobifunctional crosslinkers and heterobifunctional crosslinkers. Homobifunctional crosslinkers are symmetrical in design with the two identical reactive ends and used in one step reactions. Bis(sulfosuccinimidyl)suberate (BS3) is one of the commonly used amine-to-amine, homobifunctional crosslinker (Figure 3.8B). It contains

amine-reactive sulfo-NHS esters at each end of a short spacer arm. The effect of the negative charges provided by the sulfonate groups lends water solubility to the compound. The sulfo-NHS esters react efficiently with primary amines at pH 7-9 to form stable amide bonds, along with the release of the *N*-hydroxysulfosuccinimide as leaving group.

Heterobifunctional crosslinkers contain two different reactive groups that allow more controlled two step sequential reactions. *N*-succinimidyl-3-(2-pyridyldithio)propionate (SPDP) and succinimidyl-4-(*N*-maleimidylmethyl)cyclohexane-1-carboxylate (SMCC) are the most favorite heterobifunctional crosslinking agents. SPDP is a short-chain crosslinker for amine-to-sulfhydryl conjugation *via* NHS-ester and pyridyldithiol reactive groups that form an amide linkage and cleavable disulfide bonds, respectively (Figure 3.8C). Besides, the reagent is also effective in creating free sulfhydryls on proteins and other molecules by using dithiothreitol (DTT) or tris-(2-carboxyethyl)phosphine (TCEP) to reduce [56]. SMCC is also an amine-to-sulfhydryl crosslinker, however, containing NHS ester and maleimide group at opposite ends. The NHS ester can react with primary amine groups on the protein and the maleimide group is specific for sulfhydryls in the pH range of 6.5-7.5.

3.1.5 References

1. T. Sun, Y. S. Zhang, B. Pang, D. C. Hyun, M. Yang and Y. Xia, "Engineered nanoparticles for drug delivery in cancer therapy," Angewandte Chemie International Edition, vol. 53, no. 46, pp. 12320-12364, 2014.

2. S. D. Jo, S. H. Ku, Y.-Y. Won, S. H. Kim and I. C. Kwon, "Targeted nanotheranostics for future personalized medicine: recent progress in cancer therapy," Theranostics, vol. 6, no. 9, pp. 1362, 2016.

3. X. Chen, Nanoplatform-based molecular imaging, John Wiley & Sons, 2011.

4. P. Sapra, P. Tyagi and T. M. Allen, "Ligand-targeted liposomes for cancer treatment," Current drug delivery, vol. 2, no. 4, pp. 369-381, 2005.

5. R. Herrero-Vanrell, A. Rincon, M. Alonso, V. Reboto, I. Molina-Martinez and J. Rodriguez-Cabello, "Self-assembled particles of an elastin-like polymer as vehicles for controlled drug release," Journal of controlled release, vol. 102, no. 1, pp. 113-122, 2005.

6. J. V. Jokerst, T. Lobovkina, R. N. Zare and S. S. Gambhir, "Nanoparticle PEGylation for imaging and therapy," Nanomedicine, vol. 6, no. 4, pp. 715-728, 2011.

7. M. S. Lee, E. C. Dees and A. Z. Wang, "Nanoparticle-delivered chemotherapy: Old drugs in new packages," ONCOLOGY (United States), vol. 31, no. 3, 2017.

8. G. Bao, S. Mitragotri and S. Tong, "Multifunctional nanoparticles for drug delivery and molecular imaging," Annual review of biomedical engineering, vol. 15, pp. 253-282, 2013.

9. A. D. Bangham, M. W. Hill and N. G. A. Miller, "Preparation and use of liposomes as models of biological membranes," in Methods in membrane biology, Ed., pp. 1-68, Springer, 1974.

10. A. D. Bangham and R. W. Horne, "Negative staining of phospholipids and their structural modification by surface-active agents as observed in the electron microscope," Journal of molecular biology, vol. 8, no. 5, pp. 660IN662-668IN610, 1964.

11. G. P. van Balen, G. Caron, G. Bouchard, M. Reist, P. A. Carrupt, R. Fruttero, A. Gasco and B. Testa, "Liposome/water lipophilicity: methods, information content, and pharmaceutical applications," Medicinal research reviews, vol. 24, no. 3, pp. 299-324, 2004.

12. D. van Swaay, "Microfluidic methods for forming liposomes," Lab on a Chip, vol. 13, no. 5, pp. 752-767, 2013.

13. N. Monteiro, A. Martins, R. L. Reis and N. M. Neves, "Liposomes in tissue engineering and regenerative medicine," Journal of the Royal Society Interface, vol. 11, no. 101, pp. 20140459, 2014.

14. http://lipolife.co.uk/what-is-a-liposome/, Lipolife, "What is a liposome?".

15. D. Papahadjopoulos, S. Nir and S. Ohki, "Permeability properties of phospholipid membranes: effect of cholesterol and temperature," Biochimica et Biophysica Acta (BBA)-Biomembranes, vol. 266, no. 3, pp. 561-583, 1972.

16. S. Freeman, Ed., Eds. Biological Science, Pearson, 4 edition 2011.

17. F. Frezard, "Liposomes: from biophysics to the design of peptide vaccines," Brazilian journal of medical and biological research, vol. 32, no. 2, pp. 181-189, 1999.

18. T. Lian and R. J. Y. Ho, "Trends and developments in liposome drug delivery systems," Journal of pharmaceutical sciences, vol. 90, no. 6, pp. 667-680, 2001.

19. J. H. Collier and P. B. Messersmith, "Phospholipid strategies in biomineralization and biomaterials research," Annual Review of Materials Research, vol. 31, no. 1, pp. 237-263, 2001.

20. S. Vemuri and C. T. Rhodes, "Preparation and characterization of liposomes as therapeutic delivery systems: a review," Pharmaceutica Acta Helvetiae, vol. 70, no. 2, pp. 95-111, 1995.

21. E. Corvera, O. G. Mouritsen, M. A. Singer and M. J. Zuckermann, "The permeability and the effect of acyl-chain length for phospholipid bilayers containing cholesterol: theory and experiment," Biochimica et Biophysica Acta (BBA)-Biomembranes, vol. 1107, no. 2, pp. 261-270, 1992.

22. B. Pradhan, N. Kumar, S. Saha and A. Roy, "Liposome: method of preparation, advantages, evaluation and its application," Journal of Applied Pharmaceutical Research (JOAPR), vol. 3, no. 3, pp. 1-8, 2015.

23. A. D. Bangham, "Liposomes: the Babraham connection," Chemistry and physics of lipids, vol. 64, no. 1-3, pp. 275-285, 1993.

24. S. Batzri and E. D. Korn, "Single bilayer liposomes prepared without sonication," Biochimica et Biophysica Acta (BBA)-Biomembranes, vol. 298, no. 4, pp. 1015-1019, 1973.

25. Y. P. Patil and S. Jadhav, "Novel methods for liposome preparation," Chemistry and physics of lipids, vol. 177, pp. 8-18, 2014.

26. F. Szoka and D. Papahadjopoulos, "Procedure for preparation of liposomes with large internal aqueous space and high capture by reverse-phase evaporation," Proceedings of the National Academy of Sciences, vol. 75, no. 9, pp. 4194-4198, 1978.

27. F. Olson, C. A. Hunt, F. C. Szoka, W. J. Vail and D. Papahadjopoulos, "Preparation of liposomes of defined size distribution by extrusion through polycarbonate membranes," Biochimica et Biophysica Acta (BBA)-Biomembranes, vol. 557, no. 1, pp. 9-23, 1979.

28. C. Chen, S. Zhu, T. Huang, S. Wang and X. Yan, "Analytical techniques for single-liposome characterization," Analytical Methods, vol. 5, no. 9, pp. 2150-2157, 2013.

29. B. Ruozi, D. Belletti, A. Tombesi, G. Tosi, L. Bondioli, F. Forni and M. A. Vandelli, "AFM, ESEM, TEM, and CLSM in liposomal characterization: a comparative study," International journal of nanomedicine, vol. 6, pp. 557-563, 2011.

30. B. Lohse, P.-Y. Bolinger and D. Stamou, "Encapsulation efficiency measured on single small unilamellar vesicles," Journal of the American Chemical Society, vol. 130, no. 44, pp. 14372-14373, 2008.

31. H. Saveyn, B. De Baets, O. Thas, P. Hole, J. Smith and P. Van Der Meeren, "Accurate particle size distribution determination by nanoparticle tracking analysis based on 2-D Brownian dynamics simulation," Journal of colloid and interface science, vol. 352, no. 2, pp. 593-600, 2010.

32. O. Popovska, "An overview: methods for preparation and characterization of liposomes as drug delivery systems," International Journal of Pharmaceutical and Phytopharmacological Research, vol. 3, no. 3, pp. 182-189, 2014.

33. L. Sercombe, T. Veerati, F. Moheimani, S. Y. Wu, A. K. Sood and S. Hua, "Advances and challenges of liposome assisted drug delivery," Frontiers in pharmacology, vol. 6, 2015.

34. U. Bulbake, S. Doppalapudi, N. Kommineni and W. Khan, "Liposomal Formulations in Clinical Use: An Updated Review," Pharmaceutics, vol. 9, no. 2, pp. 12, 2017.

35. A. Akbarzadeh, R. Rezaei-Sadabady, S. Davaran, S. W. Joo, N. Zarghami, Y. Hanifehpour, M. Samiei, M. Kouhi and K. Nejati-Koshki, "Liposome: classification, preparation, and applications," Nanoscale research letters, vol. 8, no. 1, pp. 102, 2013.

36. X. Xu, M. A. Khan and D. J. Burgess, "Predicting hydrophilic drug encapsulation inside unilamellar liposomes," International journal of pharmaceutics, vol. 423, no. 2, pp. 410-418, 2012.

37. G. Haran, R. Cohen, L. K. Bar and Y. Barenholz, "Transmembrane ammonium sulfate gradients in liposomes produce efficient and stable entrapment of amphipathic weak bases," Biochimica et Biophysica Acta (BBA)-Biomembranes, vol. 1151, no. 2, pp. 201-215, 1993.

38. M. Cagdas, A. D. Sezer and S. Bucak, "Liposomes as potential drug carrier systems for drug delivery," in Application of Nanotechnology in Drug Delivery, Ed., InTech, 2014.

39. J. Gubernator, "Active methods of drug loading into liposomes: recent strategies for stable drug entrapment and increased in vivo activity," Expert opinion on drug delivery, vol. 8, no. 5, pp. 565-580, 2011.

40. V.-A. Tsotas, S. Mourtas and S. G. Antimisiaris, "Dexamethasone incorporating liposomes: effect of lipid composition on drug trapping efficiency and vesicle stability," Drug delivery, vol. 14, no. 7, pp. 441-445, 2007.

41. S. Naahidi, M. Jafari, F. Edalat, K. Raymond, A. Khademhosseini and P. Chen, "Biocompatibility of engineered nanoparticles for drug delivery," Journal of controlled release, vol. 166, no. 2, pp. 182-194, 2013.

42. A. Z. Wilczewska, K. Niemirowicz, K. H. Markiewicz and H. Car, "Nanoparticles as drug delivery systems," Pharmacological reports, vol. 64, no. 5, pp. 1020-1037, 2012.

43. X. Li, Z. Yang, K. Yang, Y. Zhou, X. Chen, Y. Zhang, F. Wang, Y. Liu and L. Ren, "Self-assembled polymeric micellar nanoparticles as nanocarriers for poorly soluble anticancer drug ethaselen," Nanoscale research letters, vol. 4, no. 12, pp. 1502, 2009.

44. M. L. Adams, A. Lavasanifar and G. S. Kwon, "Amphiphilic block copolymers for drug delivery," Journal of pharmaceutical sciences, vol. 92, no. 7, pp. 1343-1355, 2003.

45. M. Karayianni and S. Pispas, "Self-Assembly of Amphiphilic Block Copolymers in Selective Solvents," in Fluorescence Studies of Polymer Containing Systems, Ed., pp. 27-63, Springer, 2016.

46. S. S. Kulthe, Y. M. Choudhari, N. N. Inamdar and V. Mourya, "Polymeric micelles: authoritative aspects for drug delivery," Designed Monomers and Polymers, vol. 15, no. 5, pp. 465-521, 2012.

47. V. Mourya, N. Inamdar, R. Nawale and S. Kulthe, "Polymeric micelles: general considerations and their applications," Ind. J. Pharm. Edu. Res, vol. 45, pp. 128-138, 2011.

48. J. Li and J.-J. Zhu, "Quantum dots for fluorescent biosensing and bio-imaging applications," Analyst, vol. 138, no. 9, pp. 2506-2515, 2013.

49. I. L. Medintz, H. T. Uyeda, E. R. Goldman and H. Mattoussi, "Quantum dot bioconjugates for imaging, labelling and sensing," Nature materials, vol. 4, no. 6, pp. 435-446, 2005.

50. X. Wu, H. Liu, J. Liu, K. N. Haley, J. A. Treadway, J. P. Larson, N. Ge, F. Peale and M. P. Bruchez, "Immunofluorescent labeling of cancer marker Her2 and other cellular targets with semiconductor quantum dots," Nature biotechnology, vol. 21, no. 1, pp. 41-46, 2003.

51. C. Wang, X. Gao and X. Su, "In vitro and in vivo imaging with quantum dots," Analytical and bioanalytical chemistry, vol. 397, no. 4, pp. 1397-1415, 2010.

52. M. V. Yezhelyev, A. Al-Hajj, C. Morris, A. I. Marcus, T. Liu, M. Lewis, C. Cohen, P. Zrazhevskiy, J. W. Simons and A. Rogatko, "In situ molecular profiling of breast cancer biomarkers with multicolor quantum dots," Advanced Materials, vol. 19, no. 20, pp. 3146-3151, 2007.

53. Y. Park, Y.-M. Ryu, Y. Jung, T. Wang, Y. Baek, Y. Yoon, S. M. Bae, J. Park, S. Hwang and J. Kim, "Spraying quantum dot conjugates in the colon of live animals enabled rapid and multiplex cancer diagnosis using endoscopy," ACS nano, vol. 8, no. 9, pp. 8896-8910, 2014.

54. V. Biju, "Chemical modifications and bioconjugate reactions of nanomaterials for sensing, imaging, drug delivery and therapy," Chemical Society Reviews, vol. 43, no. 3, pp. 744-764, 2014.

55. A. Albanese, P. S. Tang and W. C. Chan, "The effect of nanoparticle size, shape, and surface chemistry on biological systems," Annual review of biomedical engineering, vol. 14, pp. 1-16, 2012.

56. G. T. Hermanson, Bioconjugate techniques, Academic press, 2013.

57. https://www.thermofisher.com/, "Chemistry of Crosslinking, Overview of Crosslinker Structure and Chemistry

58. M. Huang, Z. Ma, E. Khor and L.-Y. Lim, "Uptake of FITC-chitosan nanoparticles by A549 cells," Pharmaceutical Research, vol. 19, no. 10, pp. 1488-1494, 2002.

59. M. Prabaharan, J. J. Grailer, S. Pilla, D. A. Steeber and S. Gong, "Amphiphilic multi-arm-block copolymer conjugated with doxorubicin via pH-sensitive hydrazone bond for tumor-targeted drug delivery," Biomaterials, vol. 30, no. 29, pp. 5757-5766, 2009.

3.2 Smart multifunctional nanoparticles in nanomedicine

This chapter corresponds to the review "Smart multifunctional nanoparticles in nanomedicine" by M. Seleci, D. Ag Seleci, R. Joncyzk, F. Stahl, C. Blume, T. Scheper first published in *BioNanoMaterials*, 2016, 17(1-2), 33-41. It was reproduced by permission of De Gruyter Publishing House.

3.2.1 Summary

Over the past two decades, nanotechnology has emerged new opportunities by using novel nanomaterials in nanomedicine. Nanomedicine can be defined as the application of nanotechnology to medicine. The undesirable side effects and risk of overdosing of drugs are the main challenges in conventional therapy, hence efficient drugs need to be established by using selective targeting. In this regard, nanomedicine formulations provide the improvement of the biodistribution and target site accumulation of systemically administered therapeutic agents. Many different types of nanomedicines have been evaluated over the years and the results of the studies evidenced that they improve the balance between the efficacy and the toxicity of drugs. Furthermore, using nanomedicines for diagnostics offers advantages due to their higher sensitivity and selectivity compared to classical methods.

This review article summarizes design, physical properties and applications of smart nanoparticles in nanomedicine. Brief information about nanotechnology, nanobiotechnology, and nanoparticles is presented in the introduction part. The generation of multifunctional nanoparticles from different material compositions with various properties and functionalities is discussed. In the second part, the physicochemical properties of nanoparticles (size, shape, and surface chemistry) and the effect of these properties on biological applications are evaluated. In addition, the available targeting ligands for targeted therapy, passive and active targeting of nanoparticles, as well as the effects of targeting on cellular uptake mechanisms are reviewed. The correlation between nanoparticle-based drug carrier design, and drug loading and release methods are clarified. Finally, it is concluded that smart multifunctional nanoparticles would be the most promising candidates for drug delivery in nanomedicine after identification of relevant targets and production of novel molecules.

3.2.2 Abstract

Recent advances in nanotechnology caused a growing interest using nanomaterials in medicine to solve a number of issues associated with therapeutic agents. The fabricated nanomaterials with unique physical and chemical properties have been investigated for both diagnostic and therapeutic applications. Therapeutic agents have been combined with the nanoparticles to minimize systemic toxicity, increase their solubility, prolong the circulation half-life, reduce their immunogenicity and improve their distribution. Multifunctional nanoparticles have shown great promise in targeted imaging and therapy. In this review, we summarized the physical parameters of nanoparticles for the construction of "smart" multifunctional nanoparticles and their various surface engineering strategies. Outlook and questions for the further researches were discussed.

3.1.2 Introduction

Nanotechnology and nanobiotechnology have gained much momentum in recent years. The term nanotechnology mostly refers to the fabrication of new materials with at least one dimension in a size range between 1 and 100 nanometres (nm), that is one billionth (or 10–9) of a meter. It is already used in a variety of products across various industries such as agriculture, cosmetics, electronics, textiles, recycling, energy, chemicals, as well as healthcare. Nanobiotechnology is defined by science's growing ability to work at the molecular level, atom by atom, combining biological materials and the rules of physics, chemistry, and genetics to fabricate synthetic structures such as biosensors, nanosized microchips and even tissue analogs for growing skin, bones, muscle, and other organs of the body [1, 2]. The development of a wide range of nanoscale technologies currently enables new scientific approaches in disease diagnosis, treatment, monitoring, and prevention. These technological innovations of nanotechnology within medicine are referred to as "nanomedicine" by the National Institutes of Health in USA [3].

Nanoparticles with ~100 nm have been widely used to improve the drug accumulation, internalization, and therapeutic efficacy. As shown in Figure 3.9, the physicochemical and biological properties of the nanoparticles can also be finely adjusted by tailoring their chemical properties, sizes, shapes, structures, morphologies, and surface properties [4]. The conjugation chemistry strategy of the drug molecule and surface modification is very important for drug delivery. Drug molecules may be adsorbed or attached covalently to the surface of nanocarrier. Besides, the interior core can also entrap drug molecules. The surface coating of nanocarriers with molecules, for instance, hydrophilic and/or

hydrophobic polymers [e.g. polyethylene glycol (PEG) and poly(ε-caprolactone) (PCL)] or surface modifications with targeting ligands such as antibodies, aptamers, peptides or small molecules determine the mechanism of uptake for the nanocarriers by the cells. Nanoparticles can be modified by active and passive targeting to enhance the concentration of the drug molecule inside the specific area. Once the drug loaded nanocarriers reach the diseased tissue, the therapeutic agent is released through changes in physiological environment such as temperature, pH, osmolarity, or *via* an enzymatic activity [5]. Delivering of a therapeutic compound to the target site is a major problem in the treatment of many diseases. A conventional application of drugs may have limited effectiveness, poor biodistribution and lack of selectivity [6]. It has been established that nanocarriers can become concentrated preferentially in tumors or at inflammatory sites, and this is due to antigen sampling by virtue of the enhanced permeability and retention (EPR) effect of the vasculature [7]. The current treatment options for most solid tumors are surgical intervention combined with chemotherapy or radiation therapy. However, today's therapy in its very general and systemic application form damages healthy tissues and causes unwarranted toxicity to the patient [8, 9]. In recent years, nanoparticle based delivery systems have been exploited in various medical applications. Their attractive features are that they are made from biocompatible, well-characterized and easily functionalized materials [10]. On the basis of these materials' properties, nanomaterials exhibit a highly differential targeting and uptake efficiency in a cell- or tissue-specific manner. Furthermore, the drug molecule on the nanocarrier is protected from harsh conditions before it can reach the target. In contrast to conventional drug delivery, using nanomaterials a prolonged and controlled drug release can be achieved [11, 12]. Thus, nanomedicine represents an innovative field with enormous potential for treatment by combination of smart nanoparticles with small molecules carrying a wide range of functions.

Liposomes, polymeric nanoparticles, dendrimers, metal nanoparticles, and quantum dots are versatile molecules with a variety of biomedical uses, such as diagnostic assays [13, 14], radiotherapy enhancement [15, 16], as well as drug and gene delivery [17, 18]. Liposomes are artificially prepared vesicles composed of lipid bilayers. They are biocompatible and their size can be varied in broad ranges (50–500 nm). Both hydrophobic and hydrophilic drugs can be encapsulated in the hydrophobic lipid bilayer and hydrophilic aqueous core, respectively [19]. An alternative approach to liposome is the use of niosomes which are composed mainly of non-ionic surfactants [20]. Polymeric

nanoparticles made of natural polymers (e.g. chitosan, collagen) and synthetic polymers [e.g. poly(lactide-coglycolide) (PLGA) and (PCL)] are colloidal solid platforms for the controlled and sustained release of drug molecules and gene delivery. Natural polymers are less toxic and more biodegradable than synthetic polymers. The majority of these compounds are synthesized through a spontaneous self-assembly process using block polymers of two or more polymeric chains with different hydrophilicity [21]. Dendrimers are synthesized from branched monomers by stepwise a repetitive reaction sequence and it is possible to control of their structural and chemical properties, including size, shape, and number of branches. Poly(amidoamine) (PAMAM) and poly-L-lysine are largely used dendrimers in drug and gene delivery. Low polydispersity and biocompatibility are the main problems using these nanoparticles as a tool in nanomedicine [22]. Semiconductor quantum dots are utilized as fluorescent probes for imaging and labeling of the molecules due to their unique photophysical characteristics such as broad excitation and tunable emission. Nevertheless, the main components of the quantum dots are hazardous heavy metals such as cadmium and selenium, which are highly toxic to living organisms. The heavy metal core can be coated with shell and a further surface coating can be carried out to make quantum dot more biocompatible [23]. Researchers are interested in studying tracking of these nanoparticles and to investigate their physical and biological properties for their cellular uptake and delivery.
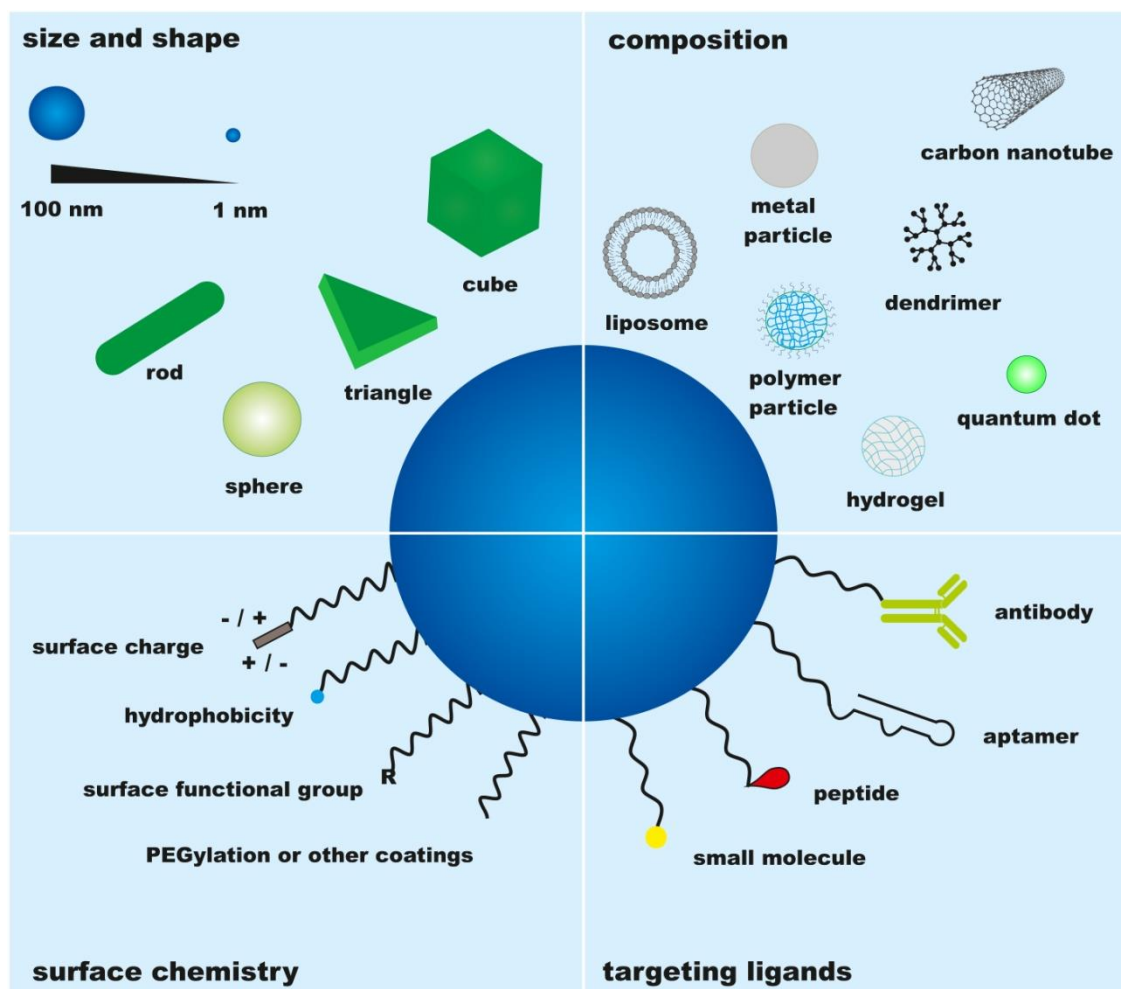
Figure 3.9 Design of nanoparticles for drug delivery. Multifunctional nanoparticles can be generated from the different materials composition with different properties and functionalities. Various strategies are used to combine therapeutic agents and imaging probes with the particles.

3.1.3 Physical properties and applications of nanoparticle based drug carriers

Size and shape

The physicochemical properties of nanoparticles, size, shape, and surface chemistry play a critical role in determining tissue penetration, cellular delivery, and therapeutic efficacy. Nanoparticles with varying size and shape are taken up to the cells at different rates. The cell membrane is composed of lipids, carbohydrates, and proteins that mediate cellular functions. The nanoparticle surface can interact with these molecules and may activate the cell's uptake mechanisms. Nanoparticle cell interactions can be remarkably different from that of small or large sized particles at nanoscale [24]. As nanoparticles with a smaller size have larger surface areas available to adhere and interact with cell membranes, the decrease of nanoparticle size may lead to an increase in mobility and interaction with cell membranes, which can result in enhanced cellular uptake of

nanoparticles [25]. Besides, because of their small size, nanoparticles are often not recognized as a foreign agent by macrophages and consequently do not enter macrophages through membrane pores to be led to the digestion apparatus for such microparticles, the reticuloendothelial system [26]. Donkor and Tang showed that the cellular and nuclear internalization of 30 nm sized single-walled carbon nanotubes (SWCNT) was higher than 50 nm SWCNT [27]. In a subsequent study, Jiang *et al.* reported that relatively small sizes of 2, 4 and 6 nm core gold nanoparticles (AuNP) were sufficient to induce dramatic changes in nanoparticle internalization efficiency and mechanism [28]. The shape of nanoparticles also plays a direct role for their function in biological systems [29]. Li and coworkers investigated the influence of nanoparticle shape on the cellular uptake. To clarify its on cellular uptake of the nanoparticles, sphere, rod, cube, and disk shaped polymer coated nanoparticles were compared. Based on a detailed free energy analysis, the effect of the nanoparticle shape was found to be mainly induced by the different membrane bending energies during endocytosis. The spherical nanoparticles needed to overcome a minimal membrane bending energy barrier, compared with non-spherical particles. The spherical nanoparticles thus demonstrated the fastest internalization rate, followed by cubic-, then rod and disk-like nanoparticles [30]. Even though nanoparticles show a certain size and shape after synthesis, they might induce aggregation into larger clumps during the *in vitro* and *in vivo* applications. The formation of these aggregates complicates the interpretation of the results [31]. Besides, although both size and shape are essential features, surface charge and functionality are also significant for the interaction of nanoparticles with the physiological system.

Surface chemistry

In addition to their size and shape, the surface chemistry of nanoparticles is an important factor for their interaction with the biological environment. Nanoparticles should ideally have a hydrophilic surface to escape macrophage capture [32]. Generally, that can be achieved by coating the surface of nanoparticles with a hydrophilic polymer such as PEG, which has favorable inherent physicochemical properties and is biocompatible (e.g. it possesses high flexibility, but a low toxicity and immunogenicity). For this purpose, nanoparticles can also be fabricated from block copolymers with hydrophilic and hydrophobic parts [33, 34]. A surface modification of nanoparticles with PEG was found to reduce nanoparticle accumulation in off-target organs such as liver and spleen. PEG-coated nanoparticles have a high solubility in a number of solvents and exhibit a reduced

adsorption of blood proteins, leading to prolonged circulation half-life compared to non-PEGylated nanoparticles [35–37]. In this way, it reduces the aggregation. PEG chains can be functionalized with alcohols, carboxylic acids amines and thiols to conjugate small molecules or targeting ligands. Yoon *et al.* demonstrated that tumor-targeting ability of hyaluronic acid nanoparticles (HANPs) could be optimized by chemical conjugation of amine-functionalized PEG, which might help escaping the unintended accumulation in the liver [38]. The charge of nanoparticle's surface is commonly characterized using the zeta potential, which variably reflects the electrostatic potential of particles and is influenced by the composition of the particles as well as by the medium in which the nanoparticles are suspended [3]. Particles with a zeta potential more positive than +30 mV or more negative than −30 mV are normally considered to be physically stable [39, 40]. The negative membrane of cells interacts differently with positively/negatively charged nanoparticles, whereby positively charged nanoparticles are generally known to be more easily internalized than neutral and negatively charged nanoparticles [41, 42]. Remarkably, some nanoparticles such as polymeric nanocomplexes and AuNP, which have the same size range, but different surface charges yielded marked discrepancies in both distribution and uptake efficiency. The particles also showed different levels of toxicity depending on their surface charges [43–46].

Targeting ligands

Nanoparticle surfaces are often bioconjugated with small molecules and/or targeting ligands to enable both *in vitro* and *in vivo* cell specific targeting [47]. Proteins and peptides, carbohydrates, vitamins, aptamers, antibodies, and antibody fragments are the mostly used molecules that bind specifically to an overexpressed target on the cell surface [48]. Immunogenicity, stability, and difficulties in site-specific conjugations with nanoparticles are the major obstacles in targeting ligands. Monoclonal antibodies (mAbs) are widely preferred targeting ligands because of their availability to research and their high affinity and specificity for molecular targets [49, 50]. Several mAbs have been used in clinics for cancer therapy, such as bevacizumab (against colorectal cancer) and trastuzumab (against breast cancer) [51]. However, they are large, complex molecules and may cause immunogenicity. Aptamers are small synthetic nucleic acid oligomers that can bind to targets with high sensitivity and high specificity. Aptamers are selected through an *in vitro* process called the systematic evolution of ligands by exponential enrichment (SELEX) to be most specific for a particular target [52]. They have potential

advantages as targeting ligands. Aptamers can be synthesized with a specific functional moiety, such as a carboxylate, amino or sulfhydryl at only one end of the nucleic acid sequence of the aptamer. They are small in size and non-immunogenic [50, 53]. Peptides are an attractive alternative as targeting molecule due to several advantages, including a smaller size, a lower immunogenicity, a higher tissue penetration capability, a higher stability and a relatively easy production process. Phage-displayed peptide libraries are a valuable screening resource for identification of the peptides that target a specific receptor [54, 55]. The most widely used peptide in targeted delivery is the integrin targeted arginine-glycine- aspartic acid (RGD) peptide. This peptide has been extensively studied by combining various nanoparticles [56]. A promising approach for overcoming the barrier of the cell membrane in drug delivery are cell penetrating peptides (CPPs). Arginine rich CPPs such as transactivator of transcription (TAT), penetratin and polyarginine are often used for intracellular delivery of the cargo conjugates [57]. It has been hypothesized that the positively charged CPPs provide a strong electrostatic interaction with anionic species presented at the extracellular surface of cell membranes, including lipid head groups, proteins such as nucleolin, and proteoglycans like heparin sulfate [58, 59].

Passive and active targeting

Targeting of the nanoparticles is performed *via* two different strategies: passive and active targeting, as schematically shown in Figure 3.10. Nanoparticles can enhance the intracellular concentration of the drugs in cancer cells while avoiding unwarranted toxicity towards healthy cells. Malignant tumors release angiogenic growth factor proteins that stimulate new blood vessels or demand rerouting of existing vessels to supply them oxygen and nutrients [61, 62]. Tumor tissue is characterized by highly disorganized vascular architecture, irregular blood flow, reduced lymphatic drainage, and vessels are leaky [63, 64]. Because of the reduced lymphatic drainage, the permeating nanocarriers are not removed efficiently and thus are retained in the tumor tissue [65]. These features provide an EPR effect, which constitutes an important mechanism for the passive targeting and the selective accumulation of nanoparticles in the tumor and also in its surrounding tissue [66]. Gabizon *et al.* showed that a PEGylated liposomal doxorubicin (Dox) formulation had a long circulation time in plasma, enhanced accumulation in murine tumors and a high therapeutic activity over free (unencapsulated) Dox [67]. The objective of the active targeting strategy is to overcome

specificity limitations of drug conjugate by using targeting moieties. Nanoparticles are typically conjugated with targeting ligands that were described in the previous section, thereby allowing preferential accumulation of the drug within selected tissues or intracellular organelles [68]. Fabricated nanoparticles may enter the cells *via* different endocytic pathways such as receptor-mediated endocytosis depending on their size, shape, and surface properties (Figure 3.11).
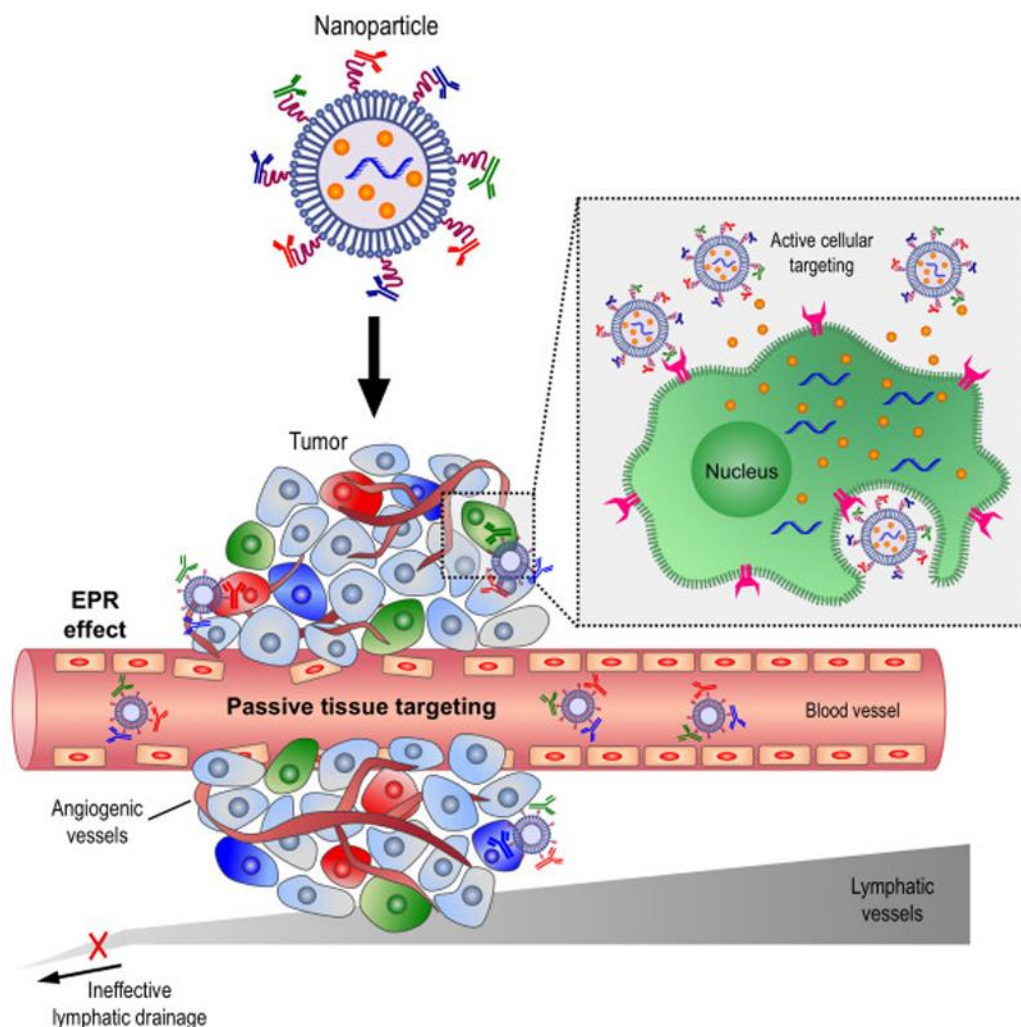
Figure 3.10 Active and passive targeting of drug loaded nanoparticles. (Reprinted with permission from Ref. [60], Copyright 2014 BioMed Central.)

Drug loading and release

High drug loading capacity is essential for a successful drug delivery system. The surface chemistry of the nanoparticles and the properties of the drug as well as some environmental factors such as release conditions have a strong influence on both drug loading and release. The loading of drug molecules into the nanoparticles can be performed by two methods. Within the incorporation method, the drug should be

incorporated at the time of nanoparticle formation. In the adsorption/absorption method, the nanocarrier should be incubated with the concentrated drug solution [69]. Drug loading and entrapment efficiency are determined by the properties of the drug and the carrier molecule. Biomolecules, drugs or proteins show the greatest loading efficiency when they are loaded at or near their isoelectric point (pI), comprising a minimal solubility and a maximal absorption. Prior studies showed, that the use of ionic interactions between the drug and the matrix material can be an effective way to increase drug loading for small molecules [70, 71]. Summarizing, while designing a nanoparticle based drug delivery system, subsequent biodegradation, and drug release should be considered. Loading the drug molecules inside or on the surface of nanoparticle carrier allows controlled release of the drug. This method bears many advantages such as improving biodistribution, reducing unwarranted side toxicity for healthy tissue and protecting the drug from physiological degradation compared to conventional free drugs administration [49]. Desorption of the drugs, drug diffusion from the nanoparticle matrix, matrix erosion or degradation of nanoparticles determine the release rate of the drug [3, 69].
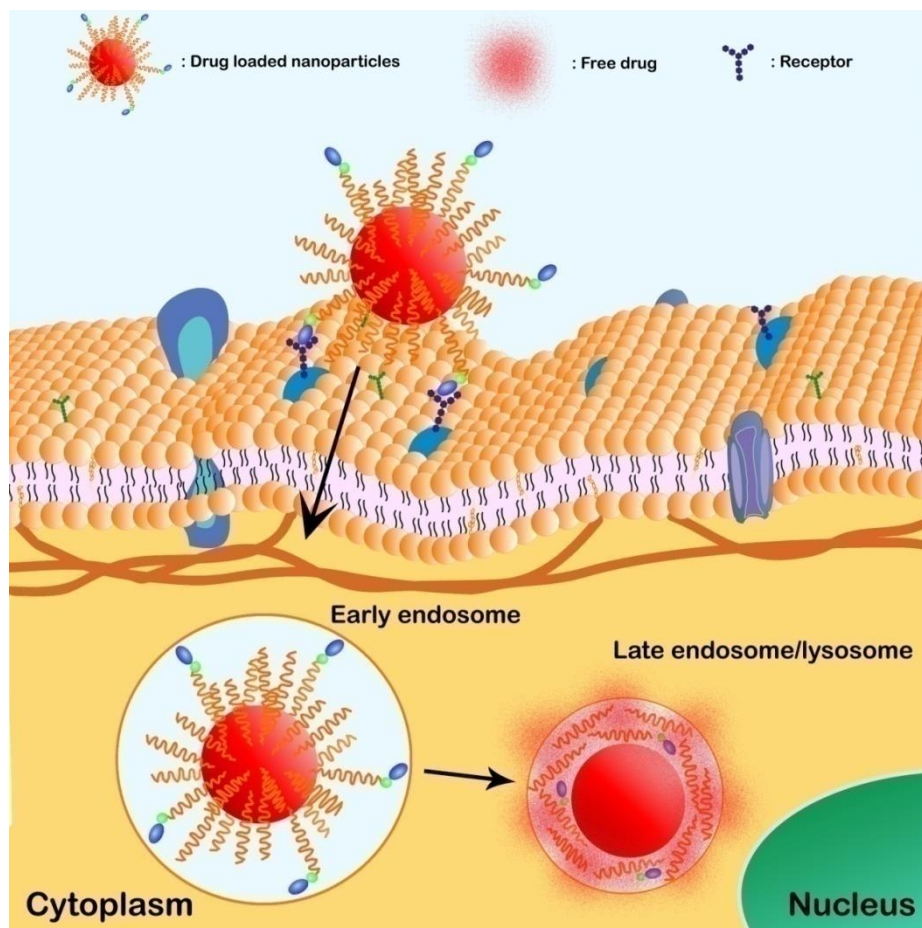
Figure 3.11 Schematic representation of the cytosolic delivery of drug loaded nanoparticles *via* receptor mediated endocytosis. The nanoparticles are engulfed in a vesicle, called early endosome after receptor mediated cell association with nanoparticles. Endosomal escape of the nanoparticles leads to the cytosolic release of the encapsulated drug molecule. (Modified reproduction with permission from Ref. [56], copyright 2015 American Chemical Society.)

3.1.4 Conclusions

Utilization of nanoparticles as drug carriers offer promising improvements in drug delivery. The loading of drug molecules into or on top of the nanocarriers can improve the pharmacokinetic properties of the drug and can protect the drug against early degradation enabling targeted and controlled drug release. Thus, accumulation of the drugs in targeted size can be increased and in this way occurrence of undesired drug effects can be prevented in healthy tissues. Furthermore, multifunctional nanoparticles with simultaneously useful capabilities such as targeting and imaging contrast enhancement can be synthesized. These nanoparticles combine both diagnostic and therapeutic features within a single formulation and therefore are denoted as "theranostic" agents [72–74]. Despite the fact that there are several nanoparticle based drug delivery systems, being developed or being currently under preclinical and/or

clinical evaluation, still only a few such nano-drugs are in use on the market [75]. This is due to the fact that some problems in clinical usage encountered such as low drug loading capacity and a low circulation half-life, leading to low release and diagnostic features. Furthermore, the still relatively low physical stability and scale up problems bring along limitations for therapeutic applications of nanoparticle based drug delivery systems. Besides, the studies show that ultrafine particles (UFPs; diameter <100 nm) are more toxic and induce more severe inflammation than larger particles in their effects [76]. Within the field of nanotoxicology, safe nanomaterials will be designed and new methods and techniques for analyzing these nanostructures in *in vitro* test platforms will be developed. The greater part of the fabricated drug delivery systems work well *in vitro*, however many systems fail in *in vivo* testing because of excessive accumulation and toxicity in the kidneys and liver [77]. In the last decade, threedimensional (3D) cell culture systems have drawn great attention because they often offer levels of cell differentiation and tissue organization not observed in conventional two-dimensional (2D) culture systems [78]. In recent years "organ-on-a-chip" systems are useful as an *in vitro* approach to test drugs and nanoparticles by mimicking the specific physiological environment found in certain organs. But both these technologies are relatively new and require further validation to predict clinical responses in human.

Consequently, smart multifunctional nanoparticles will be the most promising candidates as drug carriers in nanomedicine after identification of relevant targets and production of novel molecules. This molecules will enable the development of personalized drug delivery systems by improving the life quality and duration of the patients.

3.1.5 Acknowledgments

3.1.6 References

1. McNeil SE. Nanotechnology for the biologist. J Leukoc Biol. 2005;78:585–94.

2. Fortina P, Kricka LJ, Surrey S, Grodzinski P. Nanobiotechnology: the promise and reality of new approaches to molecular recognition. Trends Biotechnol. 2005;23:168–73.

3. Singh R, Lillard JJ. Nanoparticle-based targeted drug delivery. Exp Mol Pathol. 2009;86:215–23.

4. Xia Y. Are we entering the nano era? Angew Chem Int Edit. 2014;53:12268–71.

5. Panzarini E, Inguscio V, Tenuzzo BA, Carata E, Dini L. Nanomaterials and autophagy: new insights in cancer treatment. Cancers. 2013;5:296–319.

6. Nevozhay D, Kanska U, Budzynska R, Boratynski J. Current status of research on conjugates and related drug delivery systems in the treatment of cancer and other diseases. Postepy Hig Med Dosw. 2007;61:350–60.

7. Ge H, Hu Y, Jiang X, Cheng D, Yuan Y, Bi H, et al. Preparation, characterization, and drug release behaviors of drug nimodipine- loaded poly (epsilon-caprolactone)-poly(ethylene oxide)-poly(epsilon-caprolactone) amphiphilic triblock copolymer micelles. J Pharm Sci. 2002;91:1463–73.

8. Sunderland CJ, Steiert M, Talmadge JE, Derfus AM, Barry SE. Targeted nanoparticles for detecting and treating cancer. Drug Dev Res. 2006;67:70–93.

9. Orive G, Gascon AR, Hernandez RM, Dominguez-Gil A, Pedraz JL. Techniques: new approaches to the delivery of biopharmaceuticals. Trends Pharm Sci. 2004;25:382–7.

10. Tiwari A, Patra HK, Choi J-W, editors. Advanced theranostic materials. Beverly: Wiley-Scrivener Publishing, 2015.

11. Farokhzad OC, Langer R. Impact of nanotechnology on drug delivery. ACS Nano. 2009;3:16–20.

12. Ai J, Biazar E, Jafarpour M, Montazeri M, Majdi A, Aminifard S, et al. Nanotoxicology and nanoparticle safety in biomedical designs. Int J Nanomedicine. 2011;6:1117–27.

13. Qiu X, Hildebrandt N. Rapid and multiplexed microRNA diagnostic assay using quantum dot-based Förster resonance energy transfer. ACS Nano. 2015;9:8449–57.

14. Donolato M, Antunes P, Bejhed RS, Zardan Gomez de la Torre T, Osterberg FW, Strömberg M, et al. Novel readout method for molecular diagnostic assays based on optical measurements of magnetic nanobead dynamics. Anal Chem. 2015;87:10613–8.

15. Kim K, Oh KS, Park DY, Lee JY, Lee BS, Kim IS, et al. Doxorubicin/gold-loaded core/shell nanoparticles for combination therapy to treat cancer through the enhanced tumor targeting. J Control Release 2016;228:141–9.

16. Cifter G, Chin J, Cifter F, Altundal Y, Sinha N, Sajo E, et al. Targeted radiotherapy enhancement during electronic brachytherapy of accelerated partial breast irradiation (APBI) using controlled release of gold nanoparticles. Phys Med. 2015;31:1070–4.

17. Hwang AA, Lu J, Tamanoi F, Zink JI. Functional nanovalves on protein-coated nanoparticles for in vitro and in vivo controlled drug delivery. Small. 2015;11:319–28.

18. Look J, Wilhelm N, von Briesen H, Noske N, Günther C, Langer K, et al. Ligand-modified human serum albumin nanoparticles for enhanced gene delivery. Mol Pharm. 2015;12:3202–13.

19. Suzuki R, Omata D, Oda Y, Unga J, Negishi Y, Maruyama K. Cancer therapy with nanotechnology-based drug delivery systems: applications and challenges of liposome technologies for advanced cancer therapy. In: Lu Z-R, Sakuma S, editors. Nanomaterials in Pharmacology. New York: Springer Science + Business Media, 2016:457–82.

20. Moghassemi S, Hadjizadeh A. Nano-niosomes as nanoscale drug delivery systems: an illustrated review. J Control Release. 2014;185:22–36.

21. Wang AZ, Langer R, Farokhzad OC. Nanoparticle delivery of cancer drugs. Annu Rev Med. 2012;63:185–98.

22. Parat A, Bordeianu C, Dib H, Garofalo A, Walter A, Begin-Colin S, et al. Dendrimer–nanoparticle conjugates in nanomedicine. Nanomedicine (Lond). 2015;10:977–92.

23. Al-Ali A, Singh N, Manshian B, Wilkinson T, Wills J, Jenkins GJ, et al. Quantum dot induced cellular perturbations involving varying toxicity pathways. Toxicol Res. 2015;4:623.

24. Nel AE, Maedler L, Velegol D, Xia T, Hoek EM, Somasundaran P, et al. Understanding biophysicochemical interactions at the nano–bio interface. Nat Mater. 2009;8:543–57.

25. Ha HK, Kim JW, Lee M-R, Jun W, Lee W-J. Cellular uptake and cytotoxicity of β-lactoglobulin nanoparticles: the effects of particle size and surface charge. Asian-Australas J Anim Sci.2015;28:420–7.

26. Choi J, Zhang Q, Reipa V, Wang NS, Stratmeyer ME, Hitchins VM. Comparison of cytotoxic and inflammatory responses of photoluminescent silicon nanoparticles with silicon micronsized particles in RAW 264.7 macrophages. J Appl Toxicol. 2009;29:52–60.

27. Donkor DA, Tang XS. Tube length and cell type-dependent cellular responses to ultra-short single-walled carbon nanotube. Biomaterials. 2014;35:3121–31.

28. Jiang Y, Huo S, Mizuhara T, Das R, Lee Y-W, Hou S, et al. The interplay of size and surface functionality on the cellular uptake of sub-10 nm gold nanoparticles. ACS Nano. 2015;9:9986–93.

29. Doane TL, Burda C. The unique role of nanoparticles in nanomedicine: imaging, drug delivery and therapy. Chem Soc Rev. 2012;41:2885–911.

30. Li Y, Kröger M, Liu WK. Shape effect in cellular uptake of PEGylated nanoparticles: comparison between sphere, rod, cube and disk. Nanoscale. 2015;7:16631–46.

31. Verma A, Stellacci F. Effect of surface properties on nanoparticlecell interactions. Small. 2010;6:12–21.

32. Moghimi SM, Szebeni J. Stealth liposomes and long circulating nanoparticles: critical issues in pharmacokinetics, opsonization and protein-binding properties. Prog Lipid Res. 2003;42:463–78.

33. Harris JM, Martin NE, Modi M. Pegylation: a novel process for modifying pharmacokinetics. Clin Pharmacokinet.2001;40:539–51.

34. Adams ML, Lavasanifar A, Kwon GS. Amphiphilic block copolymers for drug delivery. J Pharm Sci. 2003;92:1343–55.

35. Sperling RA, Parak WJ. Surface modification, functionalization and bioconjugation of colloidal inorganic nanoparticles. Phil Trans R. Soc A. 2010;368:1333–83.

36. Svenson S, Prud'homme RK, editors. Multifunctional nanoparticles for drug delivery applications: imaging, targeting, and delivery. In: Nanostructure Science and Technology. Boston: Springer Science+Business Media, 2012.

37. Ulusoy M, Jonczyk R, Walter J-G, Springer S, Lavrentieva A, Stahl F, et al. Aqueous synthesis of PEGylated quantum dots with increased colloidal stability and reduced cytotoxicity. Bioconjugate Chem. 2016;27:414–26.

38. Yoon HY, Koo H, Choi KY, Lee SJ, Kim K, Kwon IC, et al. Tumor-targeting hyaluronic acid nanoparticles for photodynamic imaging and therapy. Biomaterials. 2012;33:3980–9.

39. Duman O, Tunc S. Electrokinetic rheological properties of Na-bentonite in some electrolyte solutions. Micropor Mesopor Mater. 2009;117:331–8.

40. Crooke ST, editor. Antisense drug technology: principles, strategies, and applications, 2nd ed. Boca Raton: CRC Press, 2008.

41. Yue ZG, Wei W, Lv PP, Yue H, Wang LY, Su ZG, et al. Surface charge affects cellular uptake and intracellular trafficking of chitosan-based nanoparticles. Biomacromolecules. 2011;12:2440–6.

42. Arvizo RR, Miranda OR, Thompson MA, Pabelick CM, Bhattacharya R, Robertson JD, et al. Effect of nanoparticle surface charge at the plasma membrane and beyond. Nano Lett. 2010;10:2543–8.

43. Jiang J, Oberdörster G, Biswas P. Characterization of size, surface charge, and agglomeration state of nanoparticle dispersions for toxicological studies. J Nanopart Res. 2008;11:77–89.

44. Asati A, Santra S, Kaittanis C, Perez JM. Surface-charge-dependent cell localization and cytotoxicity of cerium oxide nanoparticles. ACS Nano. 2010;4:5321–31.

45. Frohlich E. The role of surface charge in cellular uptake and cytotoxicity of medical nanoparticles. Int J Nanomed. 2012;7:5577–91.

46. Schaeublin NM, Braydich-Stolle LK, Schrand AM, Miller JM, Hutchison J, Schlager JJ, et al. Surface charge of gold nanoparticles mediates mechanism of toxicity. Nanoscale. 2011;3:410–20.

47. Zhang S, Gao H, Bao G. Physical principles of nanoparticle cellular endocytosis. ACS Nano. 2015;9:8655–71.

48. Narang AS, Mahato RI. Targeted delivery of small and macromolecular drugs. CRC Press; 2010.

49. Sun T, Zhang YS, Pang B, Hyun DC, Yang M, Xia Y. Engineered nanoparticles for drug delivery in cancer therapy. Angew Chem Int Ed. 2014;53:12320–64.

50. Friedman AD, Claypool SE, Liu R. The smart targeting of nanoparticles. Curr Pharm Des. 2013;19:6315–29.

51. Milano A, Nasti G, Iaffaioli RV, Caponigro F. First line targeted therapies in breast cancer: focus on bevacizumab. Biologics. 2007;1:3–10.

52. Tuerk C, Gold L. Systematic evolution of ligands by exponential enrichment: RNA ligands to bacteriophage T4 DNA polymerase. Science. 1990;249:505–10.

53. Wang AZ, Gu F, Zhang L, Chan JM, Radovic-Moreno A, Shaikh MR, et al. Biofunctionalized targeted nanoparticles for therapeutic applications. Expert Opin Biol Ther. 2008;8:1063–70.

54. Zhang X-X, Eden HS, Chen X. Peptides in cancer nanomedicine: drug carriers, targeting ligands and protease substrates. J Control Release. 2012;10:159:2–13.

55. Li ZJ, Cho CH. Peptides as targeting probes against tumor vasculature for diagnosis and drug delivery. J Transl Med. 2012;10:1–9.

56. Seleci M, Ag Seleci D, Ciftci M, Demirkol DO, Stahl F, Timur S, et al. Nanostructured amphiphilic star-hyperbranched block copolymers for drug delivery. Langmuir. 2015;31:4542–51.

57. Tabujew I, Marco Lelle M, Peneva K. Cell-penetrating peptides for nanomedicine – how to choose the right peptide. BioNano- Mat. 2015;16:59–72.

58. Ziegler A, Blatter X, Seelig A, Seelig J. Protein transduction domains of HIV-1 and SIV TAT interact with charged lipid vesicles. Binding mechanism and thermodynamic analysis Biochemistry. 2003;42:9185–94.

59. Goncalves E, Kitas E, Seelig J. Binding of oligoarginine to membrane lipids and heparan sulfate: structural and thermodynamic characterization of a cell-penetrating peptide. Biochemistry. 2005;44:2692–702.

60. Peer D. Harnessing RNAi nanomedicine for precision therapy. Moll Cell Ther. 2014;2:5.

61. Carmeliet P, Jain RK. Angiogenesis in cancer and other diseases. Nature. 2000;407:249–57.

62. Prabhu VV, Chidambaranathan N, Gopal V. A historical review on current medication and therapies for inducing and inhibiting angiogenesis. J Chem Pharm Res. 2011;3:526–33.

63. Escoffre JM, Bouakaz A. Therapeutic ultrasound, advances in experimental medicine and biology. Heidelberg, Germany: Springer, 2015.

64. Baronzio GF, Hager ED, editors. Hyperthermia in cancer treatment: a primer, medical intelligence unit. Berlin: Landes Bioscience and Springer Science+Business Media, 2006.

65. Maeda H. The enhanced permeability and retention (EPR) effect in tumor vasculature: the key role of tumor-selective macromolecular drug targeting. Adv Enzyme Regul. 2001;41:189–207.

66. Yu MK, Park J, Jon S. Targeting strategies for multifunctional nanoparticles in cancer imaging and therapy. Theranostics. 2012;2:3–44.

67. Gabizon A, Catane R, Uziely B, Kaufman B, Safra T, Cohen R, et al. Prolonged circulation time and enhanced accumulation in malignant exudates of doxorubicin encapsulated in polyethylene-glycol coated liposomes. Cancer Res. 1994;54:987–92.

68. Sinha R, Kim GJ, Nie S, Shin DM. Nanotechnology in cancer therapeutics: bioconjugated nanoparticles for drug delivery. Mol Cancer Ther. 2006;5:1909–17.

69. Soppimath KS, Aminabhavi TM, Kulkarni AR, Rudzinski WE. Biodegradable polymeric nanoparticles as drug delivery devices. J Control Release. 2001;70:1–20.

70. Chen Y, Mohanraj VJ, Parkin JE. Chitosan-dextran sulfate nanoparticles for delivery of an anti-angiogenesis peptide. Lett Pept Sci. 2003;10:621–9.

71. Mahapatro A, Singh DK. Biodegradable nanoparticles are excellent vehicle for site directed in-vivo delivery of drugs and vaccines. J Nanobiotechnol. 2011;9:55–66.

72. Cheng Z, Zaki AA, Hui JZ, Muzykantov VR, Tsourkas A. Multifunctional nanoparticles: cost versus benefit of adding targeting and imaging capabilities. Science. 2012;338:903–10.

73. Zheng SW, Huang M, Hong RY, Deng SM, Cheng LF, Gao B, et al. RGD-conjugated iron oxide magnetic nanoparticles for magnetic resonance imaging contrast enhancement and hyperthermia. J Biomater Appl. 2014;28:1051–9.

74. Pennakalathil J, Ozgun A, Durmaz I, Cetin A, Rengul T, Tuncel D. pH-responsive near-infrared emitting conjugated polymer nanoparticles for cellular imaging and controlled-drug delivery. Int J Polym Sci A1. 2015;53:114–22.

75. Wilczewska AZ, Niemirowicz K, Markiewicz KH, Car H. Nanoparticles as drug delivery systems. Pharmacol Rep. 2012;64:1020–37.

76. Oberdorster G, Ferin J, Gelein R, Soderholm SC, Finkelstein J. Role of the alveolar macrophage in lung injury: studies with ultrafine particles. Environ Health Perspect. 1992;97:193–9.

77. de Villiers MM, Aramwit P, Kwon GS, editors. Nanotechnology in drug delivery. In: Biotechnology: Pharmaceutical Aspects. New York: AAPS Press and Springer Science Business Media, 2008.

78. Huh D, Hamilton GA, Ingber DE. From three-dimensional cell culture to organs-on-chips.TrendsCellBiol.2011;21:745–54.

4. Experimental Investigations

Experimental part comprises two original research articles investigating the design and applications of different nanoparticles in drug delivery and theranostic. The results of these articles are presented in two chapters. The first chapter (4.1) describes the potential of targeted amphiphilic star-hyperbranched block copolymer as a drug carrier. Within this scope, synthesis, characterization and surface modification of the micelles were investigated in detail as well as i*n vitro* analysis using integrin αvβ3 receptor positive and negative cells. This article provides particular results and perspectives to create novel targeted drug delivery systems which are crucial for the development of effective therapies. The second chapter (4.2) focuses on the development of liposome-nanoparticle hybrids for co-delivery of imaging and therapeutic agents. Thus, a novel theranostic drug carrier, which could enhance bioavailability of water-insoluble quantum dot and improve the stability of the drug, was designed and characterized. The outcome of this article provides new insights into the advantages of the combination of different nanoparticles for biomedical applications.

4.1 Nanostructured amphiphilic star-hyperbranched block copolymers for drug delivery

This chapter corresponds to the article "Nanostructured amphiphilic star-hyperbranched block copolymers for drug delivery" by M. Seleci, D. Ag Seleci, M. Ciftci, D. Odaci Demirkol, F. Stahl, S. Timur, T. Scheper, Y. Yagci first published in *Langmuir*, 2015, 31, 4542-4551. It was reproduced by permission of The American Chemical Society.

Table of Contents Graphic
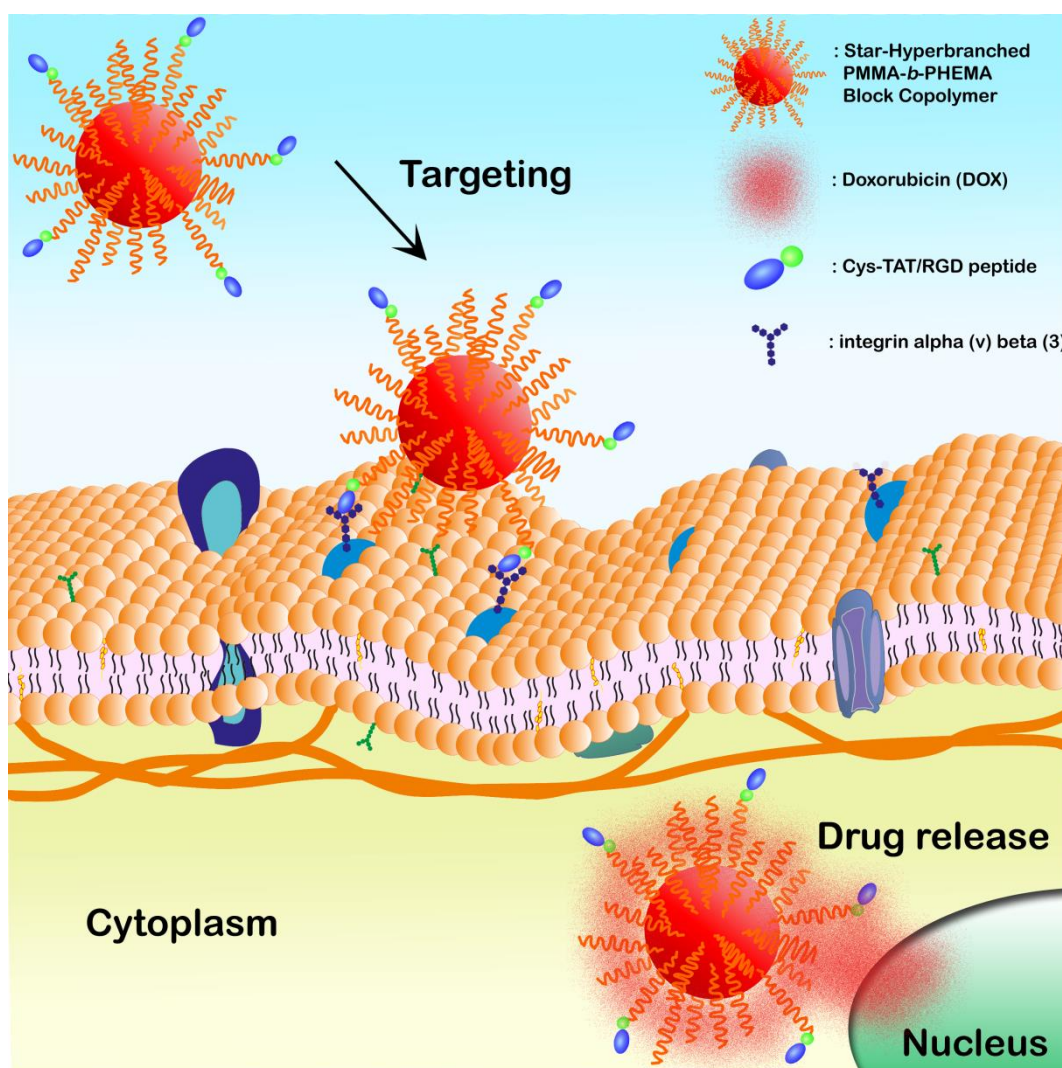
4.1.1 Summary

Polymeric nanoparticles have been extensively investigated for controlled and sustained drug delivery with a special focus on cancer therapy. Several biodegradable polymers have been used in drug delivery to improve the therapeutic effect of the drug with prolonged systemic circulation by conjugating, or adsorbing sterically amphiphilic polymers such as PEG to the nanoparticle surface. The utilization of amphiphilic polymers results in the formation of nanoparticles with a hydrophilic shell and a hydrophobic core. The hydrophilic shell provides a hydration layer that hinders interactions with the surrounding proteins in the circulation and hydrophobic core enables the encapsulation of drugs with poor aqueous solubility. Polymeric nanoparticles as drug carriers have substantial advantages such as the controlled and tunable release of therapeutics achievable by adjusting the physicochemical properties of the polymers. The main goal of the controlled and sustained release is to deliver agents to specific parts of the body by improving their pharmacological activity and stability. Thus, undesirable side effects could be reduced. Even though controlled release increases the efficacy of the drugs, lack of specificity is still the biggest limitation to achieve a desired delivery system with minimum systemic adverse effects.

The combination of active targeting with controlled and sustained release technology would significantly enhance the therapeutic efficiency of the agent. This approach allows for a large amount of the drug to be delivered to specific cells *via* receptor mediated targeting and facilitates to keep the concentration of drug constant at the targeted site over an extended period of time. Thus, targeted drug delivery reduces the relative concentration of the drug in the remaining tissues and thereby minimizes side effects. Therefore, there is a crucial need to design and develop novel targeted drug delivery systems.

In the present study, the development of an efficient dual peptide targeted copolymer based drug delivery system was aimed. For that, well characterized amphiphilic star-hyperbranched poly(methyl methacrylate)-*block*-poly(hydroxyethyl methacrylate) (PMMA-*b*-PHEMA) block copolymers were used. PMMA-*b*-PHEMA was synthesized by sequential visible light induced self-condensing vinyl polymerization (SCVP) and conventional vinyl polymerization. After the characterization, the surface of PMMA-*b*-PHEMA was functionalized using heterolinker N-(*p*-Maleimidophenyl) isocyanate (PMPI) and the model drug doxorubicin (DOX) was encapsulated into the surface activated copolymer. Arginylglycylaspactic acid (RGD) peptide was conjugated to cell

penetrating peptide (Cys-TAT) *via* the 1-ethyl-3-(3-(dimethylamino)propyl) carbodiimide/*N*-Hydroxysuccinimide (EDC/NHS) chemistry to obtain effective targeting ligand with high penetration property. High performance liquid chromatography (HPLC) analysis was used to prove the peptide conjugation. Subsequently, the obtained Cys-TAT/RGD peptide was bound to the surface of the copolymer. The physicochemical characteristics of the synthesized polymeric micelles were investigated with regard to size, polydispersity index, drug loading content and drug loading efficiency. Besides, the *in vitro* release of DOX was studied at pH 7.4 and 5.7 to mimic physiological conditions and the acidic tumor environment, respectively. Sustained release of DOX from PMMA-*b*-PHEMA/DOX/Cys-TAT/RGD was observed, especially at physiological pH 7.4, since most of the encapsulated DOX (~60%) remained within the micelle core after 48 h.

To test the targeting efficiency of the designed system, two types of cancer cell lines were selected after analysis of αvβ3 integrin receptor expression by flow cytometry. Higher expression level of integrin αvβ3 receptor in glioblastoma (U87) cells was determined compared to breast cancer (MCF-7) cells. The cellular uptakes of free drug and the conjugates were evaluated on both cell lines. According to the results targeted polymeric micelles, PMMA-*b*-PHEMA/DOX/Cys-TAT/RGD showed considerably increased uptake in U87 cells when compared to nontargeted micelles and free drug. Moreover, there was no specific cellular uptake in MCF-7 cells, which has lower integrin αvβ3 receptor expression. Afterwards, the cytotoxicity of the micelles was investigated in both cell lines by 3-(4,5-dimethylthiazol-2-yl)-2,5-diphenyltetrazolium (MTT) assay and flow cytometric analysis. The results were compared with control medium and free drug. The plain copolymer was non-toxic to both cell lines with relative cell viabilities about 90%. DOX-encapsulated copolymer and free DOX showed similar toxicity on both cell lines in comparison with nontreated control cells. The coupling of targeting peptides to the surface of DOX-encapsulated polymeric micelles resulted in enhanced toxicity in U87 cells no increasement of toxicity in MCF-7 cells. Furthermore, PMMA-*b*-PHEMA/DOX/Cys-TAT/RGD had significant cytotoxicity on U87 cells compared to free DOX. The cellular localization of free drug and drug loaded copolymers was monitored using fluorescence microscopy. Since DOX has fluorescent properties and intercalates into DNA to inhibit the progression of topo isomerase II, it accumulates in the cell nucleus. In fluorescence microscopy images it was also clearly seen that free DOX was located in the nucleus of U87 and MCF-7 cells. In the case of PMMA-*b*-

PHEMA/DOX/Cys-TAT/RGD, strong red fluorescence in the nucleus and in the cytoplasm of U87 cells was observed and this was attributed to the receptor mediated endocytosis process.

Overall, the results presented here indicate the potential of the amphiphilic hyperbranched copolymer as a drug nanocarrier with dual peptides which can specifically bind with integrin αvβ3, while Cys-TAT facilitates penetration through the cell membrane. The targeted polymeric micelle formulation might be a promising and efficient vehicle for delivery of the agents to integrin αvβ3 receptor overexpressed cells.

4.1.2 Abstract

A robust drug delivery system based on nanosized amphiphilic star-hyperbranched block copolymer, namely, poly(methyl methacrylate-block-poly(hydroxylethylmethacrylate) (PMMA-*b*-PHEMA) is described. PMMA-*b*- PHEMA was prepared by sequential visible light induced selfcondensing vinyl polymerization (SCVP) and conventional vinyl polymerization. All of the synthesis and characterization details of the conjugates are reported. To accomplish tumor cell targeting property, initially cell-targeting (arginylglycylaspactic acid; RGD) and penetrating peptides (Cys-TAT) were binding to each other *via* the well-known EDC/NHS chemistry. Then, the resulting peptide was further incorporated to the surface of the amphiphilic hyperbranched copolymer *via* a coupling reaction between the thiol (−SH) group of the peptide and the hydroxyl group of the copolymer by using N-(p-maleinimidophenyl) isocyanate as a heterolinker. The drug release property and targeting effect of the anticancer drug (doxorubicin; DOX) loaded nanostructures to two different cell lines were evaluated *in vitro*. U87 and MCF-7 were chosen as integration αvβ3 receptor positive and negative cells for the comparison of the targeting efficiency, respectively. The data showed that drug-loaded copolymers exhibited enhanced cell inhibition toward U87 cells in compared to MCF-7 cells because targeting increased the cytotoxicity of drug-loaded copolymers against integrin αvβ3 receptor expressing tumor cells.

4.1.3 Introduction

The therapeutic efficacy of many anticancer drugs for cancer treatment is limited by their poor penetration into tumors and by their adverse effects on healthy cells [1]. In solid tumors, this penetration problem could cause trouble leading to reduced efficacy and the development of drug resistance. Thus, controlled delivery of anticancer drug to the

targeted cell has recently been an academic and an industrial challenge. Taking these drugs alone may lead to the failure of therapy, early disease relapse, drug resistance, and other side effects [2]. To prevent all these shortcomings, development of novel carrier platforms for drug uptake into the cell with minimum effective dose and high efficiency is one of the long-term goals in pharmacology. Some of the existing methods are based on the introduction of multifunctional nanocarrier platforms achieving outstanding properties through nanobiomaterial based formulations and bioconjugation techniques in targeted anticancer therapy [3-5].

Self-assembled nanostructures of amphiphilic block copolymers have extensively been used with various advantages in biomedicine as carriers for drugs and biomolecules [6,7]. They are biocompatible, are highly stable, and facilitate dissolution of poorly soluble pharmaceutical agents molecules owing to accommodation of drugs in their hydrophobic core. The hydrophilic shell structure in micelles provides a stabilizing interface between the hydrophobic core and aqueous media [8]. Furthermore, many functions could be incorporated to the missile surface to reveal multifunctional polymeric micelles. The modification of surface with targeting ligands, cell penetrating moieties, and contrast agents can be used to allow for specific targeting, intracellular accumulation, and imaging, respectively [9]. Targeted drug delivery systems have enormous potential for improving the efficiency of cancer treatment. RGD peptides are one of the promising legends for targeting $\alpha v \beta 3$ integrin, which is overexpressed in various cancer cells such as U87 glioblastoma cells [10]. Cell penetrating peptides (CPPs) represent a class of peptides that include the cationic TAT peptide of the HIV-1 transactivating factor which has been shown to translocate across the negatively charged cell membrane and improve cytoplasmic delivery of the macromolecules [11,12]. Hyperbranched amphiphilic polymers are another class of materials widely used in diverse bioapplications such as drug and gene delivery, tissue engineering, and bioimaging studies [13]. Recently, an amphiphilic hyperbranched multiarm copolymer [H40-star-(PLA-*b*-PEP-OH)] was investigated as a drug delivery vesicle, and the inhibition properties of drug-loaded micelles toward the proliferation of HeLa human cervical carcinoma cell line were evaluated [14]. In another study, Durmaz *et al.* used Food and Drug Administration approved beta-cyclodextrin (β-CD) to prepare pH-sensitive, star-shaped, cone-shaped polymers and evaluated their ability to deliver anti-GPDH siRNA past the endosomal membrane and into the cytoplasm of multiple epithelial cell lines. Using atom transfer radical polymerization (ATRP) technique, they grafted P(HEMA-*co*-DMAEMA)

copolymers from the secondary face of the β-CD core *via* acid-labile hydrazone linkages [15]. In addition, an aptamer-functionalized amphiphilic hyperbranched copolymer conjugate was successfully used as a novel targeted cancer imaging system [16].

Hyperbranched polymers are generally synthesized by step-growth polycondensation or ring opening polymerization of ABx monomers and self-condensing vinyl polymerization (SCVP) of AB monomers. Among them, SCVP is the most efficient and flexible method for a variety of vinyl monomers. In this approach, monomers are copolymerized with inimers possessing both polymerizable vinyl and pendant initiating groups. Dimanganese decacarbonyl $[Mn_2(CO)_{10}]$ in conjunction with organohalogen compounds is an elegant visible light acting photoinitiating system offering molecular design flexibility for the synthesis of complex macromolecular structures [17]. This simple photoinitiating system provided different synthetic utilities in free radical promoted cationic [18], mechanistic transformation [19,20], graft copolymerization [21], controlled radical polymerization [22-25], surface patterning [26], and preparation of telechelics [27].

In continuation of our investigations into the potential of photochemically prepared polymers for biomedical applications, herein we report the use of a nanostructured amphiphilic star-hyperbranched block copolymer as a novel targeted drug delivery platform. Two-step synthesis of the block copolymers was carried out by using manganese-based photoinitiating system. Amphiphilic hyperbranched polymers are endowed with cell targeting property due to the incorporation of both cell-targeting (arginylglycylaspactic acid; RGD) and penetrating peptides (Cys-TAT). In addition, an anticancer drug doxorobucin (DOX) was chosen as a model drug and efficiently encapsulated into the copolymer. The anticancer capability of DOX-loaded targeted micelles was studied in MCF-7 and U87 cell lines by evaluating cellular uptake, cytotoxicity and apoptosis in comparison to free DOX and DOX-loaded nontargeted micelles. The *in vitro* DOX release profile from polymeric micelles was also observed under different pH conditions. All of the synthesis and characterization details of the conjugates are reported.

4.1.4 Experimental section

Materials

Methyl methacrylate (MMA, Aldrich, 99%) and 2-Hydroxyethyl methacrylate (HEMA; 99%, Aldrich) were passed through a column of basic alumina to remove the inhibitor. 2-Bromoethyl methacrylate (BEMA) was kindly donated by Bicak research group. Dimanganese decacarbonyl ($Mn_2(CO)_{10}$, 99%, Aldrich) was purified by sublimation and stored in a refrigerator in the dark. Methanol (MeOH, 99.9%, Merck) and *n*-hexane (95%, Aldrich) were used as received. Doxorobucin (hydrochloride) was purchased from Cayman Chemical. Cysteine modified cell penetrating peptide with CYGRKKRRQRRR-NH$_2$ sequence Cys-TAT (47−57) was obtained from GenScript. *N*-(*p*-Maleinimidophenyl)isocyanate (PMPI), 1-ethyl-3-(3-(dimethylamino)propyl) carbodiimide (EDC), MES hydrate, Arg-Gly-Asp (RGD) peptide, 4′,6-diamidino-2-phenylindole dihydrochloride (DAPI), 3-[4,5-dimethylthiazol-2-yl]-2,5-diphenyltetrazolium bromide (MTT), and propidium iodide (PI) solution were ordered from Sigma-Aldrich. N-Hydroxysuccinimide (NHS) and sodium dodecyl sulfate (SDS) were purchased from Fluka and Applichem, respectively. Mouse IgG1, K isotype control fluorescein isothiocyanate (FITC), and anti-human CD51/CD61 (integrin αvβ3) FITC were purchased from affymetrix eBioscience. Annexine-V-FLUOS staining kit was purchased from Roche Diagnostics GmbH (Mannheim, Germany). Phosphate buffered saline (PBS) was prepared with 137 mM sodium chloride, 2.7 mM potassium chloride, 10.1 mM disodium hydrogen phosphate, and 1.8 mM potassium dihydrogen phosphate, pH 7.4; all chemicals were also provided by Sigma-Aldrich.

Methods

Synthesis of Bromo Functional Hyperbranched Poly(methyl methacrylate) (Hyperbranched PMMA)

Bromo functional hyperbranched PMMA was synthesized by radical photopolymerization of MMA and 2-BEMA as described previously [28]. An example detailing a typical procedure is as follows: $Mn_2(CO)_{10}$ (2.96 mg, 7.60×10^{-6} mol), BEMA (76 μL, 7.06×10^{-4} mol), and 1.0 mL of MMA (9.38×10^{-3} mol) were placed in a Pyrex tube equipped with a magnetic stirring bar and filled with dry nitrogen prior to irradiation with a Ker-Vis blue photoreactor equipped with six lamps (Philips TLD 18 W) emitting

light nominally at 400−500 nm at room temperature. At the end of irradiation, the polymer was precipitated in excess methanol and dried in a vacuum.

Syntheses of Amphiphilic Star-Hyperbranched Poly(methylmethacrylate)-b-Poly(2-hydroxyethyl methacrylate) (PMMA-b-PHEMA) Block Copolymers

The above obtained macroinitiator (bromo functional hyperbranched PMMA, 250 mg, containing 1.6×10^{-4} mol bromo groups), $Mn_2(CO)_{10}$ (20.8 mg, 5.3×10^{-5} mol), and HEMA (1.25 mL, 9.5×10^{-3} mol) were put in a Pyrex tube equipped with a magnetic stirring bar and filled with dry nitrogen. The mixture was irradiated by visible light at room temperature. After the given time, the resulting polymers were precipitated in excess *n*-hexane, dried in a vacuum, and characterized by ^{1}H NMR, Fourier transform infrared (FT-IR), and dynamic light scattering (DLS) measurements.

Characterization of the Polymers

^{1}H NMR spectra of the polymers were recorded on an Agilent VNMRS 500 instrument. FT-IR analyses were performed on a PerkinElmer FT-IR Spectrum One B spectrometer.

Gel-permeation chromatography (GPC) measurements were obtained from a Viscotek GPCmax Autosampler system consisting of a pump module (GPCmax, Viscotek Corp.), a combined lightscattering detector (model 270 Dual Detector, Viscotek Corp.), and a refractive index (RI) detector (VE 3580, Viscotek Corp.). The light scattering detector ($\lambda_0 = 670$ nm) included two scattering angles: 7° and 90°. The RI detector was calibrated with polystyrene standards having narrow molecular weight distribution, and so the quoted molecular weights of the polymers are expressed in terms of polystyrene equivalents. Two columns 7.8×300 mm (LT5000L, Mixed, Medium Org and LT3000L, Mixed, Ultra-Low Org) with a guard column 4.6×10 mm (Viscotek, TGuard) were used for the chloroform eluent at 35 °C (flow rate: 1.0 mL·min^{-1}). Data were analyzed using Viscotek OmniSEC Omni-01 software.

Bioconjugation. Binding of the RGD to Cys-TAT Peptide

RGD peptide (0.5 mg) was dissolved in 500 µL of ddH$_2$O, and its carboxyl groups were activated using 0.1 M EDC and 0.05 M sulfo-NHS for 30 min at 1000 rpm. After this step, 0.1 mg/mL Cys-TAT peptide was added to the activated RGD peptide and stirred at 750 rpm for 4 h. Finally, the solution was dialyzed (MWCO: 1.0 kDa, Tube-O-

Dialyzer, G-Biosciences) against ddH$_2$O to remove unbound and excess amount of molecules.

Activation of OH-Functionalities and Drug Encapsulation

PMPI was used as a heterolinker through the interaction of thiol (−SH) groups of the peptide and hydroxyl groups of the copolymer forming carbamate bond. Prior to the drug loading, PMMA-*b*-PHEMA was activated with PMPI as follows: PMMA-*b*-PHEMA copolymer (1.0 mg) and PMPI (1.25 mg) were dissolved in 1.0 mL of DMSO and stirred at 1000 rpm in ambient conditions for 2 h. DOX solution in DMSO (0.2 mg/mL) in the presence of triethylamine was added to the modified copolymer solution and stirred at 1000 rpm in the dark for 4 h. For the encapsulation of DOX into the copolymer, the whole solution was dropwise added into 4.0 mL of ddH$_2$O and stirred for 24 h. At the end of the process, the micelle solution was dialyzed (MWCO: 4000 Da, Tube-O-Dialyzer, G-Biosciences) against ddH$_2$O for 24 h in the dark to removing unbound molecules and then filtrated using 0.45 μm filters.

Bioconjugation of Peptides to PMPI Activated PMMA-b-PHEMA/DOX

The resulting Cys-TAT/RGD peptide was added to PMPI activated PMMA-*b*-PHEMA/DOX and stirred for overnight. After bioconjugation of the peptide (Cys-TAT/RGD) to the drug−polymer conjugate, the whole solution was dialyzed (MWCO: 1.0 kDa, Tube-ODialyzer, G-Biosciences) against ddH$_2$O.

Characterization Methods of the Conjugates

The synthesized Cys-TAT/RGD, PMMA-*b*-PHEMA/DOX, and PMMA-*b*-PHEMA/ DOX/Cys-TAT/RGD were characterized *via* high performance liquid chromatography (HPLC) and DLS analysis. HPLC measurements and DLS measurements were carried out using VWR Hitachi Chromaster and Malvern Zetasizer Nanoseries-Nano-ZS instruments, respectively. The optical characteristics of DOX and the conjugates were also examined using a Nanodrop 3300 apparatus (Thermo Fisher Scientific Inc.). The peptide concentrations were measured by bicinchoninic acid (BCA) method using the Pierce BCA kit (Thermo Scientific) according to the manufacturer's instructions.

HPLC

Initially, the samples were filtered (Millex-GV, 0.22 μm, PVDF, 4 mm). For the analysis, a DAD detector and Kinetix 2.6 μm C8 100 Å, 150 × 4.6 mm (Phenomenex) column

were used. Detection was performed at 214 nm at room temperature. The mobile phase consisted of 0.065% Trifluoroacetic acid (TFA) in water and 0.05% TFA in acetonitrile with a flow rate of 1.0 mL/min.

Dynamic Light Scattering (DLS)

The hydrodynamic size of the copolymer and conjugates were analyzed using a Malvern Zetasizer Nanoseries-Nano-ZS. Measurements were performed at 25 °C at an angle of 173°, and each sample was analyzed in triplicate. Samples were filtered using a 0.45 μm membrane filter prior to measurements for all of the experiments.

Transmission Electron Microscopy (TEM)

The samples were prepared from solution by placing a droplet on a carbon coated mesh copper grid and drying in the air. Measurements were done using a FEI Tecnai G2 F20 TMP-TEM instrument with a 200 kV FEG in bright field mode.

Calculation of Drug Loading Capacity

The drug loading content was calculated *via* measuring the absorption of the lyophilized sample. The lyophilized sample was dissolved in DMSO, and spectrophotometric measurements were performed at 485 nm. A calibration curve with a known concentration of free DOX was established to determine the drug content in the solution. The percentages of DLC (drug loading content) and DLE (drug loading efficiency) were calculated according to the following equations:

$$(1)\ \text{Drug loading content (DLC)} = \left[\frac{\text{Amount of DOX in micelle } (W_1)}{\text{Amount of DOX-loaded micelles } (W_2)} \right] \times 100\%$$

$$(2)\ \text{Drug loading efficiency (DLE)} = \left[\frac{\text{Amount of DOX in micelle } (W_1)}{\text{Amount of DOX for micelle preparation } (W_3)} \right] \times 100\%$$

In Vitro Drug Release

Drug release experiments were carried out using dialysis method. The DOX-loaded micelle solutions prepared were transferred into a dialysis membrane tubing (Thermo, Slide-A-Lyzer MINI Dialysis Devices, 3.5K MWCO). The tubing was immersed in 10.0 mL of the PBS buffer (pH 5.7 and 7.4) and placed in a water bath (Memmert, Germany) at 37 °C. At specific time intervals, 0.5 mL samples were withdrawn from the release medium and replaced with the same volume of fresh buffer. The amount of released DOX

was analyzed by fluorescence emission measurements at 595 nm with a calibration curve, which was established with a known concentration of free DOX. The release studies were performed in quadruplicate for each of the samples.

Cell Culture Studies

U87 (human glioblastoma cells) and MCF-7 (breast cancer cells) cell lines were provided from the German Collection of Microorganisms and Cell Cultures (DSMZ). U87 cells were grown in DMEM containing 10% FCS and 1.0% P/S. MCF-7 cells were cultivated in Minimum Essential Medium Eagle (MEM) modified with 10% fetal calf serum, 1.0 mM sodium pyruvate, 2.0 mM L-glutamine, 10 mg/mL insulin, 1.0% nonessential amino acids, and 1.0% P/S. All cells and the samples were cultivated in medium and reagents at 37 °C in a humidified environment with 5.0% CO_2.

Conformation of Integrin αvβ3 Receptor Expression on the Cell Surface

The expression level of integrin αvβ3 in U87 cells and in MCF-7 cells was tested *via* flow cytometry analyses. Initially, cells were harvested by accutase treatment and washed once in cold PBS. After suspending in incubation buffer which consisted of PBS supplemented with 2.0% fetal calf serum, 4×10^5 cells were collected and centrifuged, and the cell surface was blocked at room temperature for 10 min in 100 μL of incubation buffer. For cell staining, 5.0 μL of FITC labeled anti-human integrin αvβ3 was added and the cell suspension was shaken at room temperature for 1 h at 450 rpm in the dark. Mouse IgG1 K isotype control antibody was used for negative control staining. Unbound antibody was removed by washing the cells once in 300 μL of incubation buffer. Before flow cytometric analysis, cells were resuspended in 500 μL of PBS and then analyzed in a COULTER EPICS XL-MCL flow cytometer. At least 10 000 gated events were observed in total, and the living cells were gated in a dot plot of forward versus side scatter signals. For drawing dot plots and histograms, the software WinMDI 2.9 was used.

Cellular Uptake

Flow cytometry studies were carried out to determine the cellular uptake level of free DOX, PMMA-*b*-PHEMA/DOX, and PMMA-*b*-PHEMA/DOX/Cys-TAT/RGD conjugates in MCF-7 and U87 cells. Cells were prepared as described above, and then samples were applied for 4 h. Before flow cytometric analysis, cells were suspended 500

µL of PBS and then analyzed in a COULTER EPICS XL-MCL flow cytometer. The analysis of measured signals was done as described above.

Cytotoxicity Assay

3-(4,5-Dimethylthiazol-2-yl)-2,5-diphenyl tetrazolium bromide (MTT) assays were used to determine the cytotoxicity effect of free DOX, PMMA-*b*-PHEMA, PMMA-*b*-PHEMA/DOX, and PMMA-*b*-PHEMA/DOX/Cys-TAT/RGD on U87 and MCF-7 cells. Cells were seeded in 96-well-tissue plates and cultivated for 3 days. Then cells were washed once in PBS and treated with samples for 24 h. Samples were removed, and cells were incubated in 110 µL/well 10% MTT solution (5.0 mg/mL in PBS) in medium for 4 h. Afterward, 100 µL of SDS solution (1.0 g SDS in 10 mL 0.01 M HCl) was added per well and incubated for 24 h. Finally, UV−vis absorption was measured at 570 nm with 630 nm as the reference wavelength using a microplate reader model 680 (BioRad).
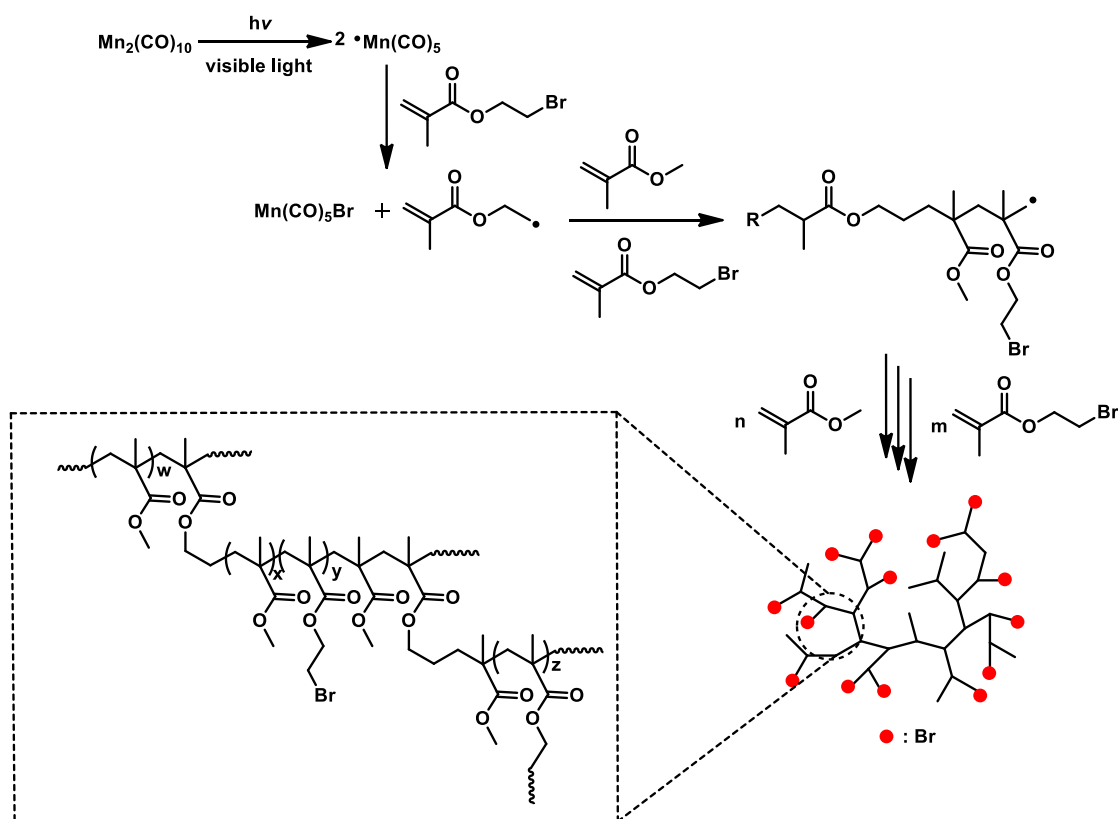
Figure 4.1 Visible Light Induced Synthesis of Hyperbranched PMMA

Annexin V/PI Staining

For flow cytometry studies, the same procedure was utilized as mentioned above. Cells were treated 4 h with DOX, PMMA-*b*-PHEM/DOX, and PMMA-*b*-PHEM/DOX/Cys-TAT/RGD, and then treated cells were stained with both Annexin V-FLUOS and PI for

dead/live discrimination. Briefly, cells were incubated in 100 μL of incubation buffer including 2.0 μL of Annexin V for 15 min at room temperature in the dark. Then 2.0 μL of the PI stock solution was added to each tube and mixed well before the analysis to determine PI fluorescence. The stained cells were then analyzed in a COULTER EPICS XL-MCL flow cytometer.

Fluorescence Microscopy

U87 and MCF-7 cells were cultivated for 2 days on a 96-well plate in a volume of 200 μL of medium. Samples were diluted with medium and then added to the cells. The cells were incubated for 6 h at 37 °C and were washed once in PBS. Afterward Fluoroshield with DAPI was dropped on the cells, and images were taken using an OLYMPUS IX50 fluorescence microscope equipped with an OLYMPUS SC30 camera.

Statistical Analysis

Statistical analysis was performed using the GraphPad Prism 6 statistical software. All experiments were repeated four times. One-way analysis of variance (ANOVA) was performed with Tukey test for multiple comparisons in statistical evaluation. The difference between two groups was considered to be significant when the P value was less than 0.05.

4.1.5 Results and discussion

Synthesis and Characterization of Amphiphilic Star Copolymer

In the first step of the approach, hyperbranched poly(methyl methacrylate) (PMMA) hydrophobic core was prepared by implementing manganese-based visible light photoinitiating system into SCVP method. Thus, methyl methacrylate (MMA) was copolymerized in bulk with 2-bromoethyl methacrylate (BEMA) possessing both polymerizing and bromide initiating sites in the structure in the presence $Mn_2(CO)_{10}$ under visible light for 2 h. The relative BEMA concentration was deliberately kept low (7.5 mol % MMA) to avoid solubility problems. The higher BEMA concentrations and prolonged irradiation times essentially lead to higher branching, but partially insoluble materials. At the end process, PMMA with highly branched structure as determined with an RM value (M_nRI/M_nLS) of 0.23 was obtained. The obtained hyperbranched polymer contains 8 mol % BEMA segments with unreacted bromo groups as determined by ^1H NMR. The suggested mechanism is outlined in Figure 4.1. In the first step of the process,

·Mn(CO)$_5$ radicals formed from the photochemical homolysis of Mn$_2$(CO)$_{10}$ abstract bromine atoms from BEMA to generate radicals on the inimer. Subsequently, these carbon centered radicals of the inimer initiate the copolymerization MMA and BEMA. Since some of the bromine groups are not activated, BEMA contributes to both the generation of branching points on the polymer chain and the existence of bromine moieties in the final product; while MMA takes place only in the formation of linear polymer chains.

As consequence of the described process, the resulting hyperbranched polymers contain bromine groups in the structure which allows further polymerization of hydrophilic monomer HEMA. Thus, visible light induced polymerization of HEMA in the presence of hyperbranched PMMA macroinitiator resulted in the formation of the amphiphilic PMMA-*b*-PHEMA copolymers possessing hydrophobic hyperbranched core and hydrophilic chains (Figure 4.2A).

The structure of the precursor hyperbranched polymer and the resulting star block copolymer was confirmed by spectral analysis. In the ^{1}H NMR spectrum of the precursor polymer, characteristic bands of the PMMA core were observed; whereas in the spectrum of the block copolymer additional bands at 3.5−4.4 ppm corresponding to −CH$_2$O, −OCHH$_2$, and –OH protons of PHEMA segments were clearly detectable (Figure S4.1, Supporting Information).

The results obtained from FT-IR spectroscopy also support the successful block copolymerization. The IR spectra of the block copolymers (Figure S4.2, Supporting Information) exhibit the OH stretching band of PHEMA star arms in addition to characteristic bands of PMMA core.
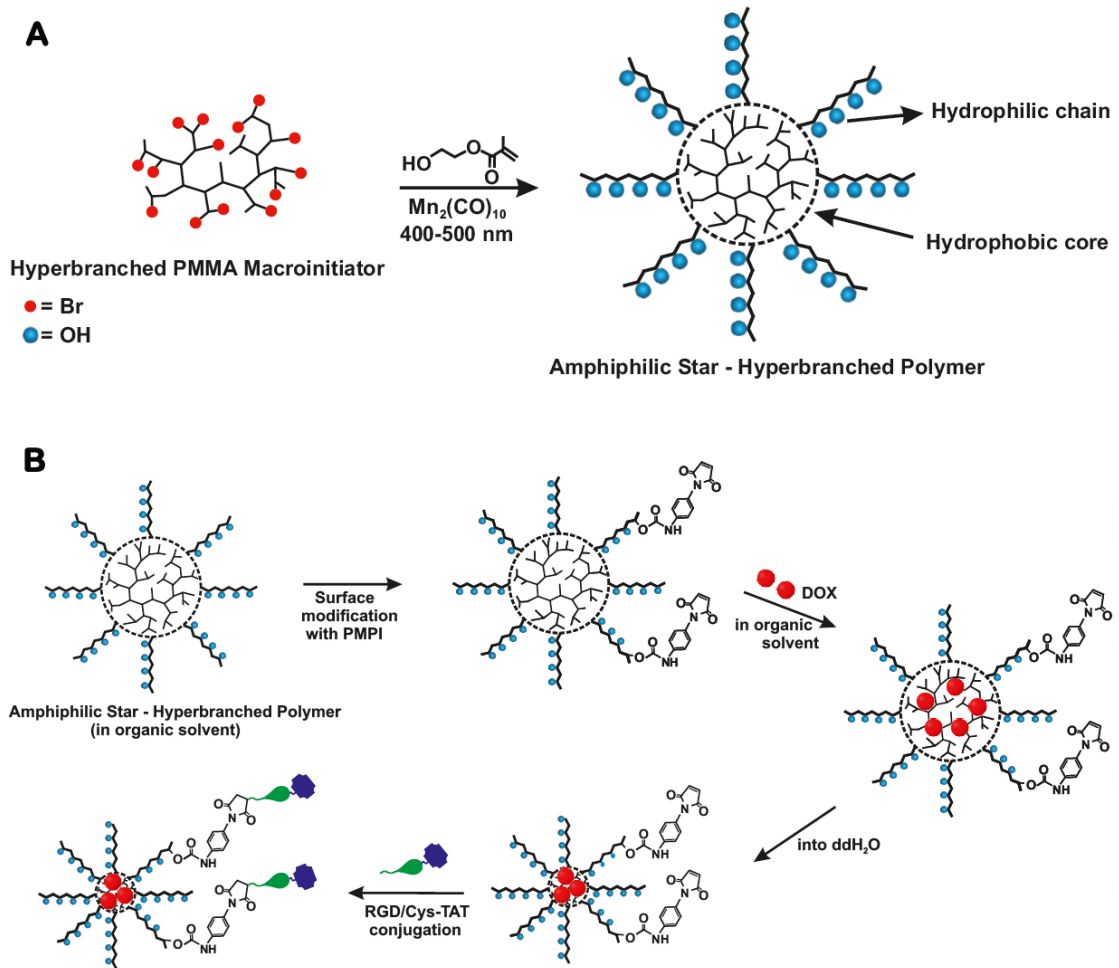
Figure 4.2 (A) Synthesis of amphiphilic star-hyperbranched PMMA-*b*-PHEMA block copolymer. (B) Schematic representation of the bioconjugation process.
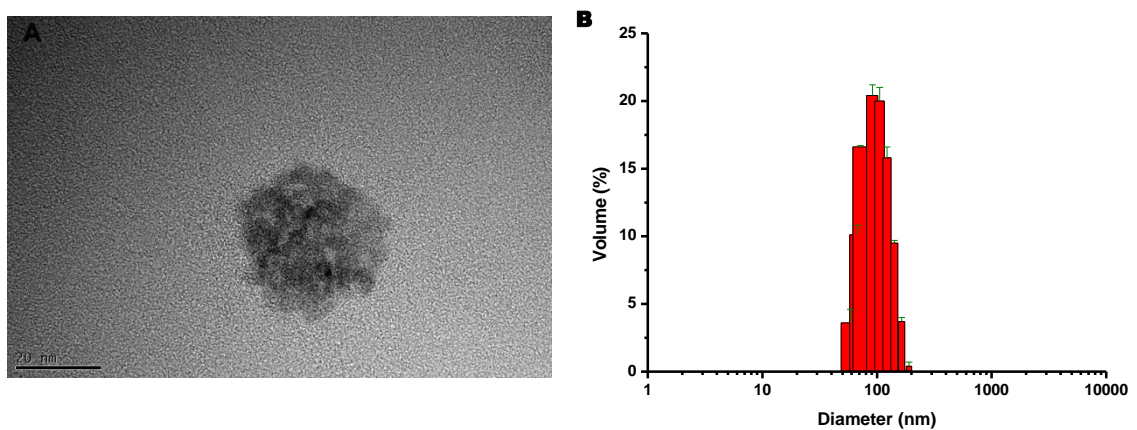
Figure 4.3 TEM micrograph showing (A) morphology and (B) a size distribution histogram of PMMA-*b*-PHEMA.

Synthesis and Characterization of PMMA-b-PHEMA Conjugates

In our study, we aimed to develop a novel micellar drug delivery system with the use of PMMA-*b*-PHEMA copolymer and RGD peptide as a carrier molecule and targeting

ligand in U87 cells, respectively. In the first step, surface modification of the PMMA-*b*-PHEMA was carried out with PMPI for facilitating peptide conjugation. At the same time, the covalent binding strategy was used between activated carboxyl groups on RGD peptide and the amino groups on Cys-TAT using EDC along with sulfo-NHS. This conjugation was proven by HPLC analysis. For this aim, chromatograms of Cys-TAT and RGD peptide were compared with chromatogram of Cys-TAT/RGD conjugate (Figure S4.3, Supporting Information). Nonconjugated RGD and Cys-TAT peptides have peaks at 2.24 and 8.25 min, respectively (Figure S4.3A and B, Supporting Information). Cys-TAT/RGD conjugate has peaks at 2.02 and 8.04 min that were assigned to RGD and Cys-TAT peptide, respectively (Figure S4.3C, Supporting Information). For the next step, model drug DOX was encapsulated in PMPI modified PMMA-*b*-PHEMA (PMMA-*b*-PHEMA/DOX), and finally Cys-TAT/RGD was conjugated with PMMA-*b*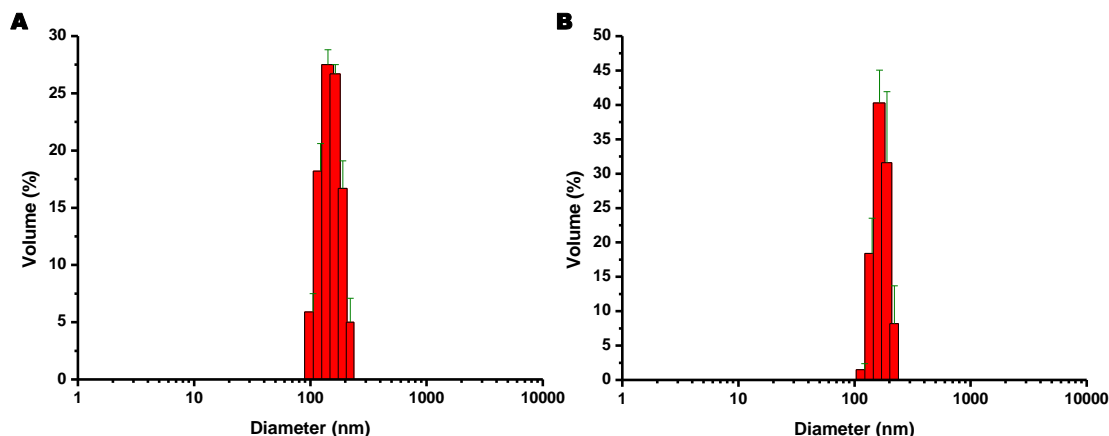-PHEMA/DOX (PMMA-*b*-PHEMA/DOX/Cys-TAT/ RGD) *via* high affinity of thiol groups present in Cys-TAT for maleimide groups of PMPI. The overall process is shown in Figure 4.2B. The binding amount of peptide for each polymer was quantified by BCA assay with a bovine serum albumin (BSA) standard curve (y = $0.0004x + 0.093$, $R^2 = 0.997$). The starting amount of Cys-TAT/RGD conjugate was 224 μg after the dialysis. The amount of Cys-TAT/RGD conjugated to PMMA-b-PHEMA/DOX was 135 μg of peptide per 1.0 mg of polymer.

The size of polymeric micelles is very important for tumor accumulation by EPR effect and cellular internalization [29]. Micelle size was analyzed to be 101.3 ± 26.15 nm (Figure 4.3B) *via* DLS, which is an ideal size range for nano particle drug delivery applications [30,31]. The hydrodynamic diameter increased to 154.1 ± 28.72 nm and 172.2 ± 22.91 nm after DOX loading and conjugation with peptides respectively (Figure 4.4). The particle morphology of copolymer observed by TEM (Figure 4.3A). TEM observation showed that the micelles had a spherical shape and had an average diameter around 35 nm which was smaller than that determined by DLS due to dehydration during sample preparation and subsequently shrinkage of the micelles for TEM [32,33].

Figure 4.4 Histograms of particle size distribution of (A) PMMA-*b*-PHEMA/DOX, and (B) PMMA-*b*-PHEMA/DOX/Cys-TAT/RGD nanoparticles.

DOX Loading Content (DLC) and Loading Efficiency (DLE)

PMMA-*b*-PHEMA/DOX prepared with the ratio of copolymer/DOX was 1/0.2 (w/w). The DLC and DLE of PMMA-*b*-PHEMA/DOX and PMMA-*b*-PHEMA/DOX/Cys-TAT/RGD are shown in Table 4.1. Drug encapsulation was affected by many factors including hydrophobic block length, hydrophobicity of core-forming block, crystallinity, drug solubility in water, and interactions between drug and copolymer [34,35].

Table 4.1 Characterization of PMMA-b-PHEMA polymeric micelles incorporating DOX.

| Micelles | Drug content (%) | | Micelle size (nm) | Polydispersity |
| | DLC | DLE | Volume (%) | index |
			(Mean ± SD)	
PMMA-*b*-PHEMA/DOX	4.62	23.08	154.1 ± 28.72	0.300
PMMA-*b*-PHEMA/DOX/Cys-TAT/RGD	4.32	21.60	172.2 ± 22.91	0.871

In Vitro Drug Release

In vitro release profiles of DOX from PMMA-*b*-PHEMA/DOX/Cys-TAT/RGD at 37 °C under physiological conditions (pH 7.4) and in an acidic environment (pH 5.7) were demonstrated in Figure 4.5. The free DOX solution was also used as a control. DOX release was much faster at pH 5.7 when compared to that at pH 7.4. It can be explained that at the lower pH doxorubicin has a higher solubility [36]. The release of a drug from polymeric micelles is not so fast and depends many factors such as polymer degradation, micelle stability, rate of drug diffusion from the micellar core, and crystallinity [37-39]. DOX released from PMMA-*b*-PHEMA/DOX/Cys-TAT/RGD occurred in a sustained manner. In contrast, the free DOX was rapidly released by 87% in just 8 h. Within 48 h,

the cumulative release of DOX was 57% and 39% for PMMA-*b*-PHEMA/DOX/Cys-TAT/RGD at pH 5.7 and 7.4, respectively. These results confirmed that DOX molecules were successfully loaded into the core of copolymer micelle.
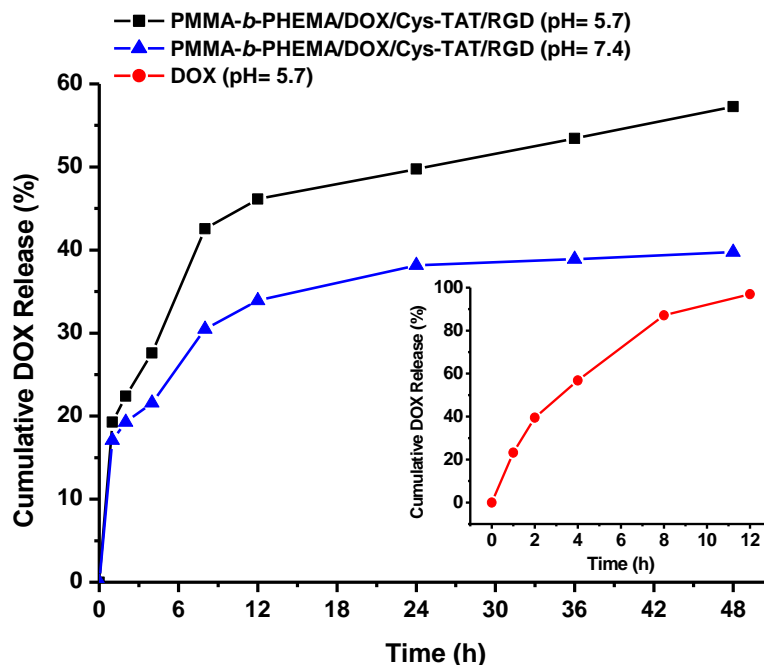
Figure 4.5 *In vitro* cumulative release of DOX from PMMA-*b*-PHEMA/DOX/Cys-TAT/RGD at pH 5.7 and 7.4. The inset shows the release profile of free DOX at pH 5.7 for 12 h.

Conformation of Integrin αvβ3 Receptor Expression on the Cell Surface

MCF-7 and U87 cells were characterized for their expression level of integrin αvβ3 receptor. In flow cytometry analysis, cell surface proteins were detected by FITC conjugated antibodies. Higher amounts of antibodies on the cell surface enhanced the measured fluorescence intensity. After cell staining, the fluorescence intensity of each cell sample was read out separately and a dot plot graph and histogram of the cells were drawn (Figure S4.4, Supporting Information). Figure S4.4A indicates fluorescence measurement of MCF-7 cells, and Figure S4.4B shows the signals of U87 cells. The mean intensity of the isotype controls for MCF-7 cells was 2.71 AU, whereas the isotype control for U87 was 2.98 AU. After the incubation with the anti-integrin αvβ3 antibody, the fluorescence intensity was 2.94 AU for MCF-7 cells, yet it was 4.61 AU for U87 cells. Results confirmed that integrin αvβ3 receptor expression was considerably higher in U87 cells than in MCF-7 cells.

Cellular Uptake

To evaluate receptor mediated cell targeting, flow cytometry analysis was performed. Cellular uptake of free DOX, PMMA-*b*-PHEMA/DOX, and PMMA-*b*-PHEMA/DOX/Cys-TAT/RGD was tested for both cell lines. MCF-7 and U87 cells treated with free DOX and had a lower fluorescence intensity similar to that of the control cells as shown in Figure 4.6. After the encapsulation of DOX in the copolymer, enhanced cellular uptake was seen for both cell lines. Because free maleimide groups, which can nonspecifically interact with cellular thiols present on the activated surface of copolymer, affect the cellular uptake and delivery of cargo molecules [40]. Conjugation of RGD peptide to the structure *via* carbamate bond caused enhanced cellular uptake of the drug carriers for integrin αvβ3 receptor positive U87 cells (Figure 4.6B). In the case of MCF-7 cells, no specific enhancement was observed in the cellular uptake of PMMA-*b*-PHEMA/DOX/Cys-TAT/RGD (Figure 4.6A).
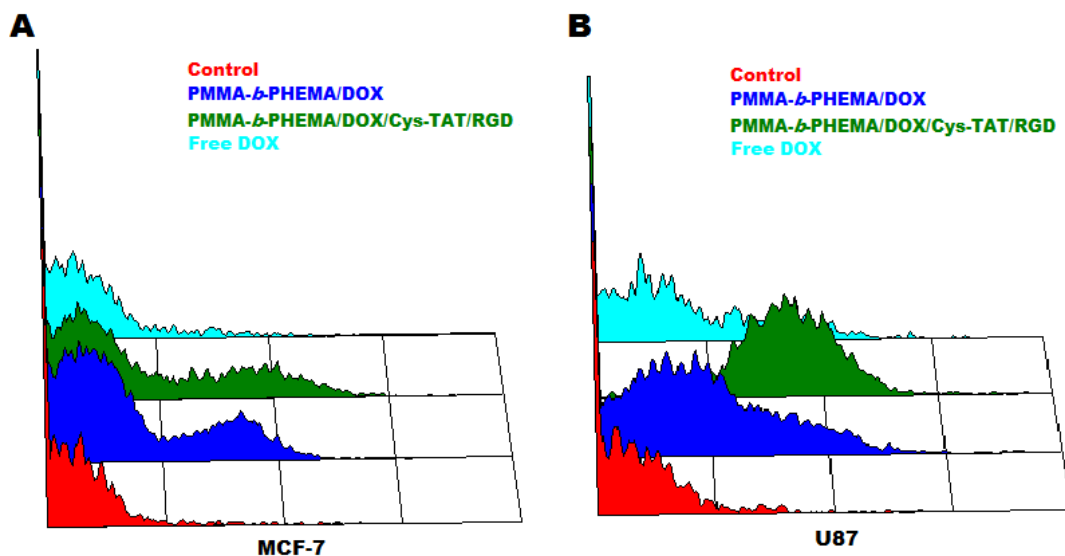
Figure 4.6 Flow cytometric analysis of (A) MCF-7 and (B) U87 cells. Cells were exposed to free DOX, PMMA-*b*-PHEMA/DOX/Cys-TAT/RGD, and PMMA-*b*-PHEMA/DOX (equivalent concentration of DOX 2.5 μg/mL) for 4 h.

Cytotoxicity

The cytotoxicity of PMMA-*b*-PHEMA copolymer and conjugates was investigated in MCF-7 and U87 cells by MTT assay. The results showed that PMMA-*b*-PHEMA copolymer was practically nontoxic to MCF-7 and U87 cells with relative cell viabilities (%) of 87.4 and 91.4, respectively (Figure 4.7). PMMA-*b*-PHEMA/DOX had a significant cytotoxic effect ($p < 0.0001$) on both cell lines in comparison with nontreated control cells due to (as explained above) nonspecific interactions. But no significant

61

differences were observed in comparison with free DOX. Due to the conjugation of the peptides to PMMA-*b*-PHEMA/DOX conjugate, PMMA-*b*-PHEMA/DOX/Cys-TAT/RGD was more toxic to U87 cells than to MCF-7 cells. Furthermore, it had significant cytotoxicity ($p < 0.01$) on U87 cells compared to free DOX.
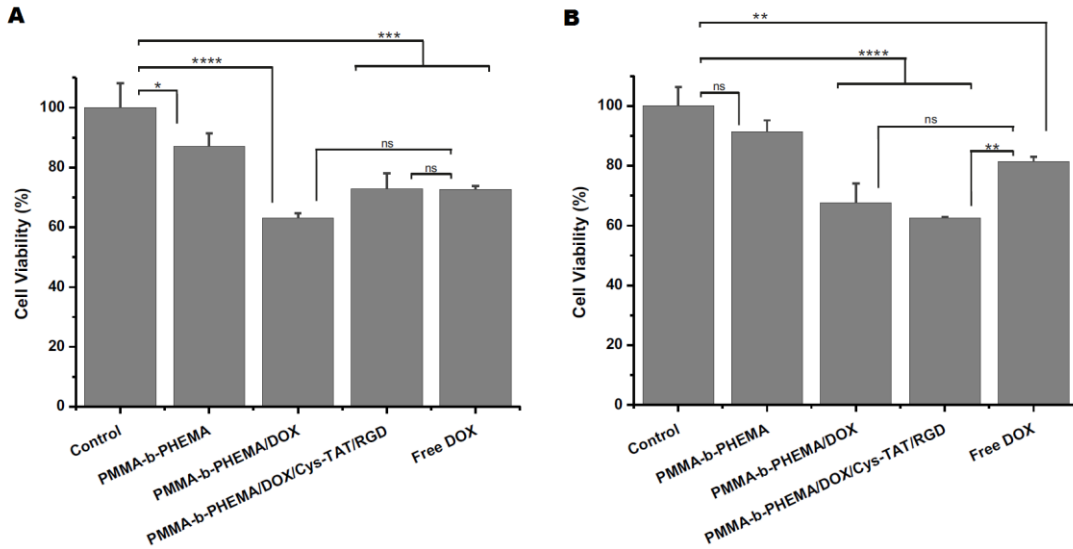
Figure 4.7 Cytotoxicity of (A) MCF-7 and (B) U87 cells. Cells were incubated with PMMA-*b*-PHEMA, PMMA-*b*-PHEMA/DOX, PMMA-*b*-PHEMA/DOX/Cys-TAT/RGD, and free DOX for 24 h. MTT assay was applied. Error bars represent the standard deviation from the mean. Data were analyzed using one-way ANOVA with Tukey test, and *$p < 0.05$ was considered significant.

Annexin V/PI Staining

The extent and mode of cell death were evaluated with Annexin V/PI staining, and fluorescence was measured by flow cytometry (Figure 4.8). Here Annexin V positive, but PI negative cells were defined as early apoptotic cells (lower-right quadrant), whereas Annexin V positive and PI positive cells were defined as late apoptotic cells (upper-right quadrant). On the other hand, Annexin V negative, but PI positive cells were defined as necrotic cells (upper-left quadrant). PMMA-*b*-PHEMA/DOX nanoparticles after treatment showed an increase in total apoptosis for both cell lines (Figure 4.8B, F). However, targeted PMMA-*b*-PHEMA/DOX nanoparticles presented a higher increase in total apoptosis than DOX and PMMA-*b*-PHEMA/DOX alone for U87 cell line (Figure 4.8G). No significant differences versus other conjugates were found in MCF-7 cells treated with PMMA-*b*-PHEMA/DOX/Cys-TAT/RGD nanoparticles (Figure 4.8A−D). Statistical data were analyzed using Win MDI software.
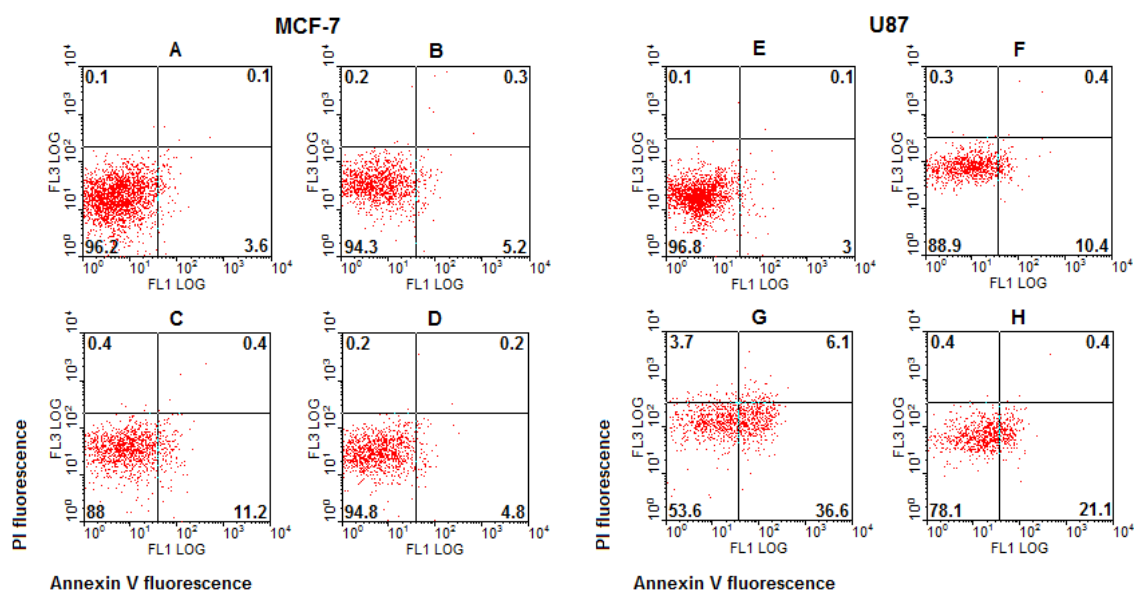
Figure 4.8 Apoptotic cell deaths by flow cytometric analysis with Annexin V/PI staining after incubating MCF-7 (left panel) and U87 (right panel) cells in PBS/FCS, with (A, E) PBS/FCS alone, (B, F) PMMA-*b*-PHEMA/DOX, (C, G) PMMA-*b*-PHEMA/DOX/Cys-TAT/RGD, and (D, H) free DOX.

Cell Imaging

Since DOX is fluorescent, drug and drug loaded polymeric micelle localization can be effectively monitored. In tumor cells, it localizes to the nucleus [41]. Free DOX molecules move to nucleus freely with red fluorescence in obtained images. The synthesized PMMA-*b*-PHEMA/DOX/Cys-TAT/RGD conjugate bound to integrin αvβ3-positive U87 cell specificity, whereas binding of that conjugate was slight with nonspecific interactions in αvβ3-negative MCF-7 cells (Figure 4.9A, D). Besides the strong red fluorescence in the nucleus, the fluorescence was observed in the cytoplasm as well. The reason is that targeted conjugate was taken into the U87 cell with endocytosis specifically and after that, it escaped from endosomal/lysosomal vesicles to the cytoplasm. The targeting process was performed successfully, and therefore, nontargeted PMMA-*b*-PHEMA/DOX micelle was taken into MCF-7 cells as against targeted micelle. These consequences are similar to the results of flow cytometry analysis and other studies performed in the literature [42].
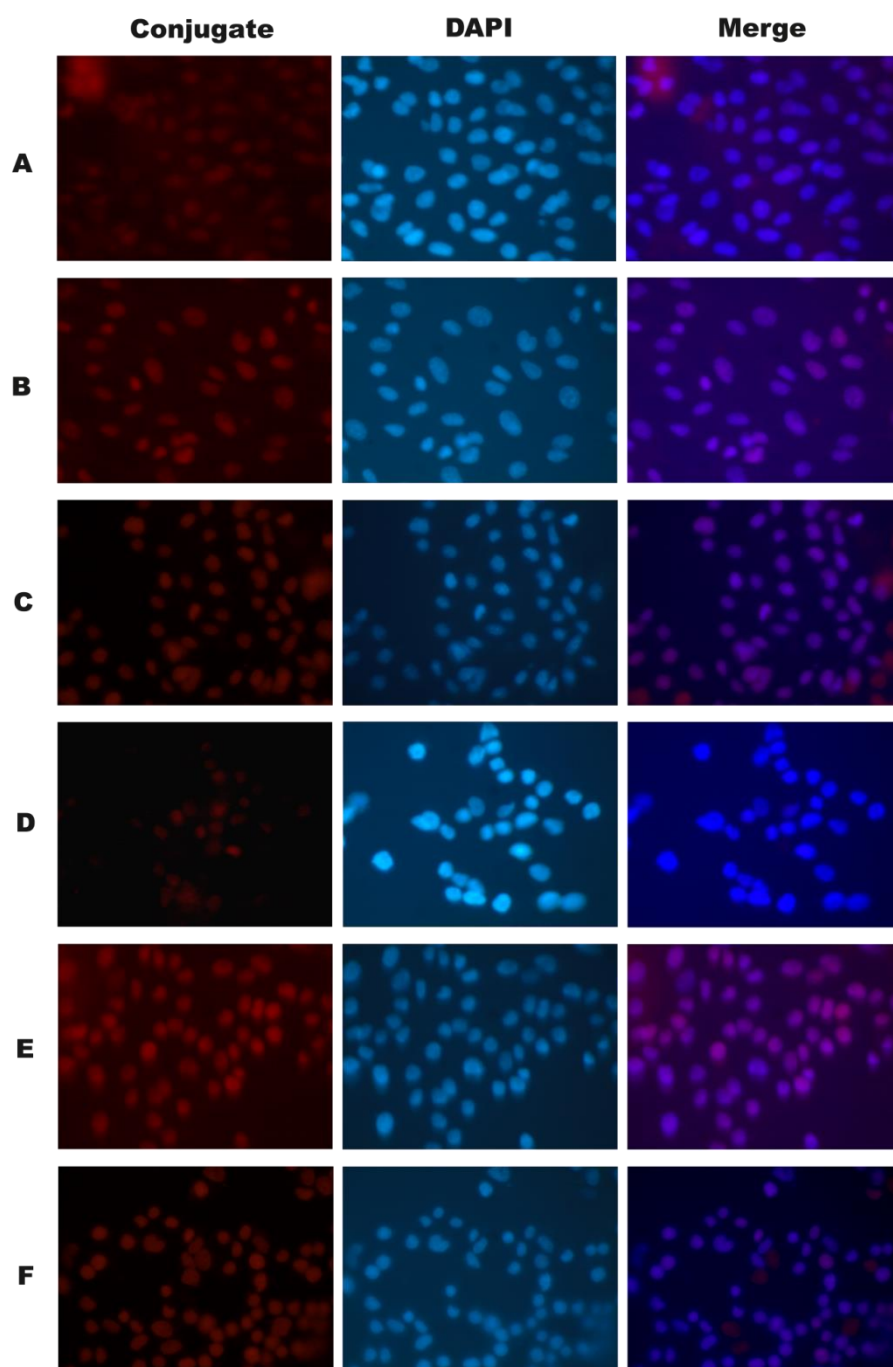
Figure 4.9 Fluorescence microscopy of U87 cells after incubation with (A) PMMA-*b*-PHEMA/DOX/Cys-TAT/RGD, (B) PMMA-*b*-PHEMA/DOX, and (C) free Dox; and MCF-7 cells after incubation with (D) PMMA-*b*-PHEMA/DOX/Cys-TAT/RGD, (E) PMMA-*b*-PHEMA/DOX, and (F) free DOX for 6 h at 37 °C (DOX equivalent concentration: 2.5 μg/mL for all formulations). All pictures are in 40× magnification.

4.1.6 Conclusion

An amphiphilic star-hyperbranched block copolymer, namely, PMMA-*b*-PHEMA, was successfully synthesized by SCVP and conventional vinyl polymerization. The hydrodynamic diameter of micelles self-assembled from PMMA-*b*-PHEMA was measured to be ~100 nm. DOX was encapsulated into the copolymer micelles, and the

targeting properties of nanostructures in the presence and in the absence of cell targeting and penetrating peptides were evaluated *in vitro*. The drug-loaded nanostructured copolymers exhibit great potential as targeting drug carriers. The targeted drug-loaded nanoparticles show stronger inhibition on the integrin αvβ3 receptor overexpressed cells because the cell internalization could be significantly enhanced due to the RGD-mediated targeting.

4.1.7 Acknowledgements

4.1.8 References

1. Minchinton, A. I.; Tannock, I. F. Drug Penetration in Solid Tumours. Nat. Rev. Cancer 2006, 6, 583−592.

2. Wu, H. C.; Huang, C. T.; Chang, D. K. Anti-Angiogenic Therapeutic Drugs for Treatment of Human Cancer. J. Cancer Mol. 2008, 4, 37−45.

3. Torchilin, V. P. Multifunctional, Stimuli-Sensitive Nanoparticulate Systems for Drug Delivery. Nat. Rev. Drug Discovery 2014, 13, 813−827.

4. Sawant, R. R.; Torchilin, V. P. Multifunctional Nanocarriers and Intracellular Drug Delivery. Curr. Opin. Solid State Mater. Sci. 2012, 16, 269−275.

5. Ag, D.; Seleci, M.; Bongartz, R.; Can, M.; Yurteri, S.; Cianga, I.; Stahl, F.; Timur, S.; Scheper, T.; Yagci, Y. From Invisible Structures of SWCNTs Toward Fluorescent and Targeting Architectures for Cell Imaging. Biomacromolecules 2013, 14, 3532−3541.

6. Kuang, H.; Wu, S.; Xie, Z.; Meng, F.; Jing, X.; Huang, Y. Biodegradable Amphiphilic Copolymer Cantaining Nucleobase: Synthesis, Self-Assembly in Aqueous Solutions, and Potential Use in Controlled Drug Delivery. Biomacromolecules 2012, 13, 3004−3012.

7. Demina, T. V.; Budkina, O. A.; Badun, G. A.; Melik-Nubarov, N. S.; Frey, H.; Müller, S. S.; Nieberle, J.; Grozdova, I. D. Cytotoxicity and Chemosensitizing Activity of Amphiphilic Poly(glycerol)-Poly-(alkylene oxide) Block Copolymers. Biomacromolecules 2014, 15, 2672−2681.

8. Diao, Y. Y.; Li, H. Y.; Fu, Y. H.; Han, M.; Hu, Y. L.; Jiang, H. L.; Tsutsumi, Y.; Wei, Q. C.; Chen, D. W.; Gao, J. Q. Doxorubicin-loaded PEG-PCL Copolymer Micelles Enhance Cytotoxicity and Intracellular Accumulation of Doxorubicin in Adriamycin-Resistant Tumor Cells. Int. J. Nanomed. 2011, 6, 1955−1962.

9. Jhaveri, A. M.; Torchilin, V. P. Multifunctional Polymeric Micelles for Delivery of Drugs and siRNA. Front. Pharmacol. 2014, 5,77.

10. Miura, Y.; Takenaka, T.; Toh, K.; Wu, S.; Nishihara, H.; Kano,M. R.; Ino, Y.; Nomoto, T.; Matsumoto, Y.; Koyama, H.; Cabral, H.; Nishiyama, N.; Kataoka, K. Cyclic RGD-Linked Polymeric Micelles for Targeted Delivery of Platinum Anticancer Drugs to Glioblastoma through the Blood-Brain Tumor Barrier. ACS Nano 2013, 7, 8583−8592.

11. ElSayed, M. E. H.; Hoffman, A. S.; Stayton, P. S. Smart Polymeric Carriers for Enhanced Intracellular Delivery of Therapeutic Macromolecules. Expert Opin. Biol. Ther. 2005, 5, 23−32.

12. Li, J.; Liu, F.; Shao, Q.; Min, Y.; Costa, M.; Yeow, E. K. L.; Xing, B. Enzyme-Responsive Cell-Penetrating Peptide Conjugated Mesaporous Silica Quantum Dot Carriers for Controlled Release of Nucleus- Targeted Drug Molecules and Real-Time Intracellular Fluorescence Imaging of Tumor Cells. Adv. Healthc. Mater. 2014, 3, 1230−1239.

13. Wang, D.; Zhao, T.; Zhu, X.; Yan, D.; Wang, W. Bioapplications of Hyperbranched Polymers. Chem. Soc. Rev. 2014, DOI: 10.1039/C4CS00229F.

14. Liu, J.; Huang, W.; Pang, Y.; Zhu, X.; Zhou, Y.; Yan, D. Self-Assembled Micelles from an Amphiphilic Hyperbranched Copolymer with Polyphosphate Arms for Drug Delivery. Langmuir 2010, 26,10585−10592.

15. Durmaz, Y. Y.; Lin, Y.-L.; ElSayed, M. E. H. Development ofDegradable, pH-Sensitive Star Vectors for Enhancing the Cytoplasmic Delivery of Nucleic Acids. Adv. Funct. Mater. 2013, 23, 3885−3895.

16. Yu, S.; Dong, R.; Chen, J.; Chen, F.; Jiang, W.; Zhou, Y.; Zhu, X.; Yan, D. Synthesis and Self-Assembly of Amphiphilic Aptamer-Functionalized Hyperbranched Multiarm Copolymers for Targeted Cancer Imaging. Biomacromolecules 2014, 15, 1828−1836.

17. Asandei, A. D.; Adebolu, O. I.; Simpson, C. P. Mild-Temperature Mn2(CO)10-Photomediated Radical Polymerization of Vinylidene Fluoride and Synthesis of Well-Defined Poly(vinylidene fluoride) Block Copolymers. J. Am. Chem. Soc. 2012, 134, 6080−6083.

18. Yagci, Y.; Hepuzer, Y. A Novel Visible Light Initiatiating System for Cationic Polymerization. Macromolecules 1999, 32, 6367−6370.

19. Acik, G.; Kahveci, M. U.; Yagci, Y. Synthesis of Block Copolymers by Combination of Atom Transfer Radical Polymerization and Visible Light Radical Photopolymerization Methods. Macromolecules 2010, 43, 9198−9201.

20. Kahveci, M. U.; Acik, G.; Yagci, Y. Synthesis of Block Copolymers by Combination of Atom Transfer Radical Polymerization and Visible Light-Induced Free Radical Promoted Cationic Polymerization. Macromol. Rapid Commun. 2012, 33, 309−313.

21. Ciftci, M.; Batat, P.; Demirel, A. L.; Xu, G.; Buchmeiser, M.; Yagci, Y. Visible Light-Induced Grafting from Polyolefins. Macromolecules 2013, 46, 6395−6401.

22. Koumura, K.; Satoh, K.; Kamigaito, K. Manganese-Based Controlled/Living Radical Polymerization of Vinyl Acetate, Methyl Acrylate, and Styrene: Highly Active, Versatile, and Photoresponsive Systems. Macromolecules 2008, 41, 7359−7367.

23. Koumura, K.; Satoh, K.; Kamigaito, K. Mn2(CO)10-Induced Controlled/Living Radical Copolymerization of Methyl Acrylate and 1-Hexane in Fluoroalcohol: High α-Olefin Content Copolymers with Controlled Molecular Weights. Macromolecules 2009, 42, 2497−2504.

24. Koumura, K.; Satoh, K.; Kamigaito, K. Mn2(CO)10-Induced Controlled/Living Radical Copolymerization of Vinyl Acetate and Methyl Acrylate: Spontaneous Formation of Block Copolymers Consisting of Gradient and Homopolymer Segments. J. Polym. Sci., Part A: Polym. Chem. 2009, 47, 1343−1353.

25. Ciftci, M.; Tasdelen, M. A.; Yagci, Y. Sunlight Induced Atom Transfer Radical Polymerization by Using Dimanganese Decacarbonyl. Polym. Chem. 2014, 5, 600−606.

26. Xiong, X.; Liu, W.; Luan, Y.; Du, J.; Wu, Z.; Chen, H. A Versatile, Fast, and Efficient Method of Visible-Light-Induced Surface Grafting Polymerization. Langmuir 2014, 30, 5474−5480.

27. Iskin, B.; Yilmaz, G.; Yagci, Y. Telechelic Polymers by Visible- Light-Induced Radical Coupling. Macromol. Chem. Phys. 2013, 214, 94−98.

28. Bektas, S.; Ciftci, M.; Yagci, Y. Hyperbranched Polymers by Visible Light Induced Self-Condensing Vinyl Polymerization and Their Modifications. Macromolecules 2013, 46, 6751−6757.

29. Jin, C.; Qian, N.; Zhao, W.; Yang, W.; Bai, L.; Wu, H.; Wang, M.; Song, W.; Dou, K. Improved Therapeutic Effect of DOX-PLGAPEG Micelles Decorated with Bivalent Fragment HAb18 F(ab`)(2) for Hepatocellular Carcinoma. Biomacromolecules 2010, 11, 2422−2431.

30. Alexis, F.; Pridgen, E.; Molnar, L. K.; Farokhzad, O. C. Factors Affecting the Clearance and Biodistribution of Polymeric Nanoparticles. Mol. Pharmaceutics 2008, 5, 505−515.

31. Nagayama, S.; Ogawara, K.; Fukuoka, Y.; Higaki, K.; Kimura, T. Time-Dependent Changes in Opsonin Amount Associated on Nanoparticles Alter Their Hepatic Uptake Characteristics. Int. J. Pharm. 2007, 342, 215−221.

32. Kim, W.; Xiao, J.; Chaikof, E. L. Recombinant Amphiphilic Protein Micelles for Drug Delivery. Langmuir 2011, 27, 14329−14334.

33. Bastakoti, B. P.; Wu, K. C.-W.; Inoue, M.; Yusa, S.-I.; Nakashima, K.; Yamauchi, Y. Multifunctional Core-Shell-Corona- Type Polymeric Micelles for Anticancer Drug-Delivery and Imaging. Chem.Eur. J. 2013, 19, 4812−4817.

34. Khoee, S.; Hassanzadeh, S.; Goliaie, B. Effects of Hydrophobic Drug-Polyesteric Core Interactions on Drug Loading and Release Properties of Poly(ethylene glycol)-Polyester-Poly(ethylene glycol) Triblock Core-Shell Nanoparticles. Nanotechnology 2007, 18, 17.

35. Mohan, P.; Rapoport, N. Doxorubicin as a Molecular Nanotheranostic Agent: Effect of Doxorubicin Encapsulation in Micelles or Nanoemulsions on the Ultrasaund-Mediated Intracellular Delivery and Nuclear Trafficking. Mol. Pharmaceutics 2010, 7, 1959−1973.

36. Qi, J.; Yao, P.; He, F.; Yu, C.; Huang, C. Nanoparticles with Dextran/Chitosan Shell and BSA/Chitosan Core-Doxorubicin Loading and Delivery. Int. J. Pharm. 2010, 393, 176−184.

37. Hu, Y.; Jiang, X. Q.; Ding, Y.; Zhang, L. Y.; Yang, C. Z.; Zhang, J. F.; Chen, J. N.; Yang, Y. H. Preparation and Drug Release Behaviors of Nimodipine-Loaded Poly(caprolactone)-Poly(ethylene oxide)-Polylactide Amphiphilic Copolymer Nanoparticles. Biomaterials 2003, 24, 2395−2404.

38. Ge, H. X.; Hu, Y.; Yang, S. C.; Jiang, X. Q.; Yang, C. Z. Preparation, Characterization, and Drug Release Behaviors of Drug- Loaded ε-Caprolactone/L-Lactide Copolymer Nanoparticles. J. Appl. Polym. Sci. 2000, 75, 874−882.

39. Wang, N. X.; Von Recum, H. A. Affinity-Based Drug Delivery. Macromol. Biosci. 2011, 11, 321−332.

40. Li, T.; Takeoka, S. Enhanced Cellular Uptake of Maleimide-Modified Liposomes via Thiol-Mediated Transport. Int. J. Nanomed. 2014, 9, 2849−2861.

41. Heibein, A. D.; Guo, B.; Sprowl, J. A.; MacLean, D. A.; Parissenti, A. M. Role of Aldo-Keto Reductases and Other Doxorubicin Pharmacokinetic Genes in Doxorubicin Resistance, DNA binding, and Subcellular Localization. BMC Cancer 2012, 12, 381.

42. Li, Y.; Zou, L.; Li, Q.; Haibe-Kains, B.; Tian, R.; Li, Y.; Desmedt, C.; Sotiriou, C.; Szallasi, Z.; Iglehart, J. D.; Richardson, A. L.; Wang, Z. C. Amplification of LAPTM4B and YWHAZ Contributes to Chemotherapy Resistance and Recurrence of Breast Cancer. Nat. Med. 2010, 16, 214−218.

4.1.9 Supplementary Information
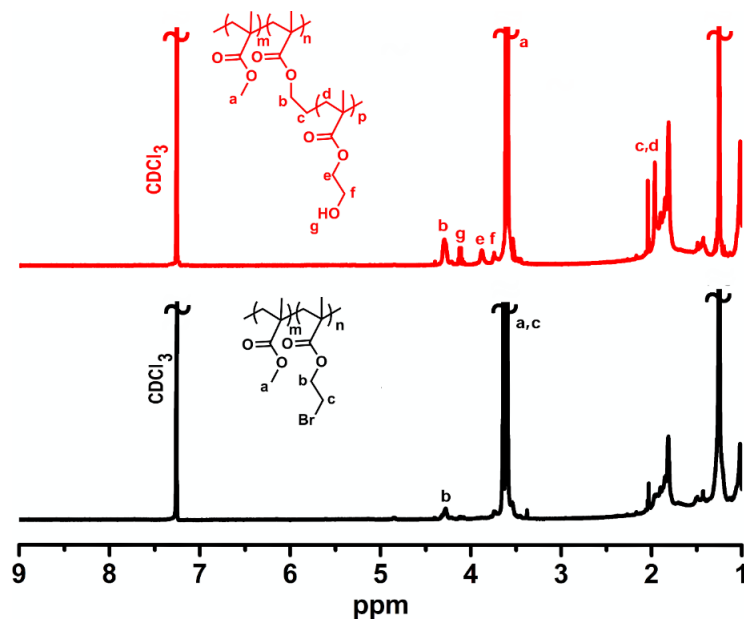
Figure S4.1 ¹H NMR spectra of hyperbranched PMMA and star-hyperbranched PMMA-*b*-PHEMA copolymer.
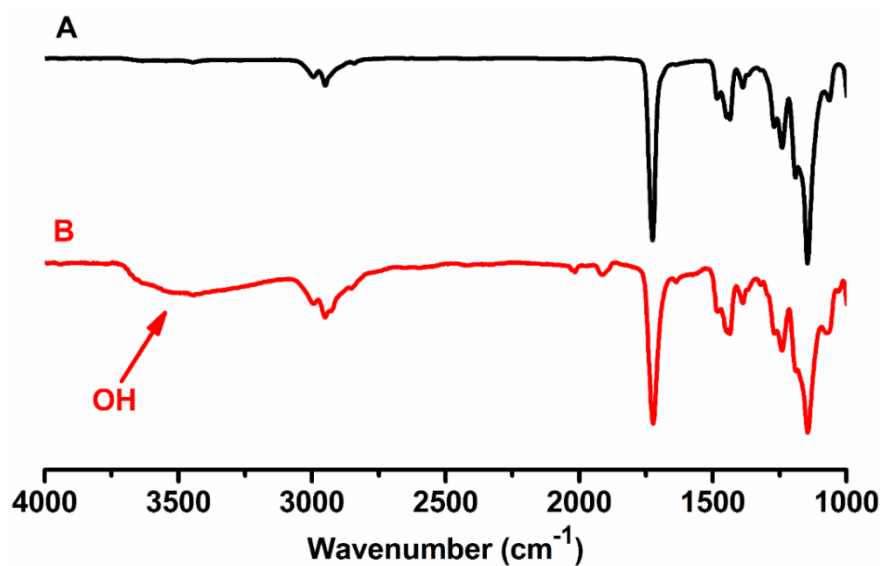
Figure S4.2 FT-IR spectra of hyperbranched PMMA and PMMA-*b*-PHEMA copolymer.
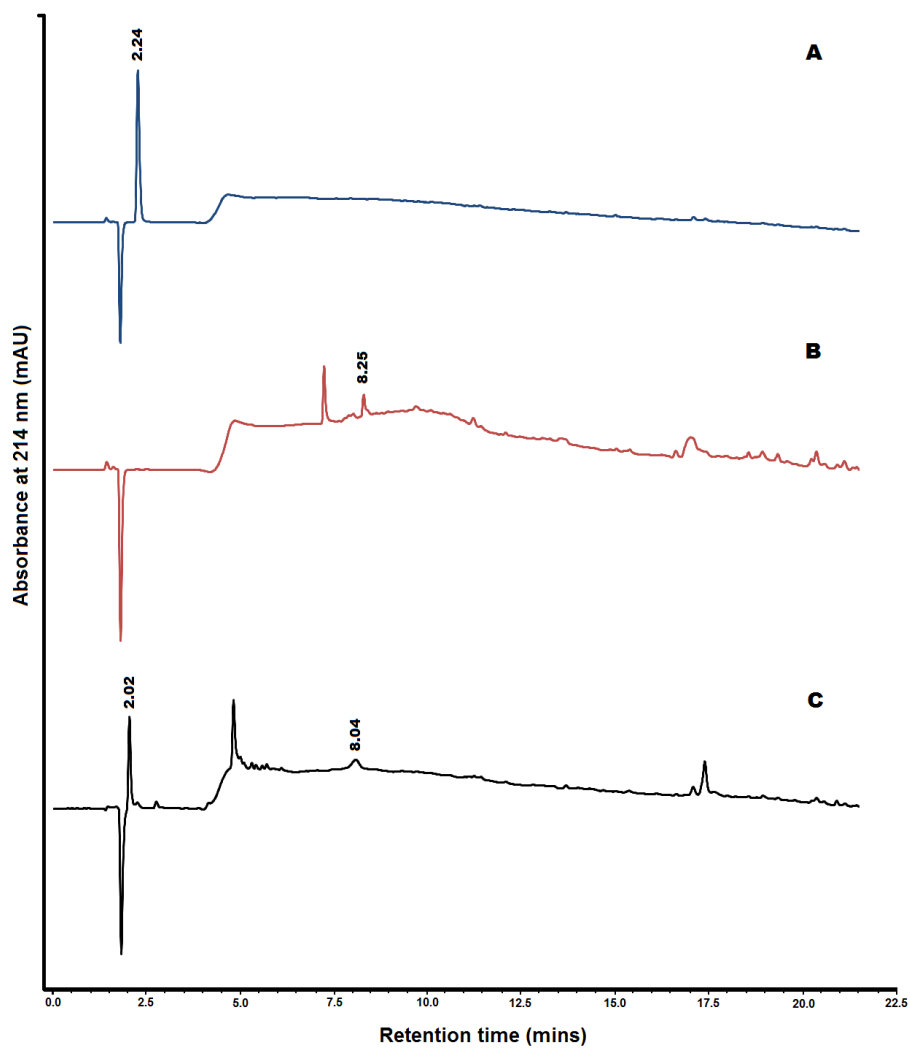
Figure S4.3 HPLC chromatogram of (A) RGD peptide, (B) Cys-TAT peptide, and (C) Cys-TAT/ RGD peptide conjugate.
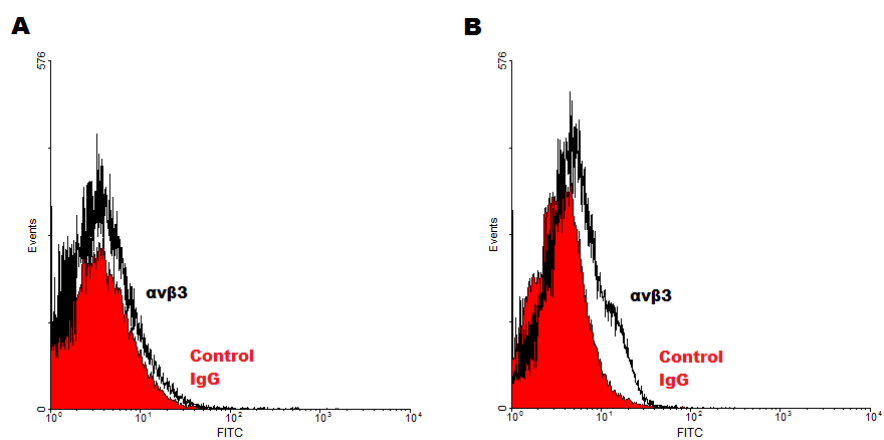
Figure S4.4 Characterization of integrin αvβ3 protein expression *via* flow cytometry in (A) MCF-7 cells and (B) U87 cells. Red histogram: IgG-FITC as negative control; Black histogram; anti-human integrin αvβ3-FITC.

4.2 Theranostic liposome-nanoparticle hybrids for drug delivery and bioimaging

This chapter corresponds to the article "Theranostic liposome-nanoparticle hybrids for drug delivery and bioimaging" by M. Seleci, D. Ag Seleci, T. Scheper, F. Stahl first published in *International Journal of Molecular Sciences,* 2017, 18(7), 1415. It was reproduced by permission of Multidisciplinary Digital Publishing Institute.

Table of Contents Graphic
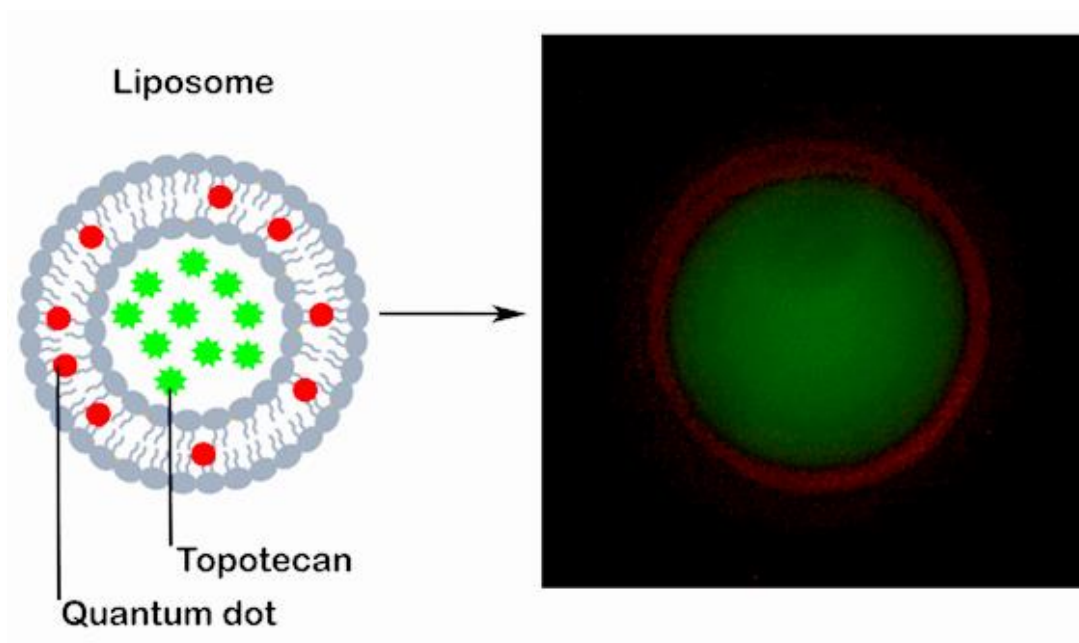
4.2.1 Summary

Personalized medicine is a promising way to address unmet medical needs. In parallel with the developments in nanotechnology, the disease treatment is moving towards tailored treatment strategies for individual patients, considering the interindividual variability in therapeutic response because of the limitations of standard diagnostic and therapeutic strategies. Novel theranostic approaches may accomplish the promise of personalized medicine.

Theranostics is a concept, which combines diagnostics and therapy into a single platform. The diagnostic part of theranostic agents provides information about the presence of a disease, its status, and its response to a specific treatment. The therapeutic effect of the agent can be realized *via* several routes of action. For example, it can be ensured through the delivery of chemotherapeutics to the intended site or theranostic agent can directly occupy the specific cell surface receptor *via* appropriate chemistry, thereby inducing a therapeutic effect. Nanoparticle-based theranostic systems can be constructed by different nanoplatforms, such as carbon nanotubes, magnetic nanoparticles, gold nanostructures, quantum dots (QDs), polymeric nanoparticles, silica nanoparticles, and liposomes. The surface of these nanoplatforms could be modified with ligands to specifically accumulate in the target tissue and/or agents could be physically encapsulated into or chemically conjugated onto the platforms. Some types of nanoparticles such as carbon nanotubes and gold nanostructures can function as theranostic nanoparticles on their own due to their light absorption properties. They can strongly absorb light energy and later scatter or emit various specific diagnostic/therapeutic signals (e.g. Raman, fluorescence, ultrasound or heat).

In this study, a novel multifunctional theranostic liposomal vehicle which contains both model drugs topotecan (TPT) and hydrophobic QDs for therapy and imaging was developed. For this aim, firstly, liposomal QDs hybrids (L-QD) were synthesized *via* the thin film hydration method. Water-insoluble QDs were successfully incorporated within the lipid bilayer of liposomes. Subsequently, TPT was encapsulated in the aqueous core of the L-QD *via* the pH gradient technique. Reduction of the particle size of liposomes was performed by sonication and subsequent extrusion. The fluorescence spectra of the free drug and liposomal formulations were measured to confirm the coexistence of both molecules in a vehicle. Both specific peaks originating from QD and TPT were observed for L-QD-TPT in the spectrum. Furthermore, fluorescence localizations of the molecules

are also observed in a large liposome using fluorescence microscopy. It was clearly seen that, the red emitting hydrophobic QDs were located in the bilayer and the green emitting TPT in the aqueous core of the liposome. Physicochemical properties of the liposomes were investigated using a variety of techniques. DLS and zeta potential analysis were carried out to determine the size and surface charge of liposomal formulations. The size and surface charge of the samples were approximately 135 nm and -10 mV which are favorable for drug delivery applications. Besides, the entrapment efficiency (EE (%)) of TPT was calculated to be 44%. The *in vitro* TPT release from L-QD-TPT was studied by the dialysis method under simulated pH conditions in normal human tissues (7.4) and tumor microenvironment (5.6). At the acidic conditions, faster release of TPT was observed compared to the neutral conditions after 32 h. This result provides an advantage to guide the anti-cancer drug to the tumor tissues.

The cellular uptake of liposomal formulations (L-QD, L-TPT, and L-QD-TPT) and free TPT by HeLa cells were tested *via* flow cytometry. Higher fluorescence signals, that are indicating the success of the uptake of the samples by the cells, were obtained from the cells treated with the samples in comparison with untreated control cells. Liposomal entrapment of TPT enhanced the cellular uptake of TPT in comparison to free drug. Additionally, the cellular internalization of multifunctional L-QD-TPT was monitored using fluorescence microscopy. As expected, TPT localized in the cell nucleus while QDs were found in the cytoplasm as well as in the nucleus. Finally, cytotoxicity of free drug and liposomal formulations were evaluated for HeLa cells using MTT assay. L-QD did not show any toxic effect to the cells after exposure for 24 h, whereas L-TPT and L-QD-TPT showed obvious toxic effects on HeLa cells when compared to free TPT. This could be attributed to the fact that the concentration of drug is higher within the cell due to the increased cellular uptake of liposomal formulations.

In summary, theranostic liposome-nanoparticle hybrids for co-delivery of imaging and therapeutic agents were successfully synthesized and characterized. This vehicle enabled the usage of water insoluble QDs by improving their bioavailability for bioimaging and, in addition, enhanced the therapeutic efficacy of TPT by increasing its stability. This approach might provide new perspectives for design, development, and application of hybrid nanoparticles in nanomedicine.

4.2.2 Abstract

Advanced theranostic nanomedicine is a multifunctional approach which combines the diagnosis and effective therapy of diseased tissues. Here, we investigated the preparation, characterization and *in vitro* evaluation of theranostic liposomes. As is known, liposome–quantum dot (L–QD) hybrid vesicles are promising nanoconstructs for cell imaging and liposomal-topotecan (L-TPT) enhances the efficiency of TPT by providing protection against systemic clearance and allowing extended time for it to accumulate in tumors. In the present study, hydrophobic CdSe/ZnS QD and TPT were located in the bilayer membrane and inner core of liposomes, respectively. Dynamic light scattering (DLS), zeta potential (ζ) measurements and fluorescence/absorption spectroscopy were performed to determine the vesicle size, charge and spectroscopic properties of the liposomes. Moreover, drug release was studied under neutral and acidic pH conditions. Fluorescence microscopy and flow cytometry analysis were used to examine the cellular uptake and intracellular distribution of the TPT-loaded L–QD formulation. 3-(4,5-Dimethylthiazol-2-yl)-2,5-diphenyltetrazolium bromide (MTT) assay was utilized to investigate the *in vitro* cytotoxicity of the formulations on HeLa cells. According to the results, the TPT-loaded L–QD hybrid has adequate physicochemical properties and is a promising multifunctional delivery vehicle which is capable of a simultaneous co-delivery of therapeutic and diagnostic agents.

4.2.3 Introduction

Nanomedicine is an innovative field with enormous potential for treatment by a combination of smart nanoparticles with small molecules carrying a wide range of functions [1]. Quantum dots (QDs) are one of the promising nanoparticles with excellent fluorescence properties, including broad absorption spectra, narrow emission spectra, high quantum yields, resistance to photobleaching, and high photochemical stability [2-4]. Due to these characteristics, they have been explored as fluorescent probes for biomedical applications and are useful in particular for *in vivo* cell labeling and imaging [5-8].

Most QDs are typically produced in organic solvents, making them unsuitable for direct use in biomedical and clinical applications. To overcome this limitation, different surface coatings have been applied to increase the hydrophilicity of QDs [9,10]. However, surface modifications often lead to decreases in the QDs' fluorescence intensity and

photostability. In an alternative approach, organic QDs are inserted into lipid bilayers to enhance their hydrophilicity, stability, and biocompatibility [11,14].

Liposomes are self-assembled, spherical lipid-bilayer vesicles that are the most clinically established nanometer-scale systems [15]. They have the capacity to entrap both lipophilic and hydrophobic compounds in a lipid membrane and aqueous core, respectively. Thus, the stability, biocompatibility, and solubility of the payloads could be enhanced with the use of several loading strategies.

Liposome–QD (L–QD) hybrid vesicles have shown a great potential for theranostic applications [16]. Tian *et al.* studied the loading of doxorubicin (DOX) into L–QD hybrid vesicles by the pH-gradient technique; they characterized these DOX-loaded vesicles using dynamic light scattering (DLS) and monitored DOX release [17]. Furthermore, Muthu *et al.* synthesized folic acid-conjugated theranostic liposomes for the targeted co-delivery of quantum dots and docetaxel [12]. In another study, apomorphine and QDs were integrated into multifunctional liposomes for brain targeting and bioimaging and the results showed that these liposomes can be accumulated to a large extent in the brain [18].

Topotecan (TPT) is a hydrophilic analog of camptothecin. It is a cell-cycle-specific drug and well established for the treatment of several cancers, including ovarian, small-cell lung and cervical cancer [19, 20]. However, TPT is unstable in physiological conditions and undergoes a pH-dependent rapid and reversible hydrolysis from a closed lactone ring to the inactive carboxylated form. This causes the loss of the antitumor activity of the drug. To protect TPT from the hydrolysis, liposome has been used for encapsulation [21]. Liposomal encapsulation of TPT enhances its efficacy by protecting it from systemic clearance, allowing greater uptake and extended tissue exposure in solid tumors [22].

In the present study, the aim was to develop multifunctional theranostic liposomes which contain both the model drug TPT and QDs for cell therapy and imaging. For this purpose, L–QD hybrids were synthesized by the incorporation of hydrophobic QD within the lipid bilayer. The biocompatibility of the QDs was increased, retaining its fluorescence characteristics. The pH-gradient technique was used to encapsulate TPT in the aqueous core of the liposome. Thus, TPT therapeutic activity and QD optical properties could be successfully integrated into one nanocarrier.

4.2.4 Results and Discussion

Synthesis and characterization of TPT-loaded liposomal formulations

The proportion of the lipids, distearoylphosphatidylcholine (DSPC) and cholesterol, was chosen to be 7:3. DSPC was selected as the bulk phospholipid component instead of egg phosphatidylcholine (EPC) or dimyristoylphosphatidylcholine (DMPC) to increase membrane rigidity, which can also increase drug retention in liposomes [23, 24]. The influence of cholesterol on the stability of the liposomes has been intensively investigated, which has revealed that cholesterol in sufficient quantity ($\leq 30\%$) reduces the leakage of loaded materials from liposome by increasing their stability and decreasing their permeability [25, 26]. Furthermore, cholesterol could enhance the hydrophobicity of the membrane [27]. Among various synthesis methods, the thin lipid layer hydration method is the most widely-used and simple method for the preparation of the liposomes. pH-gradient technique, which is based on pH gradients as a driving force for the accumulation of the weakly-basic molecules into acidic vesicles, was used to encapsulate TPT into the aqueous core of the liposomes, protecting its active lactone form until released. The fluorescence spectra of the free drug and liposomal formulations were measured and indicated that both QD and TPT peaks could be simultaneously observed in the spectrum (Figure 4.10). This indicates the coexistence of both molecules in the vesicle. Fluorescence localizations of the molecules are also photographed in a large liposome (Figure S4.5).
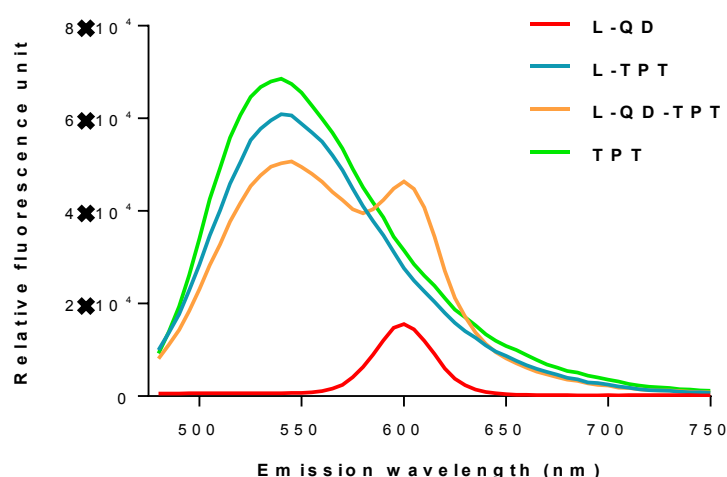
Figure 4.10 The fluorescence spectra of liposome-quantum dot (L–QD) (red), liposome-topotecan (L-TPT) (turquoise), L–QD–TPT (orange) and free TPT (green). The excitation wavelength was set at 450 nm.

The physicochemical properties of nanoparticles are an important factor in protein interactions [28]. It has been reported that nanoparticles having a size less than 150 nm are more suitable for permeating through the disorganized and leaky microvasculature of the tumor cells. Besides, their more pronounced surface curvature may also reduce the clearance of the particles as a result of reduced interaction with the surface receptors on macrophages [29, 30]. In this regard, to determine hydrodynamic diameters and the surface charge of the liposomes, DLS and ζ-potential analysis were carried out (Table 4.2). The average size of the plain liposomes was measured as ~132 nm. After QD entrapment in the lipid bilayer, a ~6 nm increase in liposome size was detected. This could be associated with the successful encapsulation of the molecules. TPT encapsulation into L–QD did not have an effect on the size (Figure S4.6). Besides, liposomes were tested for stability upon storage. Over 2 months, no significant differences in size distribution, ζ-potential as well as PDI occurred at 4 °C.

The higher surface charge of nanoparticles affects the amount of protein adsorption as well as protein corona composition on the surface [31, 32]. Studies have signified that liposomes which contain highly charged lipids are more susceptible to rapid clearance by the reticuloendothelial system (RES). However, neutral and slightly negatively charged nanoparticles have a longer circulation lifetime and less accumulation in RES [33-35]. In the present study, ζ-potential measurements revealed that the surface potential of the liposomes was slightly negative and encapsulations did not show significant alteration in surface charge. TPT encapsulation efficiency was calculated around 40%. QD incorporation into the lipid bilayer of liposomes affected just ~4% of TPT loading through the lipid membrane. Besides, the obtained polydispersity index values were lower than 0.1, confirming the homogeneity of the liposomes (Table 4.2). Accordingly, the hybrid liposomes have better physicochemical properties.

Table 4.2 Physicochemical properties and EE% of the liposomes.

Samples	Size (nm)	PDI	ζ-potential (mV)	EE (%)
L	131.8 ± 0.8	0.082	−13.6 ± 1.6	-
L–QD	138.1 ± 0.7	0.014	−7.8 ± 0.1	-
L–TPT	134.1 ± 1.2	0.073	−10.6 ± 0.1	43.8
L–QD–TPT	137.1 ± 1.7	0.069	−6.0 ± 0.1	39.5

The data are presented as the mean ± standard deviation (n = 3). PDI: Polydispersity index; ζ-potential: Zeta potential; EE: Encapsulation efficiency %.

In vitro drug release

The *in vitro* drug release profile of L–QD–TPT was investigated by the dialysis method, which is one of the most common methods for the determination of drug release from the nanoparticles. The analysis was carried out in simulated conditions of normal human tissue (pH 7.4) and a tumor microenvironment (pH 5.6) at 37 °C. The acidic environment led to an increased TPT release as compared to neutral conditions (Figure 4.11). The drug was released with an initial modest burst in the first 4 h followed by slower rates of release up to 32 h. After 32 h, the release rates of TPT were 39% at pH 7.4 and 45% at pH 5.6. The higher release rate at an acidic pH can be ascribed to the solubility of the TPT, which increased with decreasing pH as a result of protonation [36].
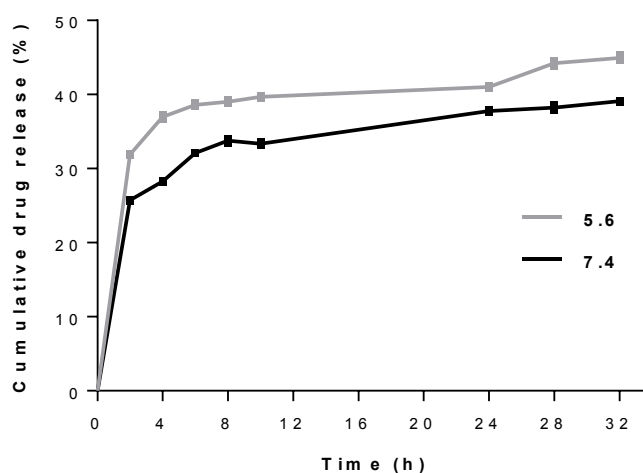
Figure 4.11 Cumulative drug release profile for L–QD–TPT at mild acidic (pH 5.6) and neutral conditions (pH 7.4). Data are presented as mean ± SD (*n* = 3).

Cellular uptake and internalization

Cellular uptake of liposomal formulations was examined *via* flow cytometry. Cells were treated with the samples for 2 h and analyzed using a flow cytometer (BD FACSAria Fusion, Becton, Dickinson and Company, Franklin Lakes, NJ, USA). A UV excitation laser (at 400 nm) was used for all measurements. Higher fluorescence signals (geometric mean values) were obtained from cells treated with the samples compared with untreated control cells. As is clear from Figure 4.12a, intracellular TPT level for L–TPT (3839 a.u.) and L–QD–TPT (4007 a.u.) in HeLa cells was higher than that of free TPT (2472 a.u.). This difference can be explained by their different uptake mechanisms. Free TPT, a small molecule, is mainly taken into the cells *via* passive diffusion, whereas liposomes enter

the cells through endocytosis [37, 38]. Besides, QD-loaded liposomes were also successfully taken up by the cells (Figure 4.12b).
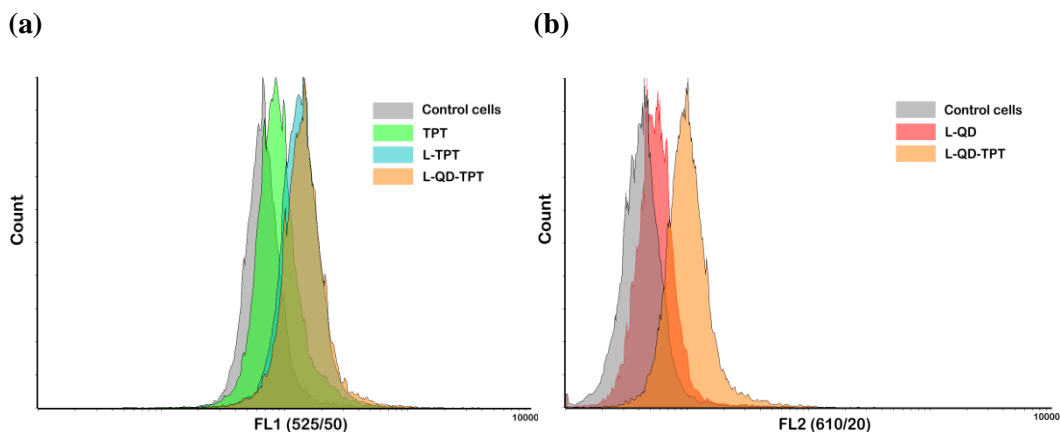
Figure 4.12 Cellular uptakes of the conjugates were determined in HeLa cells by flow cytometry. TPT, L–TPT, L–QD–TPT (a) (excitation at 400 nm, emission filter FL1 (525/50 nm)); L–QD and L–QD–TPT (b) (excitation at 400 nm, emission filter FL2 (610/20 nm)).

Fluorescence microscopy was used to observe the cellular internalization of the liposomes. The images were acquired with separate filter sets. In cells treated with L–QD–TPT, the selected fluorescent model drug TPT, which is a topoisomerase-I inhibitor, localized, unsurprisingly, in cell nuclei to exert its toxicity [39, 40]. The fluorescence from green TPT and blue 4',6-diamidino-2-phenylindole (DAPI) (nuclear stain) matched well (Figure 4.13a,c). Besides, the Figure 4.13b and merged picture (Figure 4.13d) showed punctate red spots, indicating that QDs had escaped from the endosomes and co-localized in the cytoplasm and partially in the nucleus. The results are compatible with the outcomes of flow cytometry analysis as well as with the literature [12]. Dubertret *et al.* reported the encapsulation of CdSe/ZnS QDs into phospholipid block-copolymer micelles for *in vitro* and *in vivo* imaging. The QD-micelles injected into individual cells of an early embryo and the internalized QDs were localized to both the cytosol and nuclear envelope. Besides, QD cytotoxicity was dose dependent [41].

(a)   **(b)**

(c)   **(d)**
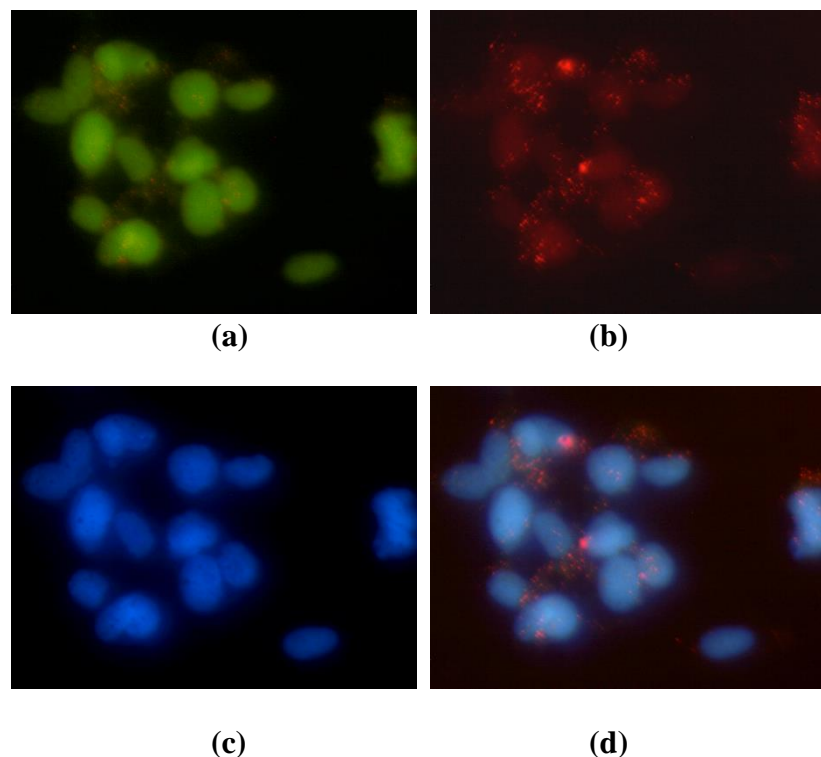
Figure 4.13 Fluorescence microscopy of HeLa cells after incubation with L–QD–TPT. Liposomes released the payload into the cell (a: TPT; b: QD). Nuclei were stained with 4',6-diamidino-2-phenylindole (DAPI) (c). The obtained images were merged into the same picture (d). All pictures are in 40× magnification.

Cytotoxicity

The cytotoxicity of the liposomal formulations and free TPT on HeLa cells were determined by 3-(4,5-Dimethylthiazol-2-yl)-2,5-diphenyltetrazolium bromide (MTT) assay. Only viable cells with active metabolism are able to convert MTT into purple-colored formazan; the quantity of the formazan is measured by recording the changes in absorbance at 570 nm to 630 nm as the reference wavelength. According to the results, L–QD had no toxic effect due to effective shielding of QD by lipid bilayer from the surroundings. Similar results were also obtained by Chinnathambi and his colleagues. They used phosphoethanolamine(polyethylene glycol)-based phospholipid micelles to encapsulate CdSe/ZnS QDs and QD-micelles showed almost no toxicity in the concentration range of 0–25 μg/mL in HeLa and A549 cell lines exposed for up to 24 h [42], whereas L–TPT and L–QD-TPT showed obvious toxic effects on HeLa cells compared to free TPT for 24 h ($p < 0.05$, Figure 4.14). This is attributed to the facts that L–TPT and L–QD–TPT were taken up into the cells more efficiently (Figure 4.12) and that the TPT concentration released from liposomes is somewhat higher compared to that

of free TPT. Hao *et al.* also found similar results regarding the enhancement of the antiproliferation ability of TPT with liposomal encapsulation [43].
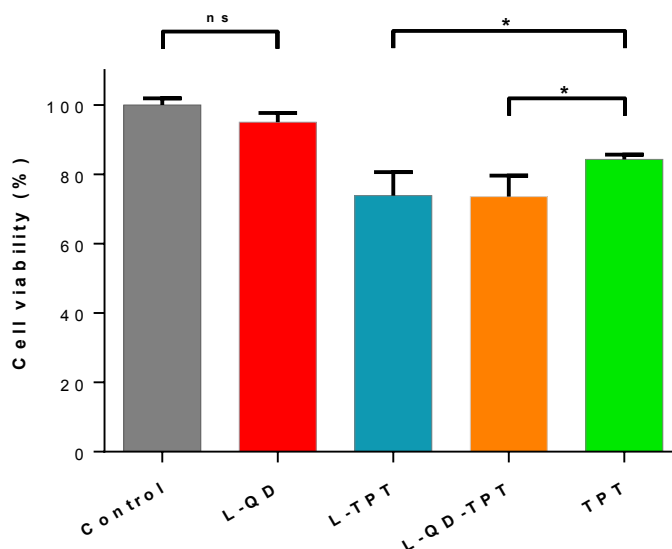
Figure 4.14 Cytotoxicity of the liposomal formulations and free TPT on HeLa cells. Cells were incubated with, L–QD, L–TPT, L–QD–TPT and free TPT (equivalent concentration of loaded TPT, 2.0 µg/mL) for 24 h. 3-(4,5-Dimethylthiazol-2-yl)-2,5-diphenyltetrazolium bromide (MTT) assay was applied. Error bars represent the standard deviation from the mean ($n = 3$). Data were analyzed using *t*-test, and * $p < 0.05$ was considered significant. ns: not significant.

4.2.5 Materials and Methods

Materials

The 3-(4,5-Dimethylthiazol-2-yl)-2,5-diphenyltetrazolium bromide (MTT), 4,6-diamino-2- phenylindol (DAPI), Dulbecco's modified eagle medium (DMEM) and cholesterol were ordered from Sigma Aldrich (Munich, Germany). CdSe/ZnS core/shell hydrophobic quantum dots (QDs) with an overall diameter of ~5 nm were obtained from PlasmaChem GmbH (Berlin, Germany). Topotecan and 1,2-distearoyl-*sn*-glycero-3-PC (DSPC) were purchased from Cayman Chemical (Ann Arbor, MI, USA).

Synthesis of L-QD hybrids

L–QD hybrids were synthesized by the thin film hydration method [44]. Briefly, DSPC:Cholesterol (7:3 molar ratio) and 30 µg/mL CdSe/ZnS QD (λ_{em} = 600 nm) solutions in chloroform were added into a round bottom flask. The mixture was placed in an evaporator to obtain a thin QD-containing lipid film and exposed to N_2 gas for just a few minutes to remove the residual of organic solvents. The dried film was hydrated with 250 mM ammonium sulphate (pH 6.5) at 60 °C, which is above the gel–liquid

melting transition temperature (Tm) of all lipids. Small unilamellar vesicles (SUVs) were prepared starting from multilamellar vesicles (MLVs) by using sonication and extruding through 0.4 μm and 0.1 μm pore size polycarbonate membranes in mini-extruder set (Avanti Polar Lipids, Alabaster, AL, USA). Afterward, liposomes were centrifuged at 11,000 rpm for 15 min to remove the excess non-incorporated quantum dots [45].

Encapsulation of model drug TPT

L–QD hybrids were loaded actively with TPT using the pH-gradient technique [46]. The obtained lipid-QD dried thin film was hydrated with 250 mM ammonium sulphate (pH 6.5) at 60 °C. After sonication, dialyzed against 10 mM HEPES buffered saline (HBS, pH 7.5) to adjust the exterior pH value of the liposomes as in physiological conditions. The suspension was then mixed with 0.1 mM TPT solution (in 0.9% NaCl) followed by 1 h incubation in a 60 °C water bath. L–QD–TPT was extruded through 0.4 μm and 0.1 μm polycarbonate membranes, respectively. Finally, liposomes were centrifuged at 11,000 rpm for 15 min to remove the excess non-incorporated molecules.

Encapsulation efficiency

The percent of encapsulation efficiency (EE%) of TPT was calculated according to the following equation (1):

$$EE\%_{\text{TPT}} = (W_{\text{en}}/\,W_{\text{total}}) \times 100\% \tag{1}$$

where W_{en} is the analyzed weight of the drug encapsulated in liposome and W_{total} is the initial amount of the drug [47]. It was determined after lysis of the liposomes by diluting purified liposomes in acidic methanol (1% trifluoroacetic acid in methanol). Calibration curves were established with known concentrations of free TPT by fluorescence emission measurements at 530 nm using a fluorospectrometer (NanoDrop 3300, Thermo Fisher Scientific Inc., Waltham, MA, USA).

Characterization

The fluorescence spectra of the free drug and liposomal formulations were measured using a spectrofluorometer. The localizations of QD and TPT in a large liposome were photographed using an Olympus BX41 fluorescence microscope (Shinjuku, Tokyo, Japan) equipped with an Olympus SC30 camera and processed by Image J software [48]. The particle size distribution and zeta potential (ζ) of the liposomes were determined by Zetasizer Nano-ZS (Malvern Instruments, Malvern, UK). The polydispersity index (PDI)

was reported as a measure of the width of size distribution. The samples were diluted at the ratio of 1:100 (v/v) with ddH_2O and equilibrated for 3 min before the measurements. Measurements were taken three times at room temperature. To test their stability, liposomal formulations were stored at 4 °C in the dark. After 2 months, their size distribution, ζ-potential and PDI were analyzed.

In vitro drug release

The dialysis technique was used for drug release experiments. L–QD–TPT was prepared and transferred into a pre-washed dialysis tubing (Slide-A-Lyzer MINI Dialysis Devices, 10K MWCO, Thermo Fisher Scientific Inc., Waltham). The tubing was immersed in 10 mL of the Phosphate buffered saline (PBS) buffer (pH 5.6 and 7.4), placed in an incubator at 37 °C and stirred at 100 rpm. At specific time intervals, 0.5 mL samples were removed from the release medium and replaced with the same volume of fresh buffer. The amount of released TPT was calculated according to the calibration curves. They were established with a known concentration of free TPT by fluorescence emission measurements at 530 nm using a spectrofluorometer.

Cell culture

Human cervical cancer cell (HeLa cell) line was provided from the German Collection of Microorganisms and Cell Cultures (DSMZ) (Braunschweig, Germany). Cells were grown in DMEM containing 10% fetal calf serum (FCS) and 1.0% penicillin/streptomycin (P/S). HeLa cells were cultivated in this medium and incubated with samples and reagents at 37 °C in a humidified environment with 5.0% CO_2.

Cytotoxicity

The MTT (3-(4,5-dimethylthiazol-2-yl)-2,5-diphenyltetrazolium bromide) assays were used to determine the cytotoxicity of the liposomal formulations. Cells (8×10^3) were seeded out in 96-well tissue plates (Sarstedt, Newton, MA, USA) in a volume of 200 μL and cultivated for three days. After this cultivation period, cells were washed once with PBS and treated with L–QD, L–TPT, L–QD–TPT and free TPT for 24 h. The equivalent concentration of free TPT was used in liposomal formulations. The samples were then removed and the cells were incubated in 110 μL/well 10% MTT solution (5.0 mg/mL in PBS) in the medium for 4 h. During this incubation time, formazan complex was produced by the cells. A 100 μL SDS solution (1.0 g SDS in 10 mL 0.01 M HCl) was added to each well to release the purple-colored salt from the cells. After 24 h of

incubation, UV-Vis absorption was measured at 570 nm to 630 nm as the reference wavelength using a microplate reader (Epoch BioTek, Winooski, VT, USA).

Cellular uptake and internalization

The cellular uptake of TPT and liposomal formulations by HeLa cells was examined through flow cytometry. Cells (5×10^5) were collected and incubated with the samples for 2 h, followed by washing two times with PBS. Just before the analysis, cells were resuspended in 500 µL of PBS and then analyzed in a BD FACSAria Fusion flow cytometer (Becton, Dickinson and Company, Franklin Lakes, NJ, USA). At least 20,000 gated events were observed in total and living cells were gated in a dot plot of forward versus side scatter signals. The dot plot and histogram data were analyzed by Flowing Software 2 [49].

Cellular internalization of L–QD–TPT was determined *via* fluorescence microscopy studies. HeLa cells were cultivated for 2 days on the chamber slides (8-well µ slides purchased from ibidi GmbH, Germany) in a volume of 200 µL of the medium. Samples were diluted with the medium and then added to the cells. The cells were incubated for 4 h at 37 °C and washed twice in PBS. Afterwards, 100 µL DAPI solution (1.0 mg/mL) was added to the cells, which were then incubated for 15 min. Cells were washed with PBS once following DAPI staining. Images were taken using an Olympus BX41 fluorescence microscope equipped with an Olympus SC30 camera and processed by Image J software.

Statistical analysis

Statistical data analysis was performed using the Student's *t*-test. The difference between two groups was considered to be significant when the *p*-value was less than 0.05.

4.2.6 Conclusion

The theranostic liposomes, with a mean size of about 135 nm, were developed for the co-delivery of imaging and therapeutic agents. Both hydrophobic QD and hydrophilic TPT were encapsulated into liposomes by thin film hydration and pH-gradient methods, respectively. Thus, the bioavailability of a poorly water-soluble molecule was enhanced and moreover, the therapeutic efficacy and stability of the drug were improved. The well-characterized liposomal TPT formulations showed significantly higher cellular uptake as well as higher cytotoxicity than free TPT. QD internalization into cells was achieved and

enabled simultaneous imaging. This liposome–nanoparticle hybrid system might offer new opportunities for the development of novel co-delivery platforms.

Supplementary Materials: The following are available online at www.mdpi.com/link, Figure S4.5: Fluorescence localizations of the molecules in a large liposome, magnification 100×. From left to right: (A) L, (B) L–QD, (C) L–TPT, and (D) L–QD–TPT. Figure S4.6: Size distributions of the liposomal formulations: (A) L, (B) L–QD, (C) L–TPT, and (D) L–QD–TPT.

Author Contributions: Muharrem Seleci designed and performed the experiments, analyzed data and wrote the paper; Didem Ag Seleci carried out the cytotoxicity and cellular uptake experiments; Thomas Scheper and Frank Stahl contributed writing the paper.

Conflicts of Interest: The authors declare no conflict of interest.

4.2.7 References

1. Seleci, M.; Ag Seleci, D.; Joncyzk, R.; Stahl, F.; Blume, C.; Scheper, T. Smart multifunctional nanoparticles in nanomedicine. BioNanoMat. 2016, 17, 33–41.

2. Bruchez, M.; Moronne, M.; Gin, P.; Weiss, S.; Alivisatos, A.P. Semiconductor nanocrystals as fluorescent biological labels. Science 1998, 281, 2013–2016.

3. Jaiswal, J.K.; Mattoussi, H.; Mauro, J.M.; Simon, S.M. Long-term multiple color imaging of live cells using quantum dot bioconjugates. Nat. Biotechnol. 2003, 21, 47–51.

4. Resch-Genger, U.; Grabolle, M.; Cavaliere-Jaricot, S.; Nitschke, R.; Nann, T. Quantum dots versus organic dyes as fluorescent labels. Nat. Methods 2008, 5, 763–775.

5. Rizvi, S.B.; Rouhi, S.; Taniguchi, S.; Yang, S.Y.; Green, M.; Keshtgar, M.; Seifalian, A.M. Near-infrared quantum dots for HER2 localization and imaging of cancer cells. Int. J. Nanomed. 2014, 9, 1323–1337.

6. Ag, D.; Bongartz, R.; Dogan, L.E.; Seleci, M.; Walter, J.-G.; Demirkol, D.O.; Stahl, F.; Ozcelik, S.; Timur, S.; Scheper, T. Biofunctional quantum dots as fluorescence probe for cell-specific targeting. Colloids Surf. B 2014, 114, 96–103.

7. Gao, X.; Cui, Y.; Levenson, R.M.; Chung, L.W.K.; Nie, S. In vivo cancer targeting and imaging with semiconductor quantum dots. Nat. Biotechnol. 2004, 22, 969–976.

8. Sounderya, N.; Zhang, Y. Use of core/shell structured nanoparticles for biomedical applications. Recent Pat. Biomed. Eng. 2008, 1, 34–42.

9. Akin, M.; Bongartz, R.; Walter, J.G.; Demirkol, D.O.; Stahl, F.; Timur, S.; Scheper, T. PAMAM-functionalized water soluble quantum dots for cancer cell targeting. J. Mater. Chem. 2012, 22, 11529–11536.

10. Smith, A.M.; Duan, H.; Rhyner, M.N.; Ruan, G.; Nie, S. A systematic examination of surface coatings on the optical and chemical properties of semiconductor quantum dots. Phys. Chem. Chem. Phys. 2006, 8, 3895–3903.

11. Al Jamal, W.T.; Al Jamal, K.T.; Bomans, P.H.; Frederik, P.M.; Kostarelos, K. Functionalized Quantum Dot Liposome Hybrids as Multimodal Nanoparticles for Cancer. Small 2008, 4, 1406–1415.

12. Muthu, M.S.; Kulkarni, S.A.; Raju, A.; Feng, S.-S. Theranostic liposomes of TPGS coating for targeted co-delivery of docetaxel and quantum dots. Biomaterials 2012, 33, 3494–3501.

13. Gopalakrishnan, G.; Danelon, C.; Izewska, P.; Prummer, M.; Bolinger, P.Y.; Geissbahler, I.; Demurtas, D.; Dubochet, J.; Vogel, H. Multifunctional lipid/quantum dot hybrid nanocontainers for controlled targeting of live cells. Angew. Chem. Int. Ed. 2006, 45, 5478–5483.

14. Yang, C.; Chen, W.; Bui, B.Q.; Xiang, G. Recent progress on the liposomes loaded with quantum dots. Rev. Nanosci. Nanotechnol. 2012, 1, 257–270.

15. Riehemann, K.; Schneider, S.W.; Luger, T.A.; Godin, B.; Ferrari, M.; Fuchs, H. Nanomedicine-challenge and perspectives. Angew. Chem. Int. Ed. 2009, 48, 872–897.

16. Muthu, M.S.; Leong, D.T.; Mei, L.; Feng, S.-S. Nanotheranostics-application and further development of nanomedicine strategies for advanced theranostics. Theranostics 2014, 4, 660–677.

17. Tian, B.; Kostarelos, K. The engineering of doxorubicin-loaded liposome-quantum dot hybrids for cancer theranostics. Chin. Phys. B. 2014, 23, 087805–4.

18. Wen, C.J.; Zhang, L.-W.; Al-Suwayeh, S.A.; Yen, T.-C.; Fang, J.-Y. Theranostic liposomes loaded with quantum dots and apomorphine for brain targeting and bioimaging. Int. J. Nanomed. 2012, 7, 1599–1611.

19. Grahn, A.Y.; Bankiewicz, K.S.; Dugich-Djordjevic, M.; Bringas, J.R.; Hadaczek, P.; Johnson, G.A.; Eastman, S.; Luz, M. Non-PEGylated liposomes for convection-enhanced delivery of topotecan and gadodiamide in malignant glioma: Initial experience. J. Neurooncol. 2009, 95, 185–197.

20. Chen, Z.J.; Zhang, Z.; Xie, B.B.; Zhang, H.Y. Development and evaluation of topotecan loaded solid lipid nanoparticles: A study in cervical cancer cell lines. J. Photochem. Photobiol. B 2016, 165, 182–188.

21. Hao, Y.L.; Deng, Y.-J.; Chen, Y.; Wang, X.M.; Zhong, H.-J.; Suo, X.-B. In vitro and in vivo studies of different liposomes containing topotecan. Arch. Pharm. Res. 2005, 28, 626–635.

22. Tardi, P.; Choice, E.; Masin, D.; Redelmeier, T.; Bally, M.; Madden, T.D. Liposomal encapsulation of topotecan enhances anticancer efficacy in murine and human xenograft models. Cancer Res. 2000, 60, 3389–3393.

23. Mayer, L.D.; Tai, L.C.; Ko, D.S.; Masin, D.; Ginsberg, R.S.; Cullis, P.R.; Bally, M.B. Influence of vesicle size, lipid composition, and drug-to-lipid ratio on the biological activity of liposomal doxorubicin in mice. Cancer Res. 1989, 49, 5922–5930.

24. Lim, H.J.; Masin, D.; McIntosh, N.L.; Madden, T.D.; Bally, M.B. Role of drug release and liposome-mediated drug delivery in governing the therapeutic activity of liposomal mitoxantrone used to treat human A431 and LS180 solid tumors. J. Pharmacol. Exp. Ther. 2000, 292, 337–345.

25. Semple, S.C.; Chonn, A.; Cullis, P.R. Influence of cholesterol on the association of plasma proteins with liposomes. Biochemistry 1996, 35, 2521–2525.

26. Bozzuto, G.; Molinari, A. Liposomes as nanomedical devices. Int. J. Nanomed. 2015, 10, 975–999.

27. Magarkar, A.; Dhawan, V.; Kallinteri, P.; Viitala, T.; Elmowafy, M.; Róg, T.; Bunker, A. Cholesterol level affects surface charge of lipid membranes in saline solution. Sci. Rep. 2014, 4, 5005.

28. Rahman, M.; Laurent, S.; Tawil, N.; Yahia, L.H.; Mahmoudi, M. Nanoparticle and protein corona. Protein–Nanoparticle Interactions; Springer: Berlin, Germany, 2013; pp. 21–44, ISBN: 978-3-642-37554-5.

29. Farokhzad, O.C.; Jon, S.; Langer, R. A. Ptamers and cancer nanotechnology. In Nanotechnology for Cancer Therapy; Amiji, M.M., Ed.; CRC Press: Boca Raton, FL, USA, 2006; pp. 289–314; ISBN: 978-0-8493-7194-3.

30. Brigger, I.; Dubernet, C.; Couvreur, P. Nanoparticles in cancer therapy and diagnosis. Adv. Drug Deliv. Rev 2002, 54, 631–651.

31. Deng, Z.J.; Liang, M.; Toth, I.; Monteiro, M.; Minchin, R.F. Plasma protein binding of positively and negatively charged polymer-coated gold nanoparticles elicits different biological responses. Nanotoxicology 2013, 7, 314–322.

32. Gessner, A.; Lieske, A.; Paulke, B.R.; Muller, R.H. Influence of surface charge density on protein adsorption on polymeric nanoparticles: Analysis by two-dimensional electrophoresis. Eur. J. Pharm. Biopharm. 2002, 54, 165–170.

33. Blanco, E.; Shen, H.; Ferrari, M. Principles of nanoparticle design for overcoming biological barriers to drug delivery. Nat. Biotechnol. 2015, 33, 941–951.

34. Levchenko, T.S.; Rammohan, R.; Lukyanov, A.N.; Whiteman, K.R.; Torchilin, V.P. Liposome clearance in mice: The effect of a separate and combined presence of surface charge and polymer coating. Int. J. Pharm. 2002, 240, 95–102.

35. Zhao, W.; Zhuang, S.; Qi, X.-R. Comparative study of the in vitro and in vivo characteristics of cationic and neutral liposomes. Int. J. Nanomed. 2011, 6, 3087–3098.

36. Padhi, S.; Mirza, M.A.; Verma, D.; Khuroo, T.; Panda, A.K.; Talegaonkar, S.; Khar, R.K.; Iqbal, Z. Revisiting the nanoformulation design approach for effective delivery of topotecan in its stable form: An appraisal of its in vitro Behavior and tumor amelioration potential. Drug Deliv. 2016, 23, 2827–2837.

37. Yingchoncharoen, P.; Kalinowski, D.S.; Richardson, D.R. Lipid-based drug delivery systems in cancer therapy: What is available and what is yet to come. Pharmacol. Rev. 2016, 68, 701–787.

38. Torchilin, V.P. Recent advances with liposomes as pharmaceutical carriers. Nat. Rev. Drug Discov. 2005, 4, 145–160.

39. Zoorob, G.; Burke, T. Enzymology and drugs, In DNA Topoisomerase Protocols; Osheroff, N., Bjornsti, M.A., Eds.; Humana Press: Totowa, NJ, United States, 2001; Volume II, pp. 215–227; ISBN: 978-1-59259-057-5.

40. Kollmannsberger, C.; Mross, K.; Jakob, A.; Kanz, L.; Bokemeyer, C. Topotecan—A novel topoisomerase I inhibitor: Pharmacology and clinical experience. Oncology 1999, 56, 1–12.

41. Dubertret, B.; Skourides, P.; Norris, D.J.; Noireaux, V.; Brivanlou, A.H.; Libchaber, A. In vivo imaging of quantum dots encapsulated in phospholipid micelles. Science 2002, 298, 1759–1762.

42. Chinnathambi, S.; Abu, N.; Hanagata, N. Biocompatible CdSe/ZnS quantum dot micelles for long-term cell imaging without alteration to the native structure of the blood plasma protein human serum albumin. RSC Adv. 2017, 7, 2392–2402.

43. Hao, Y.L.; Deng, Y.J.; Chen, Y.; Hao, A.J.; Zhang, Y.; Wang, K.Z. In Vitro cytotoxicity, in vivo biodistribution and anti-tumour effect of PEGylated liposomal topotecan. J. Pharm. Pharmacol. 2005, 57, 1279–1287.

44. Tian, B.; Al-Jamal, K.T.; Kostarelos, K. Doxorubicin-loaded lipid-quantum dot hybrids: Surface topography and release properties. Int. J. Pharm. 2011, 416, 443–447.

45. Sonali; Singh, R.P.; Singh, N.; Sharma, G.; Vijayakumar, M.R.; Koch, B.; Singh, S.; Singh, U.; Dash, D.; Pandey, B.L. Transferrin liposomes of docetaxel for brain-targeted cancer applications: Formulation and brain theranostics. Drug Deliv. 2016, 23, 1261–1271.

46. Abraham, S.A.; Edwards, K.; Karlsson, G.; Hudon, N.; Mayer, L.D.; Bally, M.B. An evaluation of transmembrane ion gradient-mediated encapsulation of topotecan within liposomes. J. Control. Release 2004, 96, 449–461.

47. Yang, S.; Liu, C.; Liu, W.; Yu, H.; Zheng, H.; Zhou, W.; Hu, Y. Preparation and characterization of nanoliposomes entrapping medium-chain fatty acids and vitamin C by lyophilization. Int. J. Mol. Sci. 2013, 14, 19763–19773.

48. Image J, 1.47v; software for image processing; National Institutes of Health: Bethesda, ML, USA, 1997. Available online: https://imagej.nih.gov/ij/index.html (accessed on 27 June 2017)

49. Flowing Software, 2.5.1v; software for flow cytometry data analysis; Turku Centre for Biotechnology: Turku, Finland, 2013. Available online: http://flowingsoftware.btk.fi/index.php?page=1 (accessed on 27 June 2017).

4.2.8 Supplementary Information
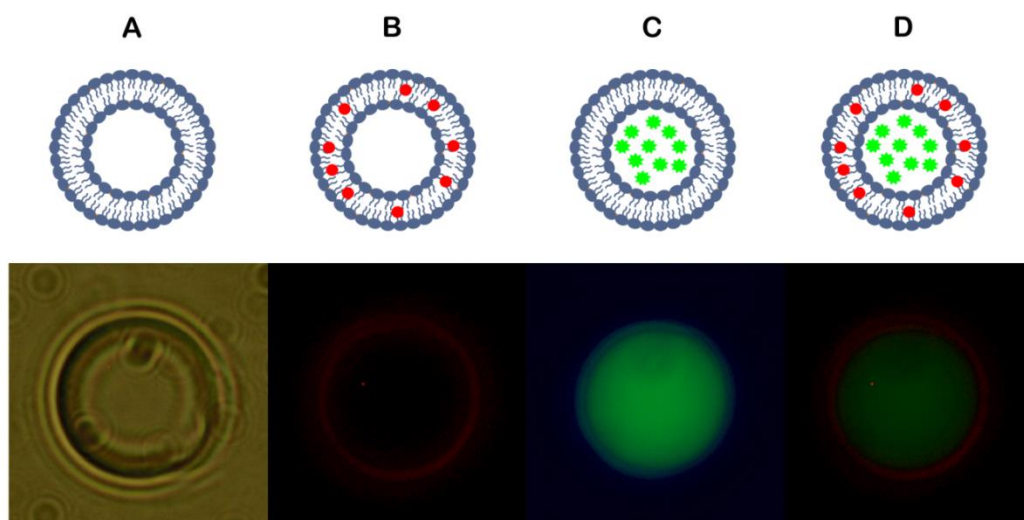
Figure S4.5 Fluorescence localizations of the molecules in a large liposome, magnification 100×. From left to right: (A) L, (B) L-QD, (C) L-TPT, and (D) L-QD-TPT.
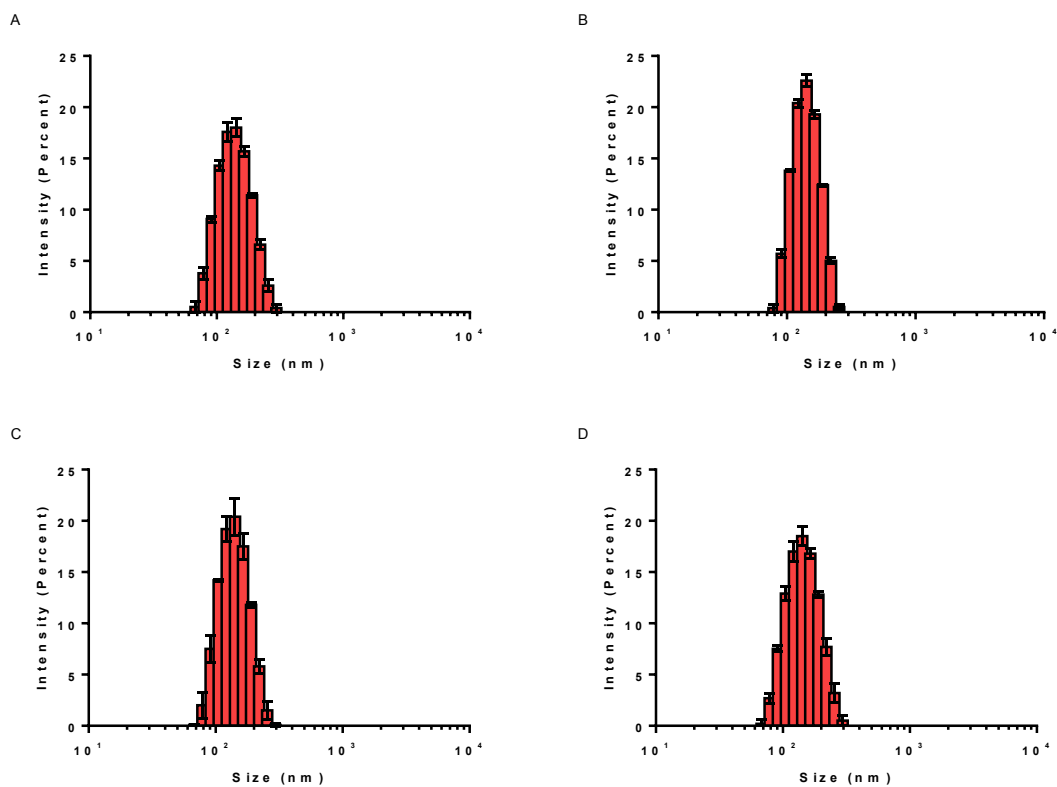
Figure S4.6 Size distributions of the liposomal formulations: (A) L, (B) L-QD, (C) L-TPT, and (D) L-QD-TPT.

5. Conclusion and Outlook

The objectives of this thesis were to design novel targeted-nanocarriers for sustained drug delivery and bioimaging, and to test their applicability in *in vitro* studies. Polymeric micelles and liposomes were utilized as nanocarriers. Active and passive targeting strategies, respectively, were performed to target the agents in a specific tissue. The characterization of the synthesized nanoparticles was carried out in detail. As a summary, nanoparticles exhibited good physicochemical properties and great potential to deliver payloads. Cellular uptake studies showed that nanocarriers were uptaken into the target cells more efficiently and hence their cytotoxicity was higher compared to free drug.

In this way poor solubility, stability, and bioavailability of the conventional therapeutic agents were enhanced. The developed multifunctional nanocarriers had high loading capacity and feasibility of incorporation of both hydrophobic and hydrophilic agents. Both therapeutic and diagnostic agents could be entrapped into a vehicle. Moreover, the developed systems showed site specific sustained drug release either by using targeting ligand on the nanoparticle surface or drug accumulation in the areas around the tumors with enhanced permeability and retention effect. Furthermore, bioimaging allowed to visualize the fate of the nanocarriers in the cells.

Amphiphilic star-hyperbranched block copolymers for drug delivery

In the first project, a polymeric micellar drug carrier was designed and characterized for controlled drug delivery studies. Firstly, an amphiphilic star-hyperbranched block copolymer, namely, poly(methyl methacrylate-block-poly(hydroxylethylmethacrylate) (PMMA-*b*-PHEMA) was prepared by sequential visible light induced self-condensing vinyl polymerization (SCVP) and conventional vinyl polymerization. A heterobifunctional cross-linking agent, *p*-Maleimidophenyl isocyanate (PMPI) which is useful for thiol to hydroxyl coupling, was utilized to functionalize micelle surface. On the other hand, Cys-TAT and RGD peptides were conjugated each other using EDC/NHS chemistry to obtain effective targeting ligand with high penetration property. After the characterization through HPLC, conjugated peptides were attached to nanoparticle surface *via* PMPI, interacted through thiol (-SH) groups of the peptide and hydroxyl (-OH) groups of the copolymer forming carbamate bond.

Selected model anticancer drug doxorubicin (DOX), is a topoisomerase II inhibitor, was encapsulated into the copolymer. The physicochemical characteristics of the synthesized

polymeric micelles were investigated in terms of size, polydispersity index, drug loading content and drug loading efficiency. The hydrodynamic diameter of the micelle before the conjugation of the peptides was measured around 100 nm by DLS. In the TEM observation, the same micelle had a smaller size, was approximately 35 nm, due to dehydration during sample preparation and subsequently shrinkage of the micelles. After targeting moiety conjugation, hydrodynamic size was determined around 170 nm. Besides, the *in vitro* drug release was studied at pH 7.4 and 5.7 to mimic physiological conditions and the acidic tumor environment, respectively. The sustained release of DOX from PMMA-*b*-PHEMA/DOX/Cys-TAT/RGD was observed, especially at physiological pH 7.4, since most of the DOX (~60%) encapsulated micelle core remained after 48 h. Synthesized and well-characterized probes were tested in two types of cancer cell lines that were selected in accordance with αvβ3 integrin receptor expression levels determined by flow cytometry. In glioblastoma (U87) cells, the higher expression level of integrin αvβ3 receptor was determined compared to breast cancer (MCF-7) cells.

In vitro active targeting capability of the micelles was evaluated and compared with the results of nontargeted DOX-loaded micelle and free drug. Within this scope, the cellular uptake levels of the PMMA-*b*-PHEMA/DOX, PMMA-*b*-PHEMA/DOX/Cys-TAT/RGD and free drug were analyzed on both cell lines for 4 h. According to the results, targeted polymeric micelle was taken significantly more than nontargeted micelle and free drug in U87 cells. Besides, there was no specific cellular uptake in MCF-7 cells, which has lower integrin αvβ3 receptor expression. Afterwards, the cytotoxicity of the micelles was investigated in both cell lines by MTT assay and as well as flow cytometric analysis through Annexin V/PI staining. The plain copolymer was non-toxic to both cell lines with relative cell viabilities about 90%. Nontargeted PMMA-*b*-PHEMA/DOX and free DOX showed almost similar toxicity on both cell lines in comparison with nontreated control cells. However, targeted PMMA-*b*-PHEMA/DOX had significant toxicity and presented a higher increase in total apoptosis than nontargeted PMMA-*b*-PHEMA/DOX and free DOX for U87 cells. Since DOX has fluorescent properties, the cellular localization of free drug and drug loaded copolymers was monitored using fluorescence microscopy. In fluorescence microscopy images it was also clearly seen that free DOX was located in the nucleus of the cells, unsurprisingly.

Overall, polymeric micelle synthesized and utilized as a drug carrier. The surface of the micelle was functionalized and Cys-TAT/RGD peptide, which has targeting potential to integrin αvβ3 receptor with high increased cellular uptake property, was conjugated to

the surface. After detailed physicochemical characterization, the applicability of the micelles was evaluated *in vitro*. The targeted PMMA-*b*-PHEMA/DOX showed higher cellular uptake and as well as higher toxicity on integrin αvβ3 receptor overexpressed cells. These findings indicate that designed multifunctional micelle might be a powerful strategy for overcoming the challenges faced in targeted cancer therapy through combining RGD with cell penetrating peptide.

Theranostic liposome-nanoparticle hybrids for drug delivery and bioimaging

In the other project, a theranostic nanoparticle-liposome hybrid, which integrates therapeutic function and diagnostic imaging into a single agent, was designed for co-delivery of the agents. Initially, liposomes were synthesized using DPSC-Chol (7:3) by thin-film hydration method. The nanoparticle that could be successfully entrapped into the lipid bilayer was added to the lipid solution before the synthesis. Encapsulation of CdSe/ZnS QD into liposomes can protect QDs from oxidation by limiting transport of oxygen to the surface. Thereby, the inherent toxicity of QDs can be reduced. Hydration was carried out through pH-gradient technique which is based pH gradient as a driving force for the accumulation of weakly basic molecules into acidic vesicles. Thus, ammonium sulphate (pH 6.5) buffer was used to hydrate QD-lipid film followed by changing of extracellular pH as 7.5 with HBS buffer. Then, the suspension was mixed with TPT solution over Tc values of the lipids. Therefore, both hydrophilic anticancer drug topotecan (TPT) and hydrophobic CdSe/ZnS quantum dot (QD) were loaded into one vehicle.

Physicochemical properties of the vehicles were investigated in detail. The presence of the fluorescent agents in liposome was analyzed with spectroscopic and microscopic methods. The simultaneous observations of fluorescence emission peaks belong to TPT (535 nm) and QD (600 nm) could be successfully performed. The localizations of the TPT and QD in aqueous core and lipid bilayer of the liposome, respectively, were monitored in a large liposome. The size and charge of the liposomes were approximately 135 nm and almost neutral, respectively. The polydispersity index (PDI) which shows distribution of the particles in solution, values were less than 0.1. Besides, they showed no significant difference in size, zeta potential and as well as PDI over 2 months when stored in 4 °C to test their stability. The encapsulation efficiency for TPT was around 44% and QD loaded liposomes showed 4% less encapsulation efficiency. That could be attributed the steric effect of the QDs in lipid membrane. These properties were well

enough for an ideal nanocarrier system. Afterwards, cellular uptake efficiency and cell viability of the liposomal formulations were investigated by different techniques. Human cervical cancer cell line HeLa was used during this study. Flow cytometric analysis were done to quantify cellular uptake levels of the molecules. According to the results, L-QD-TPT was uptaken into the cells more than the other formulations. This could be a slightly more positive charge of L-QD-TPT (-6 mV). Moreover, free TPT was entered into the cells less than liposomal formulations. This could be explained by different uptake mechanisms of the molecules. Liposomes are mainly taken up into the cell through endocytosis, whereas as a small molecule, free TPT is taken *via* passive diffusion.

The locations of the agents inside the cells were observed with fluorescence microscopy. TPT which is a topoisomerase I inhibitor was localized cell nucleus, unsurprisingly. QDs, which are seen as punctate red spots on the images, were co-localized in the cytoplasm and partially in the nucleus. Liposomal TPT formulations showed significantly higher toxicity (for 24 h, $p < 0.05$) on HeLa cells compared to free TPT due to higher and efficient cellular uptake of the agent.

Consequently, TPT and QD were encapsulated simultaneously into one liposome for theranostic applications. The stability and biocompatibility of the hydrophobic QDs were increased due to the shielding by lipid bilayer. Besides, therapeutic efficacy of the TPT was enhanced by keeping its pharmacologically active form. Liposomal formulations showed higher efficiency in uptake and higher toxicity by passive accumulation. The internalization of QD and TPT into the cells was achieved and enabled simultaneous imaging. This theranostic liposome-nanoparticle hybrid may also offer new opportunities for development of novel co-delivery platforms.

List of Publications

1. **M. Seleci**, D. Ag Seleci, F. Stahl, and T. Scheper, Theranostic liposome-nanoparticle hybrids for drug delivery and bioimaging, *International Journal of Molecular Sciences,* 2017, 18, 1415.

2. **M. Seleci**, D. Ag Seleci, R. Joncyzk, F. Stahl, C. Blume, and T. Scheper. Smart multifunctional nanoparticles in nanomedicine, *BioNanoMaterials,* 2016,17, 33–41.

3. **M. Seleci**, D. Ag Seleci, M. Ciftci, D. Odaci Demirkol, F. Stahl, S. Timur, T. Scheper, and Y. Yagci, Nano-structured Amphiphilic Star-Hyperbranched Blockcopolymers for Drug Delivery*, Langmuir*, 2015, 31, 4542–4551.

4. D. Ag Seleci, **M. Seleci**, F. Stahl, and T. Scheper, Tumor homing and penetrating peptide-conjugated niosomes as multidrug carriers for tumor-targeted drug delivery*, RSC Advances,* 2017,7, 33378-33384.

5. D. Ag Seleci, **M. Seleci**, A. Jochums, J.G. Walter, F. Stahl, and T. Scheper Aptamer mediated niosomal drug delivery, *RCS Advances*, 2016, 6, 87910–87918.

6. D. Ag Seleci, **M. Seleci**, J.G. Walter, F. Stahl, and T. Scheper Niosomes as Nanoparticular Drug Carriers: Fundamentals and Recent Applications. *Journal of Nanomaterials*, 2016. doi:10.1155/2016/7372306.

List of Presentations

Oral presentations

1. **M. Seleci** and A. Jayagopal, Molecular Imaging Approaches for Ophthalmology, March 24th 2017, Roche Pharma Research and Early Development (pRED) Neuroscience Research Forum, Basel/Switzerland

Poster presentations

1. **M. Seleci**, D. Ag Seleci, F. Stahl, and T. Scheper, Multifunctional theranostic quantum dot-liposome hybrids for drug delivery and imaging, November 9-11th 2015, Crossing Bioligical Barriers - Advances in Nanocarrier Design for Targeted Drug Delivery, Dresden/Germany

2. **M. Seleci**, D. Ag Seleci, M. Ciftci, D. Odaci Demirkol, F. Stahl, S. Timur, T. Scheper, and Y. Yagci, Nano-structured Amphiphilic Star-Hyperbranched Blockcopolymers for Drug Delivery, March 10-11th 2015, 2nd Conference of Scientific Cooperation between Lower Saxony and Israel, Hanover/Germany

3. D. Ag Seleci, **M. Seleci**, Frank Stahl, and Thomas Scheper, Design of Aptamer Based Drug Delivery, November 9-11th 2015, Crossing Biological Barriers - Advances in Nanocarrier Design for Targeted Drug Delivery, Dresden/Germany

Curriculum Vitae

Personal data

Name	Muharrem Seleci
Date of Birth	27.09.1986
Place of Birth	Giresun
Nationality	Turkish

Education

06.2014 –present

Dr. rer. nat. in Chemistry

Leibniz University of Hanover, Germany

Thesis title: Development of multifunctional nanoparticles for drug delivery and bioimaging

Supervisor: Prof. Dr. rer. nat. Thomas Scheper

09.2011 –12.2013

Master`s Degree in Biochemistry

Ege University, Izmir, Turkey

Thesis title: Quantum dots modification, investigation of drug delivery potential to cancer cells *in vitro*

Supervisor: Prof. Dr. Suna Timur

09.2006 –06.2011

Bachelor`s Degree in Biochemistry (majored in Biotechnology)

Ege University, Izmir, Turkey

Thesis title: Preparation and characterization of electrochemical malate dehydrogenase biosensor

Supervisor: Prof. Dr. Suna Timur

Work experience

07.2016 –06.2017

Roche Internships for Scientific Exchange (RiSE)
Molecular Pharmacology & Biomarkers, Ophthalmology
F. Hoffmann- La Roche AG, Basel, Switzerland

08.2014–07.2016

Research Fellow
Institute of Technical Chemistry
Leibniz University of Hanover, Hanover, Germany